

DOCTORAL THESIS NO. 74

# Performance of Engineered Timber Floor Systems: Structural Behavior and Environmental Impacts

Honghao Ren



Gävle University Press

Dissertation for the Degree of Doctor of Philosophy in Sustainability Science to be publicly defended on 21 May 2026, University of Gävle.

Opponent: Associate Professor Mahbube Subhani, Chalmers University of Technology, Sweden

© Honghao Ren 2026  
Cover illustration: Honghao Ren

Gävle University Press  
ISBN 978-91-89593-95-4  
ISBN 978-91-89593-96-1 (pdf)  
urn:nbn:se:hig:diva-49495

Distribution:  
University of Gävle  
Faculty of Engineering and Sustainable Development  
Department of Building Engineering, Energy  
Systems and Sustainability Science  
SE-801 76 Gävle, Sweden  
+46 26 64 85 00  
[www.hig.se](http://www.hig.se)

## Abstract

Cross-laminated timber (CLT) slab systems rely on edge connections to turn prefabricated individual components into continuous systems. This thesis proposes and evaluates six adhesive-free timber edge connections (Belt-BC, T shape-TS, Grove and tongue-GT, Grove-GC, Double surface-DS, Half lapped-HL) against a screw-spline CLT reference and a reinforced-concrete (RC) slab, integrating structural performance and life cycle assessment (LCA). In the LCA assessment, adhesive-free CLT slab systems without connection (AFCLT1: dovetail-jointed with service gaps; AFCLT2: dowel-laminated; and AFCLT3: solid dovetail without internal gaps) were also studied under a cradle-to-cradle framework (includes production A1-A5, partly use B1, End-of-life (EOL) C1-C4, and D modules) with a focus on ten impact categories: abiotic depletion (ADP), global warming potential (GWP), ozone depletion (ODP), human toxicity (HTP), freshwater aquatic ecotoxicity (FAETP), marine aquatic ecotoxicity (MAETP), terrestrial ecotoxicity (TETP), photochemical ozone creation (POCP), acidification (AP), and eutrophication (EP). The LCA studies are assumed to have a 50-year span of service life, and timber slabs are recycled and reused at the EOL stage. Additionally, four-point bending on glulam specimens, together with a validated FE framework establishes load capacity, displacement, effective stiffness ( $EI_{eff}$ ), strength, ductility and failure mechanisms for the timber floors with edge connections. This thesis unifies experimentally validated structural performance with LCA to show that adhesive-free edge connections can deliver competitive structural performance while materially lowering embodied impact relative to steel and RC.

Structurally, ultimate loads of CLT panels with the studied edge connections span 2.85–11.74 kN. Parametric analysis identifies clear levers: DS benefits from longer tongues, suitable dowels diameter, and additional dowels; for HL, preserving the upper-part thickness yields and optimizing dowel number/layout could increase capacity. A twin narrow-plate GC layout boosts  $EI_{eff}$  and capacity substantially relative to a single wide plate, demonstrating rotation control as a stiffness driver.

Environmentally (function unit defined as 1 m<sup>2</sup> top surface area of slab including edge connection), timber systems decisively outperform RC across most indicators; for GWP, CLT solutions were ten times lower than RC. Among adhesive-free CLT panels, AFCLT2 is consistently the lowest-impact solution, while AFCLT3 is highest within adhesive-free products due to high mass. Furthermore, electricity-mix sensitivity changes environmental performance's magnitudes but not the ranking.

The contributions of this thesis are: (i) a validated modeling-and-testing basis for six connection families; (ii) actionable design rules with quantified sensitivities for geometry, dowel size/number, and plate layout; and (iii) an LCA framework that links connection choices to cradle-to-cradle outcomes,

including electricity-mix and EOL effects. These results give designers and standard makers glue-free CLT floors that are robust, repairable, and compatible with circular construction, and provide a template for optimizing structural and environmental performance in future mass-timber systems.

**Keywords:** Cross-laminated timber, glued-laminated timber, adhesive-free connections, four-point bending, finite element modeling, life cycle assessment, global warming potential, environmental impact

## Sammanfattning

Korslimmade träskivsystem (CLT) är beroende av kantförband för att omvandla prefabricerade enskilda komponenter till kontinuerliga system. Denna avhandling föreslår och utvärderar sex limfria kantförband i trä (Belt-BC, T shape-TS, Grove and tongue-GT, Grove-GC, Double surface-DS, Half lapped-HL) i jämförelse med en skruv-spline-baserad CLT-referens samt en armerad betongplatta (RC), där strukturell prestanda och livscykelanalys (LCA) integreras. I LCA-bedömningen studerades även limfria CLT-plattsystem utan förband (AFCLT1: laxstjartssammanfogad med serviceglipor; AFCLT2: dymlingslaminerad; och AFCLT3: massiv laxstjart utan interna glipor) inom ett cradle-to-cradle-ramverk (inklusive produktion A1–A5, delvis bruksskede B1, end-of-life (EOL) C1–C4 samt modul D), med fokus på tio påverkningsskategorier: abiotisk resursutarmning (ADP), global uppvärmningspotential (GWP), ozonedbrytning (ODP), humantoxicitet (HTP), sötvattentekoticitet (FAETP), marin ekotokicitet (MAETP), terrestrisk ekotokicitet (TETP), fotokemisk ozonbildning (POCP), försurning (AP) och övergödning (EP). LCA-studierna antas ha en brukstid på 50 år, och träbjälklag återvinns och återanvänds i EOL-skedet. Därtill etablerar fyrpunktsböjning på limträprovkroppar, tillsammans med ett validerat FE-ramverk, bärförmåga, nedböjning, effektiv böjstyvhet ( $EI_{eff}$ ), hållfasthet, duktilitet och brottmekanismer för träbjälklag med kantförband. Avhandlingen förenar experimentellt validerad strukturell prestanda med LCA och visar att limfria kantförband kan ge konkurrenskraftig bärförmåga samtidigt som den inbyggda miljöpåverkan kan minska väsentligt jämfört med stål och armerad betong.

Strukturellt varierar brottlasten för CLT-paneler med de studerade kantförbanden mellan 2.85–11.74 kN. Parameterstudier identifierar tydliga styrparametrar: DS gynnas av längre spontar, lämplig dymlingsdiameter och extra dymlingar; för HL ger bibehållen tjocklek i överdelen samt optimering av antal och layout av dymlingar potential att öka bärförmågan. En GC-layout med två smala plåtar ökar  $EI_{eff}$  och bärförmågan avsevärt jämfört med en enda bred plåt, vilket visar att rotationskontroll är en drivande faktor för styvhet.

Miljömässigt (funktionell enhet definierad som 1 m<sup>2</sup> överyta av platta inklusive kantförband) presterar träbaserade system tydligt bättre än RC över de flesta indikatorer; för GWP var CLT-lösningar tio gånger lägre än RC. Bland limfria CLT-paneler är AFCLT2 genomgående lösningen med lägst påverkan, medan AFCLT3 är högst bland de limfria alternativen på grund av hög massa. Vidare påverkar känslighetsanalys för elmix storleken på miljöprestandan men inte rangordningen.

Avhandlingens bidrag är: (i) en validerad modellerings- och provningsgrund för sex förbandsfamiljer; (ii) handlingsbara designregler med kvantifierade känsligheter för geometri, dymlingsstorlek/antal och plåtlayout; samt (iii) ett LCA-ramverk som kopplar förbandsval till cradle-to-cradle-utfall,

inklusive effekter av elmix och EOL. Resultaten ger konstruktörer och standardiseringsaktörer limfria CLT-bjälklag som är robusta, reparerbara och kompatibla med cirkulärt byggande, och tillhandahåller en mall för optimering av strukturell och miljömässig prestanda i framtida stommar av massivt trä.

**Nyckelord:** Korslimmat trä, limträ, limfria förband, fyrapunktsböjning, finita element-modellering, livscykelanalys, global uppvärmningspotential, miljöpåverkan

## Acknowledgements

This doctoral thesis was carried out at the Department of Building Engineering, Energy Systems and Sustainability Science, Faculty of Engineering and Sustainable Development, University of Gävle, Sweden.

I am deeply grateful to my main supervisor, Dr. Alireza Bahrami, who introduced me to research and enabled me to work on a topic I am passionate about. Since autumn 2021 you have been unfailingly supportive and kind, consistently prioritizing my work. Your creativity, work ethic, and deep knowledge have profoundly influenced and inspired me. Your steady guidance and mentorship helped me overcome countless challenges both professionally and personally. This thesis would not have been possible without your support.

I also wish to thank my co-supervisors, Dr. Mathias Cehlin and Dr. Marita Wallhagen, for their patient discussions, supervisions, and continuous help throughout this journey.

My appreciation also goes to Rickard Larsson, workshop manager at the University of Gävle, for coordinating many aspects of the laboratory work. I warmly thank our research engineers, Dario Senkic and Mikael Sundberg, for their invaluable assistance during the experimental campaign: Mikael for providing instrumentation, and Dario for helping plan, design, install, and operate the equipment. Thank you, Dario, for your practical ingenuity in turning ideas into working solutions. To my colleagues, fellow doctoral students, and friends at the University of Gävle: thank you for the stimulating discussions, helpful feedback, and the many moments we shared at seminars, meetings, after-work events, and PhD gatherings, which inspired and encouraged me deeply.

Finally, my deepest gratitude goes to my parents, Zhihe Ren and Jun Li, for their unwavering belief in me and for keeping their door and heart open, even when I doubted myself. I am equally thankful to my partner, Xiaofang Cheng, for her companionship, patience, and support throughout these years.

Gävle, Sweden, March 2026

*Honghao Ren*



## List of Papers

This thesis is based on the following papers, which are referred to in the text by Roman numerals.

### Paper I

Ren, H., Bahrami, A., Cehlin, M., & Wallhagen, M. (2024). A state-of-the-art review on connection systems, rolling shear performance, and sustainability assessment of cross-laminated timber. *Engineering Structures*, 317, 118552. <https://doi.org/10.1016/J.ENGSTRUCT.2024.118552>

### Paper II

Ren, H., Bahrami, A., Cehlin, M., & Wallhagen, M. (2024). Proposing new adhesive-free timber edge connections for cross-laminated timber panels: A step toward sustainable construction. *Case Studies in Construction Materials*, 20, e02975. <https://doi.org/10.1016/J.CSCM.2024.E02975>

### Paper III

Ren, H., Bahrami, A., Cehlin, M., & Wallhagen, M. (2024). Flexural behavior of cross-laminated timber panels with environmentally friendly timber edge connections. *Buildings*, 14. <https://doi.org/10.3390/buildings14051455>

### Paper IV

Ren, H., Bahrami, A., Cehlin, M., & Wallhagen, M. (2024). Performance of innovative adhesive-free connections for glued-laminated timber under flexural load. *Structures*, 70, 107904. <https://doi.org/10.1016/j.istruc.2024.107904>

### Paper V

Ren, H., Wallhagen, M., Bahrami, A., & Cehlin, M. Life cycle assessment on cross laminated timber slab with different edge connections and reinforced concrete slab: Sustainability of timber connectors and metal fasteners. (*submitted to journal for publication*).

### Paper VI

Ren, H., Wallhagen, M., Bahrami, A., & Cehlin, M. (2025). Life cycle impacts of timber and reinforced concrete floor slabs: a comparative assessment. *Infrastructures*, 10(12), 346. <https://doi.org/10.3390/infrastructures10120346>

## **Additional publications (not included in the thesis)**

### **Paper VII**

Ren, H., Bahrami, A., Cehlin, M., & Wallhagen, M. (2023). Literature review on development and implementation of cross-laminated timber. *Proceedings of the 5th International Conference on Building Energy and Environment (COBEE2022)*, pp 331–339, July 25-29, 2022, Concordia University, Montreal, Canada. [https://doi.org/10.1007/978-981-19-9822-5\\_36](https://doi.org/10.1007/978-981-19-9822-5_36)

# Nomenclature

Abbreviations		Units
ADP	Abiotic depletion potential	[kg Sb eq]
AFCLT1	Adhesive-free CLT variant 1	
AFCLT2	Adhesive-free CLT variant 2	
AFCLT3	Adhesive-free CLT variant 3	
AP	Acidification potential	[kg SO <sub>2</sub> eq]
BC	Belt connection	
CML	Leiden midpoint LCIA method	
CLT	Cross-laminated timber	
CNC	Computer-numerical-control machining	
CW	Compressed/densified wood (connector material)	
DS	Double-surface tongue connection	
DSS	Double-surface spline with screws	
EP	Eutrophication potential	[kg PO <sub>4</sub> <sup>3-</sup> eq]
EOL	End-of-life	
FAETP	Freshwater aquatic ecotoxicity potential	[kg 1.4-DB eq]
FE	Finite elements	
FEM	Finite element method	
FU1	Functional unit 1: 1 m <sup>2</sup> structural floor including joint	[1 m <sup>2</sup> ]
FU2	Functional unit 2: 1 m length of edge connection	[1 m]
GC	Grooved connection	
GHG	Greenhouse gas	[CO <sub>2</sub> eq]
GLT / glulam	Glued-laminated timber	
GT	Groove-and-tongue connection	
GWP	Global warming potential	[kg CO <sub>2</sub> eq]
HL	Half-lap connection	
HTP	Human toxicity potential	[kg 1.4-DB eq]
LCA	Life cycle assessment	
MAETP	Marine aquatic ecotoxicity potential	[kg 1.4-DB eq]
MC	Moisture content	[%]

ODP	Ozone depletion potential	[kg CFC-11 eq]
POCP	Photochemical ozone creation potential	[kg C <sub>2</sub> H <sub>4</sub> eq]
PTS8160	Partial-thread self-tapping screw ( $\approx 8 \times 160$ mm)	
RC	Reinforced concrete	
SCLT	Standard/glued CLT (reference)	
SCMs	Supplementary cementitious materials	
STS	Self-tapping screws	
TS	T-shape connection	
TETP	Terrestrial ecotoxicity potential	[kg 1.4-DB eq]
VUSDFLD	ABAQUS user subroutine for field/failure checks	

<b>Symbols</b>		<b>Units</b>
a	Distance from support to load (four-point bending)	[mm]
b	Specimen width	[mm]
D	Dowel diameter	[mm]
$E_m$	Bending modulus	[GPa]
$E_X$	Young's moduli (longitudinal)	[MPa]
$E_Y$	Young's moduli (radial)	[MPa]
$E_Z$	Young's moduli (tangential)	[MPa]
$EI_{eff}$	Effective flexural rigidity including joint stiffness	[N·m <sup>2</sup> ]
F	Maximum applied load	[kN]
$G_{XY}$	Shear moduli in longitudinal–radial planes	[MPa]
$G_{XZ}$	Shear moduli in longitudinal–tangential planes	[MPa]
$G_{YZ}$	Shear moduli in radial–tangential planes	[MPa]
h	Specimen depth (thickness)	[mm]
K	Elastic stiffness matrix in FE constitutive relation	
L	Clear span (or dowel length, by context)	[mm]
$S_{1t}$	Longitudinal tensile strengths	[MPa]
$S_{2t}$	Radial/tangential tensile strengths	[MPa]
$S_{1c}$	Longitudinal compressive strengths	[MPa]
$S_{2c}$	Radial/tangential compressive strengths	[MPa]
$S_{12}$	Shear strengths in longitudinal–radial planes	[MPa]
$S_{13}$	Shear strengths in longitudinal–tangential planes	[MPa]
$S_{23}$	Shear strengths in radial–tangential planes	[MPa]
TB	Sectional thickness at mid-span	[mm]

$w$	Mid-span deflection	[mm]
$\varepsilon$	Strain vector	
$\mu$	Friction coefficient	
$\mu_{XY}$	Poisson's ratio in longitudinal–radial planes	
$\mu_{XZ}$	Poisson's ratio in longitudinal–tangential planes	
$\mu_{YZ}$	Poisson's ratio in radial–tangential planes	
$\rho$	Density	[kg/m <sup>3</sup> ]
$\sigma$	Stress vector	[MPa]



# Table of Contents

1.	Introduction .....	1
1.1.	Background .....	1
1.2.	Summary of literature review (Paper I).....	3
1.3.	Motivation .....	5
1.4.	Focus and scope .....	6
1.5.	Aims and research questions .....	7
1.6.	Thesis structure .....	8
2.	Material and methods .....	9
2.1.	FE modeling on CLT with edge connections (Papers II & III).....	9
2.1.1.	Numerical simulation and verification .....	9
2.1.2.	Material .....	13
2.1.3.	Panel and connection geometries .....	14
2.2.	Experiments on glulam with edge connections (Paper IV) .....	19
2.2.1.	Materials.....	19
2.2.2.	Fabrication and machining .....	21
2.2.3.	Experimental testing.....	21
2.2.4.	Data acquisition and analysis procedure .....	22
2.3.	LCA on slab systems and connections (Papers V & VI).....	23
2.3.1.	Functional units for structure type 1: CLT with edge connections.....	24
2.3.2.	Functional unit for structure type 2: Adhesive-free CLT .....	26
2.3.3.	System boundaries and included life cycle modules.....	28
2.3.4.	Inventory data and modeling assumptions .....	29
2.3.5.	Impact assessment method and impact categories .....	32
3.	Results and discussion.....	33
3.1.	Out-of-plane bending performance on CLT with edge connections (Papers II & III).....	33
3.1.1.	Verification of numerical framework (models 1, 2, 3).....	33
3.1.2.	Global behavior of six baseline connections .....	34
3.1.3.	Strain evolution and lamination effects.....	36
3.1.4.	Failure mode .....	37
3.1.5.	Parametric studies and performance within each type .....	39
3.1.6.	Design implications and scope.....	49

3.2.	Out-of-plane bending performance on glulam with edge connections (Paper IV) .....	49
3.2.1.	Load–displacement response .....	49
3.2.2.	Ductility .....	51
3.2.3.	Flexural properties (strength, modulus, effective stiffness) .....	51
3.2.4.	Rotation and moment resistance .....	52
3.2.5.	Failure modes and connection mechanics.....	52
3.2.6.	Design recommendations.....	55
3.3.	Comparisons between proposed timber connections and typical steel connection .....	56
3.3.1.	Results of verification model 4 .....	56
3.3.2.	Geometries of timber connections on 5-ply CLT panel.....	57
3.3.3.	Results of proposed timber connections .....	57
3.4.	Structure type 1: Environmental performance of edge connections and CLT with edge connections (Paper V) .....	59
3.4.1.	Scenario 1 (FU1: 1 m <sup>2</sup> slab including edge connection).....	59
3.4.2.	Scenario 2 (FU2: 1 m of connection; panels excluded).....	62
3.4.3.	Cross-scenario synthesis .....	65
3.4.4.	Implications for design and manufacturing .....	66
3.4.5.	Generalizability and limitations.....	66
3.4.6.	Conclusions and discussion .....	67
3.5.	Structure type 2: LCA on CLT, adhesive-free CLT, and RC slabs (Paper VI).....	67
3.5.1.	Whole-life performance across ten CML indicators.....	68
3.5.2.	Phase-resolved contributions and controlling mechanisms.....	68
3.5.3.	Geographic electricity scenarios .....	71
3.5.4.	Practical implications for designers and policy makers.....	72
3.6.	Uncertainty considerations in LCA results .....	73
3.7.	Limitations .....	74
4.	Conclusions and future work .....	76
4.1.	Conclusions .....	76
4.1.1.	Structural performance .....	76
4.1.2.	Environmental performance .....	78
4.1.3.	Reflections and summary.....	79
4.2.	Future work.....	80
	References.....	82

# 1. Introduction

This Chapter offers the following contents: (1) background, (2) focus and scope, (3) motivation, (4) research objectives and questions, (5) limitations, and (6) thesis structure.

## 1.1. Background

The buildings and construction sector accounts for roughly 40% of final global energy use and greenhouse gas (GHG) emissions, making material choices a primary lever for decarbonization (International Energy Agency. & Global Alliance for Buildings and Construction., 2019). Against this backdrop, mass-timber systems (and cross-laminated timber (CLT) in particular) have gained prominence as low-carbon, high-performance alternatives to conventional concrete and steel. Over the past decade, CLT research output and market adoption have expanded rapidly in Europe and beyond, reflecting both regulatory interest and industry uptake (Kurzinski et al., 2022; Younis & Dodoo, 2022). The emergence of tall-timber exemplars (e.g., Ascent, Mjøstårnet, HoHo) has further demonstrated the feasibility of CLT in mid-to high-rise applications, signaling a broader transition toward industrialized, low-emission building systems.

CLT is an engineered wood product (EWP) formed by laminating dimensional boards in alternating, mostly perpendicular orientations. This cross-lamination produces plate-like elements with two-way action, a high stiffness-to-weight ratio, and superior dimensional stability (CEN. EN 16351, 2021; Swedish Wood, 2022). Beyond structural efficiency, CLT offers advantages in pre-fabrication, erection speed, thermal performance, and predictable fire behavior via charring. Furthermore, timber is an environmentally friendly material due to its ability to store biogenic carbon during service life, and case studies in Sweden indicate that substituting timber for reinforced concrete (RC) can reduce structure mass by up to ~86% and foundation reactions by ~31% while meeting deflection, fire, and acoustic criteria (Bahrami et al., 2021, 2022). These attributes position CLT as a material system capable of delivering both structural performance and carbon benefits across multiple building typologies (Australian Bureau of Agricultural and Resource Economics and Sciences, 2017; Forest Service & Products Laboratory, 2010; Liu et al., 2016; Ramage et al., 2017).

As CLT adoption scales, connection systems emerge as decisive for safety, serviceability, and robustness. Because CLT is panelized for transport and manufacturing efficiency, floors and walls are assembled from multiple elements whose global behavior is governed by the joints that link them. In floor diaphragms and continuous slabs, edge connections (which join adjacent panels along their longitudinal edges) control shear transfer, limit separation,

manage rotation, and help distribute localized stresses under gravity, wind, and seismic actions. Their detailing therefore affects stiffness, ductility, energy dissipation, durability under hygro-thermal cycling, and ultimately the life cycle performance and longevity of CLT buildings.

A wide spectrum of edge-connection strategies is used in practice and research: glued butt-joints and splines; mechanical fasteners (screws, nails, bolts, dowels); interlocking profiles (e.g., tongue-and-groove, timber splines); and hybrids combining adhesives with mechanical reinforcement. Steel and adhesive-based solutions often deliver high initial stiffness and strength, but reported behaviors include brittle or low-ductility responses and early cracking in certain assemblies, particularly when connectors concentrate shear in cross layers. Moreover, the environmental burdens and indoor-air implications of some adhesives (e.g., formaldehyde-emitting chemistries) are increasingly scrutinized: Life cycle studies attribute roughly one-third of CLT's global warming potential (GWP) and energy demand to adhesives across cradle-to-grave scopes (Adhikari & Ozarska, 2018; Hemmilä et al., 2017; Puettmann et al., 2019b). These concerns motivate intensified interest in adhesive-free, timber-to-timber methods that leverage mechanical interlock and friction.

Recent advances in computer-numerical-control (CNC) fabrication have revived and industrialized carpentry-type joints at the building scale (Kurzynski et al., 2022), e.g., dovetails, tongues and grooves, depressed plates, and compressed-wood (CW) dowels and plates. Experimental and numerical studies indicate that densified-wood connectors can approach or replace steel or glued joints in selected configurations while enhancing recyclability and end-of-life (EOL) options (Mehra et al., 2022; Tétreault et al., 2023). At the same time, results also show geometry- and placement-sensitive behaviors: for example, vertical dowels or interlocks in cross layers may shift demand to rolling-shear or delamination-prone interfaces, and certain hybrid layouts can trade stiffness for ductility depending on fastener angles and spacing (e.g., mixed-angle hold-downs). Collectively, these findings suggest a promising yet nuanced design space in which connector form, material, and position must be tuned to engage the outer lamellae effectively, manage interlaminar stresses, and ensure rotation restraint while remaining compatible with fabrication tolerances and assembly sequencing.

While the structural performance of CLT connections has been broadly investigated, environmental assessments of connection systems remain comparatively sparse (Younis & Doodoo, 2022). Many life cycle assessments (LCAs) consider whole buildings or slabs, often aggregating connectors or treating them as secondary contributors (Kellenberger & Althaus, 2009; Kraenzlein et al., 2026). Yet emerging evidence indicates that connectors can contribute materially to energy demand as well as other indicators in load-bearing timber assemblies, and that choices among adhesives, metals, and all-timber fasteners can shift impact profiles across categories (e.g., GWP, Abiotic Depletion - ADP, Human Toxicity - HTP) (Lukić et al., 2021; Puettmann et al., 2019a). Accordingly, the key gap is the lack of consistent, component-level comparisons that determine impact differences between edge-connection concepts (especially adhesive-free all-wood variants) under the same functional units,

system boundaries, and lifespan assumptions. This gap constrains designers seeking to align structural performance with carbon and toxicity targets under evolving policy frameworks while supporting the transition from conventional concrete- and steel-based solutions toward more sustainable timber systems.

Concurrently, standardization for timber-fastened CLT and glued-laminated timber (glulam/GLT) edge joints remains limited. Eurocode 5 (CEN. EN, 2004) provides robust foundations for timber design, but dedicated guidance for wood-element connectors in panel-to-panel joints is still developing, especially for new carpentry-type and densified-wood solutions. As a result, design practice must often extrapolate from member- or fastener-level rules or rely on project-specific testing and modeling to establish stiffness, strength, and ductility parameters at the system level. Addressing this shortfall requires integrated programs that pair validated structural models and experiments with life cycle inventory datasets and impact assessments, situating connection choices within both structural and environmental performance envelopes.

Based on this context, the present thesis positions CLT edge connections as an interface where structural behavior and environmental performance intersect, focusing on investigating adhesive-free, all-timber concepts alongside conventional solutions (evaluating them under consistent structural demands and life cycle scopes).

## **1.2. Summary of literature review (Paper I)**

Over the past decade, research on CLT has developed rapidly, including areas such as panel structures, connection techniques, and environmental performance (Erol & Brad, 2013; Ren et al., 2024a). Therefore, paper I conducted a systematic literature study based on these three topics among CLT products in order to reveal and summarize the key findings, needs, and research gaps.

From a structural perspective, CLT connection studies can be grouped by interaction: base-to-wall, panel-to-panel splicing, and CLT-concrete composite connections. Base-to-wall systems (e.g. hold-downs and angle brackets) are decisive for lateral resistance and uplift force, where experimental outcome shows that axial-shear interaction can occur in hold-downs under drift demands, and this interaction may not be reflected by simplified design assumptions (Pozza et al., 2018). Research has also shown that detailed parameters such as end distance, spacing, and fastener arrangement influence not only strength but also deformation capacity and damage localization. (Brown & Li, 2021; J. Chen et al., 2022). This emphasizes the need for connection designs with improved ductility mechanisms and stable hysteresis instead of brittle failure. For panel-to-panel splicing in floors, conventional solutions based on steel screws, plates, and splines remain common due to their reliability and ease of design, but they may concentrate stresses in the cross layers and can limit circular EOL options when the goal is dismantling or reuse. Composite CLT-concrete floors have also been studied to improve stiffness and vibration response. Recent work emphasizes demountable shear connections to balance composite action with disassembly and material separation at EOL (Eslami et al., 2024).

In the connection literature, a clear trend is the development of timber-based and adhesive-free connection strategies that aim to reduce metal content and avoid the use of petrochemical adhesives while maintaining competitive structural performance. Development in CNC fabrication has enabled building-scale carpentry-type connections and interlocking profiles (e.g., tongue-and-groove and dovetail-inspired forms) (Ilgin et al., 2025; Larsson et al., 2020; Z. Li et al., 2021; Rogeau et al., 2021), expanding the design potential beyond the limitations of traditional fasteners. Meanwhile, the use of CW for dowels and slabs has been investigated due to its higher density and embedment resistance that led to favorable load transfer while preserving recyclability and reusability (Conway et al., 2021; Mehra et al., 2018; Xu et al., 2023). However, the literature also emphasize that performance is sensitive to geometry and placement: certain interlocks and dowel layouts may shift demand to cross-layer rolling shear (RS) or delamination interfaces, which means that connector concepts must be adapted to join outer lamellae effectively and to control interlayer stress rather than only increasing connector strength.

In CLT, RS is also one of the most important topics because it often determines the failure of floor panels in out-of-plane bending, where transverse layers are subjected to shear along planes perpendicular to the grain direction. RS strength and stiffness are sensitive to wood species, defects, lamination configuration, moisture content, and manufacturing quality, but they are also highly dependent on the test method and interpretation procedure. The literature employs various experimental methods, including short-span bending and planar shear variants. Comparative studies show that RS parameters derived from different methods are not always directly comparable, which complicates design calibration and numerical verification across studies (M. Li et al., 2019; Nero et al., 2022). Standards provide frameworks for the CLT requirements and test methods, but methodological diversity still exists in research and product development (American National Standards Institutes (ANSI), 2018; ASTM D2718, 2000; British Standards Institution, 2004; CEN. EN 16351, 2021). This challenge is particularly important for FE modeling because RS modulus and strength affect predicted stiffness, crack initiation, and ultimate failure modes. Multi-scale and cohesive-zone methods have been proposed to represent RS-driven damage, but they require further validation on consistent experimental datasets (Flores et al., 2016).

The environmental assessment literature (especially LCA) generally reports that CLT solutions can reduce embodied global warming impacts compared with conventional RC alternatives. However, the conclusions can vary significantly depending on the system boundary definition, electricity mix, transport assumptions, biogenic carbon accounting, and EOL scenarios (Andersen et al., 2022; Younis & Dodoo, 2022). Comparative building LCAs indicate that mass-timber structures may have lower embodied impacts. However, the assessment results also show that the choice of carbon storage methods and storage time can change the magnitude of reported benefits (Andersen et al., 2022; Z. Chen et al., 2020). Component-level comparisons further emphasize that ‘equivalent structural performance’ (strength, stiffness, fire/acoustic constraints, and span requirements) is necessary for benchmarking of timber and

concrete slabs (Oh et al., 2023). Case studies also highlight that impacts outside the CLT superstructure (e.g., foundations and cement-intensive groundworks) can dominate the total footprint, emphasizing the need for transparent scope definition when interpreting results (Nakano et al., 2020).

Paper I indicates that: (i) connection technologies are linked to achieving continuous CLT slab behavior and reliable ductility, (ii) RS remains a major and method-sensitive failure mechanism requiring further parameterization and validation, and (iii) the environmental impacts of alternative connection methods have not been systematically quantified under consistent scenario. These gaps motivate this thesis to adopt a comprehensive approach, where adhesive-free edge connections are evaluated through combined experiments, FE modeling, and LCA, aiming to connect mechanical performance with life cycle impacts under unified assumptions.

### **1.3. Motivation**

Reducing the climate impact of buildings requires structural systems that deliver high performance while minimizing life cycle burdens and increasing recyclability (Global Alliance for Buildings and Construction, 2024). While CLT is competitive in terms of quality, construction speed, and biocarbon storage, overall performance in precast slabs depends on the edge connections that link the individual slabs into a system. Many widely used designs in the market rely on numerous steel fasteners and adhesives embedded in multiple interfaces (MIT Climate Portal Writing Team, 2023). Although these properties are robust and durable, they also introduce environmental impacts, increase dismantling difficulty, and may limit the reuse potential of components.

Adhesive-free wood connectors offer a promising alternative. By designing their geometry to effectively connect the panel's edge, couple the tension and compression zones, and avoiding negative mechanisms, high stiffness and load-bearing capacity can be achieved without relying on traditional solutions like steel or adhesives. Beyond structural performance, these design details align with circular economy goals, enabling dry assembly, convenient inspection, and the reuse or replacement of components, thereby extending service life and reducing the overall environmental impact throughout the life cycle (Mehra et al., 2022).

From a practical perspective, designers face two interconnected challenges. First, there is a lack of comprehensive evidence regarding how specific geometric choices at edge connections (such as tongue thickness, lap length, rib angles, and pin locations) translate into predictable floor slab bending moment-rotation response and system-level stiffness (Ljunggren et al., 2025). Secondly, environmental impact assessments often stop at the panel level, failing to differentiate between different connection methods, while factors such as fasteners, adhesives, manufacturing processes, and EOL disposal methods can substantially change the final impact (Atnoorkar et al., 2023; Younis & Dodoo, 2022). Bridging these gaps requires systematic development, validation, and comparison of various connection methods.

The motivation for this thesis is therefore twofold: to improve the structural performance and predictability of CLT edge connections (especially adhesive-free concepts that enable reversible assembly) and to couple those gains with LCA results so that connection choices can be justified in both engineering and environmental fields. Consequently, the work supports climate-aligned timber construction and provides a clearer basis for specifications, designs, and future code development.

#### **1.4. Focus and scope**

This thesis examines the CLT slab system as a structural system while considering its life cycle environmental impacts with an emphasis on the structural performance and environmental performance of panel edge connections for slab applications. The structural part of this thesis developed and evaluated a series of adhesive-free timber-based joints alongside conventional references. It spans the full process from concept geometry and material selection, through finite element (FE) modeling and parameter studies, to laboratory tests under four-point bending. Particular attention is paid to how the connection engages each lamella, how load is transferred across the joint line, and how these features affect stiffness, strength, ductility, and failure modes at both joint and system levels.

The environmental part of this thesis quantified environmental impact over the life cycle of a slab system, comparing CLT with proposed edge connections, CLT with metallic connections, standard CLT (SCLT - with lamination adhesive), adhesive-free CLT (AFCLT) variants, and an RC reference under harmonized functional units, system boundaries, and scenarios. It focuses on carbon-related indicators while retaining a broader set of midpoint categories to reveal potential impact shifting between categories across phases A1–A3 (product stage), A4–A5 (construction), B (use/maintenance where applicable), C (EOL), and D (beyond the system). The LCA is designed to be decision-oriented: it keeps inventory datasets, assumptions, and scenarios transparent so that designers can adapt the results to their own projects.

This study is intentionally structured to integrate these components. It begins by analyzing the structural performance of the prototype connections, then applies this to LCA while maintaining consistent geometry, material composition, and transport/processing assumptions. This allows for comparisons (e.g., comparing all-wood connections with connections utilizing steel) not only in terms of load-bearing capacity or stiffness, but also in terms of implicit effects and end-of-life behavior. While the primary application is out-of-plane floor bending, the findings are also applicable to diaphragm effects and other edge connections that determine the overall response of plate members. In addition, this thesis explores adhesive-free solutions under practical construction constraints, including prefabrication and reusability.

## 1.5. Aims and research questions

The work aims to clarify how connection architecture, material selection, and fabrication strategy co-determine capacity, stiffness, ductility, and environmental burdens. Consequently, it contributes to the development of mass-timber systems that are not only strong and serviceable, but also materially efficient and climate-aligned across their life cycles. By combining validated structural principles with consistent life cycle models, the main objective of this research is to provide the results that should be able to be used in evidence-based guidance (based on CLT edge-connection design) for designers and researchers to help them determine in which aspects connection designs deliver the greatest structural gains and the most significant environmental benefits. This objective is pursued through five specific objectives:

1. Review the state-of-the-art to identify research gaps and design a set of adhesive-free timber edge-connection concepts for CLT/GLT slab systems.
2. Develop and apply an FE modeling framework to analyze the structural response and the influence of key parameters (stiffness, capacity, failure modes) of the proposed connections for CLT panels subjected to out-of-plane bending.
3. Conduct experimental testing of the proposed connections for GLT panels under the out-of-plane bending to validate the FE results.
4. Quantify the cradle-to-cradle life cycle impacts of CLT slabs with the proposed edge connections under unified assumptions.
5. Evaluate the cradle-to-cradle life cycle impacts of adhesive-free CLT variants (without connectors) and compare them with conventional CLT and RC reference systems.

These objectives are operationalized through the following research questions and corresponding papers (Figure 1).

RQ1: How can edge connections for CLT panels be designed and analyzed to achieve adjustable and high-performance CLT slab systems?

RQ2: How can adhesive-free connections for GLT panels be designed, and what are the key influencing design factors?

RQ3: How can LCA be used to compare different connection design solutions for CLT building systems (e.g., wood species, adhesive type)?

RQ4: How can the environmental impacts of CLT building systems be reduced and evaluated from a life cycle perspective by using LCA?

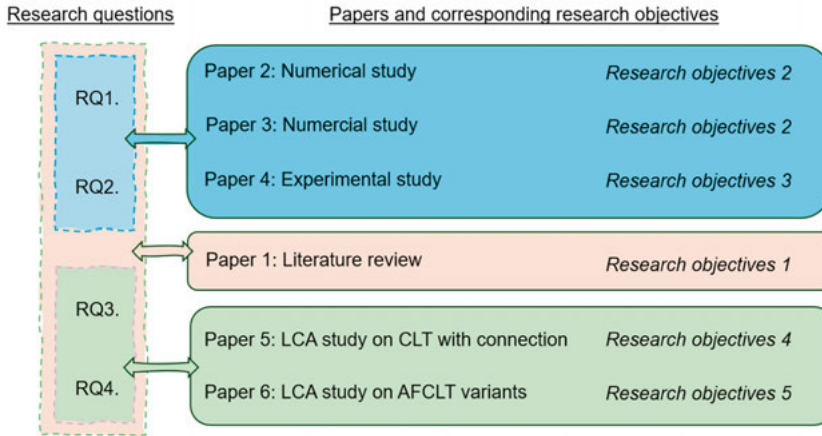


Figure 1 Research questions and corresponding papers.

## 1.6. Thesis structure

The thesis is organized to present the cover essay while investigating EWP slab system with edge connections:

- Chapter 1 introduces the context, literature review, motivation, objectives, questions, and structure.
- Chapter 2 details materials and methods: the FE framework and connection geometries for CLT edge joints; the experimental program on glulam with adhesive-free connections; and the LCA goal and scope definition, functional unit, system boundaries, inventory datasets, and impact assessment.
- Chapter 3 presents and discusses results. Sections 3.1 and 3.2 report the numerical and experimental structural performance of CLT/glulam connections (Papers II–IV). Sections 3.3 and 3.4 evaluate life cycle performance of slabs and connections across indicators and stages (Papers V–VI).
- Chapter 4 concludes and outlines future work.

## 2. Material and methods

Based on the study aims and objectives, this Chapter illustrates the corresponding investigation methodology, materials, test design, procedures, and the boundary conditions. In total, three types of studies were implemented: (1) numerical study on the CLT slab with timber edge connections, (2) experimental study on the glulam with timber edge connections, and (3) LCA study on timber connections, steel connection, CLT slabs, and RC slab.

### 2.1. FE modeling on CLT with edge connections (Papers II & III)

Papers II and III developed and evaluated six adhesive-free edge connections for CLT floor-scale panels using a validated FE framework in ABAQUS. This Section describes the applied methodologies, materials, and assumptions.

#### 2.1.1. Numerical simulation and verification

In this study, timber is treated as a 3D orthotropic composite (Mirianon et al., 2008). Strength and failure are evaluated with a quadratic, stress-based composite criterion (Sitnikova et al., 2014) (Hashin-type (Hashin, 1980)) implemented via a VUSDFLD user subroutine. The workflow is:

- (i) Build and verify FE models according to three external experimental tests (GLT slabs with CW plates/dowels (Mehra et al., 2021); AF-CLT panels reinforced with vertical CW dowels (Sotayo, Bradley, Bather, Oudjene, et al., 2020)); and CLT panels connected by steel connectors (Zhang & Chui, 2020).
- (ii) Define panel and connection geometries based on verified properties.
- (iii) Apply a four-point bending configuration consistent with EN 16351 (CEN. EN 16351, 2021) and Eurocode 5 (CEN. EN, 2004).
- (iv) Perform parametric studies for each connection family.  
Extract global and local responses (load-displacement; nine-point strain field) to interpret stiffness, capacity, and failure localization.

This approach ensures that the connection concepts are assessed under identical boundary conditions and measurement protocols, and that the model's constitutive and failure assumptions are validated by laboratory studies before being used in design exploration. The constitutive relation of studied timber is:

$$\sigma = C \cdot \varepsilon \quad (1)$$

where,

$C$ : elastic stiffness,

$\varepsilon$ : strain vector,

$\sigma$ : stress vector.

The stress vector is illustrated as:

$$\sigma = \begin{bmatrix} \sigma_{11} \\ \sigma_{22} \\ \sigma_{33} \\ \sigma_{12} \\ \sigma_{23} \\ \sigma_{31} \end{bmatrix} \quad (2)$$

Principal material axes align with fiber (longitudinal), radial, and tangential directions in each part. This allows direction-dependent stiffness and shear coupling to be evaluated consistently in the 3D stress state at each increment. A quadratic, stress-based composite criterion evaluates tensile–shear and compressive failures in longitudinal and tangential directions, with shear interaction terms (Gama & Gillespie, 2011; Hashin, 1980; Sitnikova et al., 2014). The four checks are (using directional tension and compression strengths  $S_{1t}$ ,  $S_{2t}$ ,  $S_{1c}$ ,  $S_{2c}$  and shears  $S_{12}$ ,  $S_{23}$ ,  $S_{31}$ ):

- Longitudinal tensile-shear:

$$f_{1t} = \left(\frac{\sigma_{11}}{S_{1t}}\right)^2 + \left(\frac{\sigma_{12}}{S_{12}}\right)^2 + \left(\frac{\sigma_{31}}{S_{31}}\right)^2 - 1 = 0 \quad \sigma_{11} > 0 \quad (3)$$

- Tangential tensile-shear:

$$f_{2t} = \left(\frac{\sigma_{22}}{S_{2t}}\right)^2 + \left(\frac{\sigma_{12}}{S_{12}}\right)^2 + \left(\frac{\sigma_{23}}{S_{23}}\right)^2 - 1 = 0 \quad \sigma_{22} > 0 \quad (4)$$

- Longitudinal compression:

$$f_{1c} = \left(\frac{\sigma_{11}}{S_{1c}}\right)^2 - 1 = 0 \quad \sigma_{11} < 0 \quad (5)$$

- Tangential compression:

$$f_{2c} = \left(\frac{\sigma_{22}}{S_{2c}}\right)^2 - 1 = 0 \quad \sigma_{22} < 0 \quad (6)$$

The model assumes instantaneous failure when any criterion reaches unity (i.e., no progressive damage evolution). The checks and strength sets are coded in VUSDFLD, called at each integration point, enabling direct use of tabulated strengths for standard wood and CW during the analysis and post-processing. All timber–CW and timber–timber mating faces use frictional contact with  $\mu = 0.3$  (applied to all deformable components' surfaces). In verification models that include glued internal laminations, cohesive behavior and damage properties are defined on each glued surface with zero thickness and the stiffness/damage parameters listed in Section 2.1.2. These interface settings are held constant across the verification and connection analyses.

### **Verification models 1 & 2: GLT beam-to-beam with CW plates/dowels**

Based on the verification models 1 and 2, two GLT beams ( $130 \times 160$  mm; total length 3160 mm; support span 2880 mm) are joined at their ends with external CW plates/dowels and tested in four-point bending (Figure 2 (a)) (Mehra et al., 2021). The connections are BB-8-20 (four CW plates with 20 mm thickness, sixteen dowels) and BB-6-20 (same geometry with 10 mm-thick CW plates, twelve dowels). The FE model reproduces beams, CW plates, and dowels; standard wood is Douglas fir ( $\rho = 570 \text{ kg/m}^3$ ), and CW is Scots pine densified 54% to  $1285 \text{ kg/m}^3$ . In the tests, the simulation of glued interfaces employed the same coefficient of friction ( $\mu = 0.3$ ) and cohesive parameters as those from Section 2.1.2. Moreover, gaps in experimental data are supplemented using information from literature on the same materials.

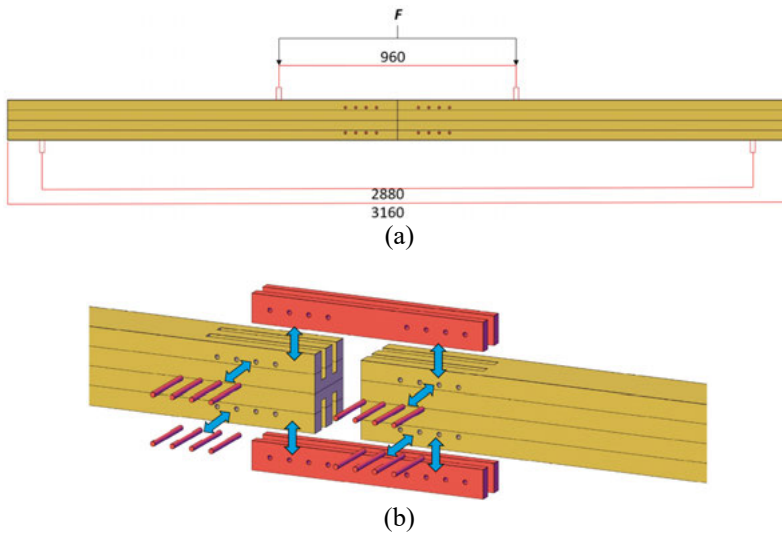


Figure 2 Geometries of verification models 1 & 2, (a) front view under loading and (b) CW connection's detail. (unit in mm)

### **Verification model 3: AF-CLT panel with vertical CW dowels**

In verification model 3 (Figure 3), three-layer AF-CLT panels (lamella thickness 20 mm) with  $\text{Ø}10 \times 60$  mm vertical CW dowels are tested under four-point bending (support span 1440 mm, load spacing 960 mm) (Sotayo, Bradley, Bather, Oudjene, et al., 2020). Analyses were performed in ABAQUS 2022 using 3D continuum elements (C3D8R). A convergence study led to a uniform 10 mm mesh ( $\approx 94\,920$  elements for the validation model). Furthermore, quasi-static loading was enforced with a minimum time increment of  $5 \times 10^{-6}$ . These simulation settings were also applied to verification models 1 and 2.

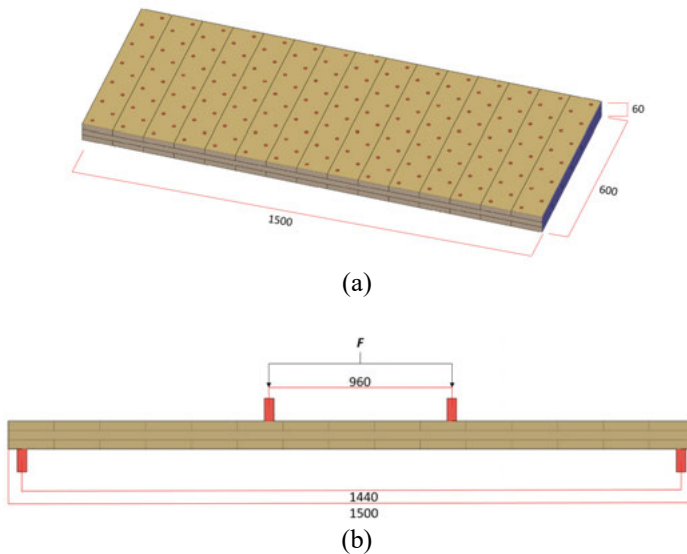


Figure 3 Geometries of verification model 3, (a) overview of AF-CLT and (b) under loading view. (unit in mm)

***Verification model 4: CLT panel with steel connection***

Verification model 4 (Figure 4) was considered to include a commonly used steel connection for CLT floor slabs in the market in order to compare its structural performance with self-developed timber connections. The double surface spline (DSS) connection was chosen which has been experimentally tested by Zhang & Cui (Zhang & Chui, 2020). In the numerical model, the specimen DSS-6160- 8/150- 19W was chosen to be numerically verified. In this specimen, the connected 5-ply CLT panel (spruce-pine-fir) had dimensions of 1600 mm × 400 mm × 175 mm (length/width/thickness), which was connected at the mid-span with two plywood splines (130 mm × 400 mm × 19 mm - length/width/thickness) and eight self-tapping steel screws (PTS6160, Ø6 × 160 mm).

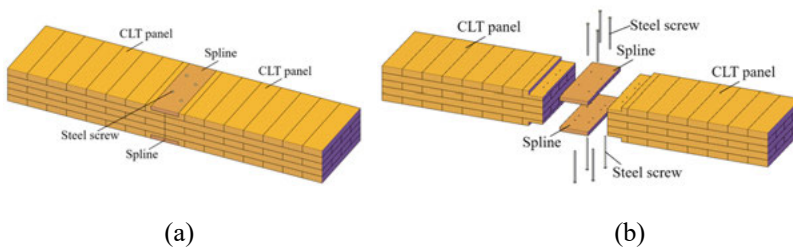


Figure 4 Geometries of verification model 4, (a) connected and (b) assembly description.

### 2.1.2. Material

Verification models mirrored the species and densities used in the experimental tests: Douglas fir ( $\rho = 570 \text{ kg/m}^3$ ) for the GLT beam-to-beam verification dowels (Mehra et al., 2021); Scots pine ( $\rho = 556 \text{ kg/m}^3$ ) for the AF-CLT panel verification (Sotayo, Bradley, Bather, Oudjene, et al., 2020); and Spruce-pine-fir ( $\rho = 450 \text{ kg/m}^3$ ) for the 5-ply CLT (Zhang & Chui, 2020). Additionally, directional elastic constants (Young's modulus  $E_x$ ,  $E_y$ , and  $E_z$ ; shear modulus  $G_{xy}$ ,  $G_{xz}$ , and  $G_{yz}$ ) and Poisson's ratios ( $\mu_{xy}$ ,  $\mu_{xz}$ , and  $\mu_{yz}$ ) were extracted from literature with experiments under similar conditions; where test programs lacked complete orthotropic sets, values were compiled from similar studies of the same materials. Furthermore, the resulting properties used for verification models are summarized in Table 1. In all subsequent connection studies, these orthotropic properties define the lamellae of the CLT panels and connectors. The assignments reflect the principal material axes (longitudinal, radial, tangential) and are used consistently across meshes and boundary conditions to enable comparison between connection families.

Table 1 Directional elastic constants and Poisson's ratios of verification models 1, 2, and 3.

Element	Young's Modulus (MPa)			Shear Modulus (MPa)			Poisson's Ratio		
	$E_x$	$E_y$	$E_z$	$G_{xy}$	$G_{xz}$	$G_{yz}$	$\mu_{xy}$	$\mu_{xz}$	$\mu_{yz}$
Standard wood – verification of numerical models 1 and 2 (Kretschmann, 2010; Yvonne, 2007)	1519 0	779	1062	784	643	116	0.44 9	0.29 2	0.37 4
CW – verification of numerical models 1 and 2 (Anshari et al., 2011)	3285 8	5061	3111	5717	1590	878	0.51	0.33	0.4
Standard wood – verification of numerical model 3 (Kretschmann, 2010)	8000	286. 3	286. 3	536. 8	536. 8	70	0.76 6	0.41 4	0.57 8
CW – verification of numerical model 3 (Dan et al., n.d.)	3151 0	2622	5152	2438	1058	3703	0.76 6	0.41 4	0.57 8
SPF - verification of numerical model 4 (American Wood Council, 2018; Kretschmann, 2010)	5516	430	209	270	253	16.6	0.34 1	0.32 2	0.43 7
Plywood - verification of numerical model 4 (Swedish Wood, 2022; Wang et al., 2022)	500	500	553	220	7.3	7.3	0.04	0.44	0.43

In addition, CW is used as a high-stiffness, high-strength, all-timber connector material. For the GLT verification, Scots pine dowels were radially

compressed by 54% to a final density of 1285 kg/m<sup>3</sup>. For the AF-CLT verification, beech dowels were hot-pressed at 130 °C to ≈1300 kg/m<sup>3</sup>. Moreover, strengths for CW vs. uncompressed wood were determined via reported correlations, enabling definition of the seven strength components required by the failure checks ( $S_{1t}$ ,  $S_{2t}$ ,  $S_{1c}$ ,  $S_{2c}$ ,  $S_{12}$ ,  $S_{13}$ , and  $S_{23}$ ). In addition, uncompressed Plywood ( $\rho = 350 \text{ kg/m}^3$ ) was used for verification model 4. The strength components values used in all verification models are summarized in Table 2. Within the proposed connection families, all external connectors (belts, T-inserts, grooved plates, etc.) are modeled as CW, with geometric details and placements given in Section 2.1.3.

Table 2 Strength components of verification models 1, 2, and 3.

Element	Strength Component (MPa)						
	$S_{1t}$	$S_{2t}$	$S_{1c}$	$S_{2c}$	$S_{12}$	$S_{13}$	$S_{23}$
Standard wood – verification of numerical models 1 and 2 (Yvonne, 2007)	123.1	2.7	51.9	5.1	5.4	7.5	9
CW – verification of numerical models 1 and 2 (Dan et al., n.d.)	250	10	112	17	9.9	13.5	15.3
Standard wood – verification of numerical model 3 ( European Scots Pine Wood, n.d.; Sotayo, Bradley, Bather, Sareh, et al., 2020)	102	2.9	54	7.5	4.7	4.7	1.1
CW – verification of numerical model 3 (Dan et al., n.d.; Gao et al., 2016)	299	8.05	105.8	18.2	25	18	28
SPF – verification of numerical model 4 (Akter et al., 2025; Kulak et al., 2023; Larsen & Munch-Andersen, 2011; Swedish Wood SWEDISH WOOD, n.d.)	104	2.9	59.8	5.19	10	10	4.61
Plywood – verification of numerical model 4 (Group, 2002)	45.8	29.2	34.8	26.5	9.5	3.2	2.46

On the other hand, two interface types are used. First, friction with  $\mu=0.3$  was applied to all timber/CW mating surfaces (based on Scots pine data); this governs sliding at interlocks and contact faces in both verification and connection models. Secondly, for verification cases that include glued internal laminations, cohesive traction–separation laws are assigned with  $K_{nn} = K_{ss} = K_{tt} = 10^5 \text{ N/mm}^3$ ,  $t_{nn} = t_{ss} = t_{tt} = 100 \text{ N/mm}^2$  (Dadej & Surowska, 2016), and fracture energy was 1.7 N/mm (Dadej & Surowska, 2016), with zero glue thickness. These values follow the sources cited in the paper and are held constant across the CLT/glulam verifications.

### 2.1.3. Panel and connection geometries

This Section provides the geometry of self-developed timber connections and the corresponding CLT panels for numerical testing (four-point out-of-plane bending). Additionally, the lumbers of CLT were assumed as Scot Pine, and the connectors were made of compressed Beech. The material properties were taken from the verification models.

Two identical CLT panels are joined along a longitudinal edge and subjected to four-point bending. Supports are 2310 mm apart; two equal top loads are applied with 480 mm spacing (Figure 5). Furthermore, the global mid-span displacement is taken at the intersection of the mid-span axis and the bottom surface. Nine strain points (P1–P9) are defined on the top, side, and bottom surfaces along the mid-span axis (Figure 5 (b)-(c)), enabling simultaneous tracking of compression, tension, and interlaminar effects. Moreover, this geometry/load set complies with EN 16351 and Eurocode 5 (CEN. EN, 2004; CEN. EN 16351, 2021) conventions for timber plate bending, allowing interpretation of stiffness and capacity within a recognized testing framework.

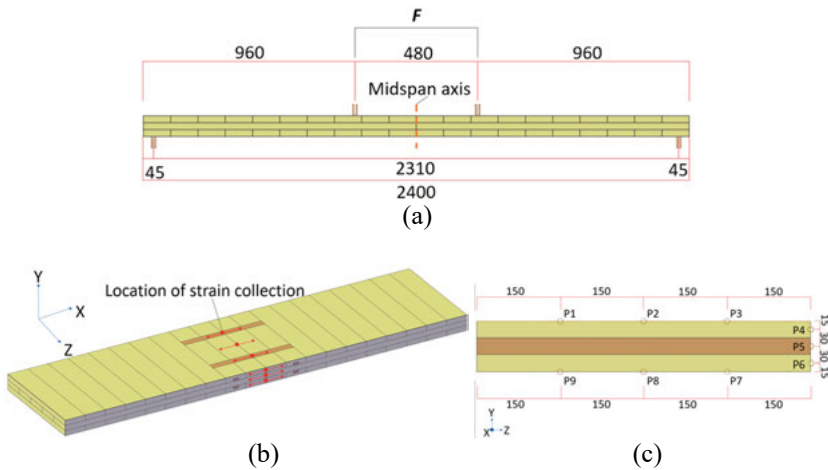


Figure 5 Loading setup and measurement placement, (a) connected CLT under four-point bending test, (b) placements of strain's collection points, and (c) geometry of 9 points for strain collection in section view (all dimensions are in mm).

Moreover, the geometries and assembly details of the studied six adhesive-free edge connections are illustrated as follows. The Belt connection (BC) uses eight CW elements per joint: four dovetail-section boards ( $480 \times 40 \times 100 \times 30$  mm: length  $\times$  min width  $\times$  max width  $\times$  thickness, each with a  $30 \times 15$  mm locking opening cut 45 mm from each end) and four rectangular locking boards ( $600 \times 30 \times 15$  mm). Assembly positions locking boards in lamellae layers 1 and 3, with dovetails inserted longitudinally so that half their length seats in each panel (Figure 6). The FE discretization for the baseline BC model uses  $\approx 43816$  solid elements.

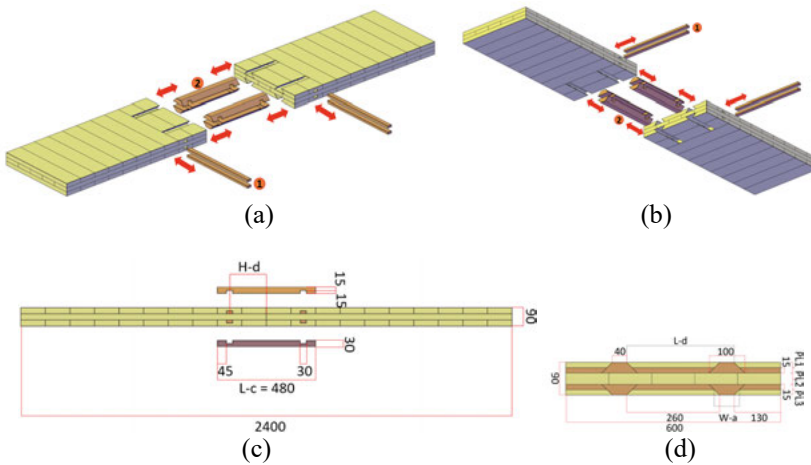
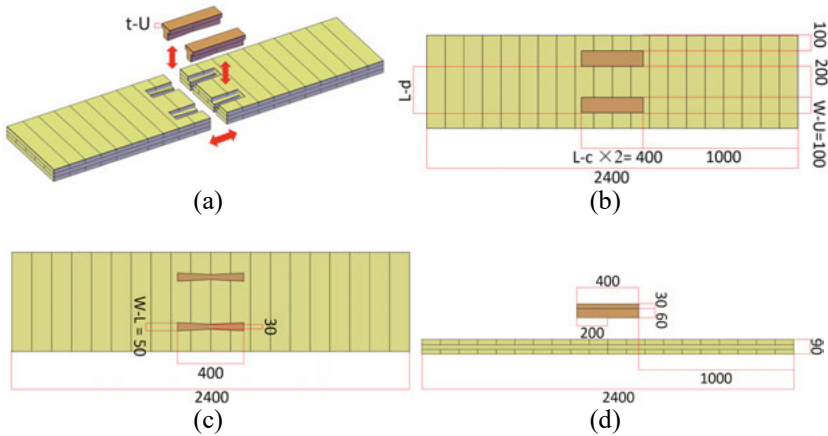
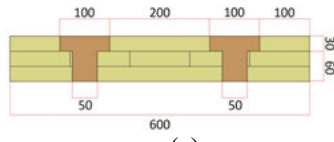


Figure 6 Overview of BC connection, (a) top view before assembly, (b) bottom view before assembly, (c) front view, and (d) section view at mid-span. (unit in mm)

Based on the T-shaped (TS) connection (Figure 7), it consists of two identical T-shaped CW inserts installed from the top surface (web first, then flange). Baseline dimensions: web  $400 \times 50 \times 60$  mm (length  $\times$  width  $\times$  thickness), flange  $400 \times 100 \times 30$  mm, with the insert thickness 90 mm matching the panel thickness. The two TS-inserts run parallel to the panel length with their mid-span axes aligned with the joint mid-span; lateral spacing between insert webs is 200 mm, each 100 mm from a side edge. FE discretization for the TS baseline uses  $\approx 41012$  elements.





(e)

Figure 7 Illustrations of TS connection, (a) 3D view, (b) top view, (c) bottom view, (d) front view, and (e) section view at mid-span. (unit in mm)

In the Groove-and-Tongue (GT) connection, it cuts a tongue in one panel and a groove in the other, both confined to the second (transverse) lamella, with non-flat mating surfaces to enhance interlock (Figure 8). The tongue panel is inserted into the grooved panel along the z-axis; the assembly is analogous to the BC connection (position/fix one panel, then insert the other from the side). Additionally, the GT's FE model employs  $\approx 78388$  elements.

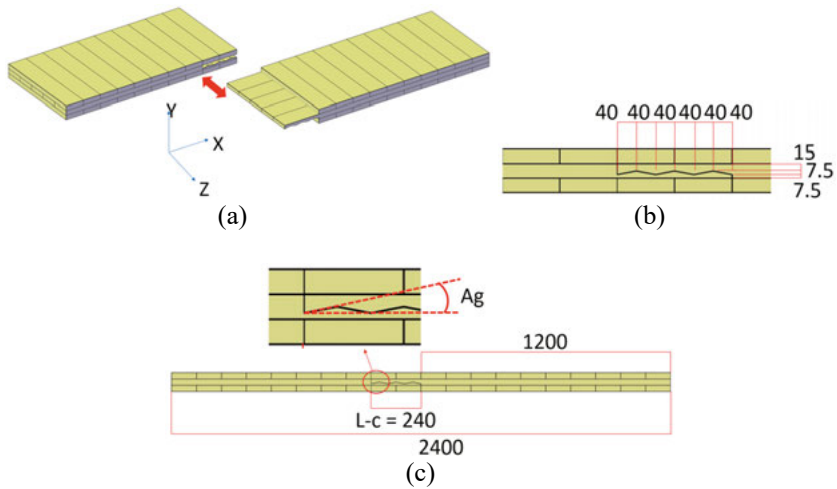


Figure 8 Geometries of GT connection, (a) 3D view, (b) dimensions of GT connection, and (c) front view. (unit in mm)

Moreover, the Grooved (GC) connection uses a single external CW plate seated in grooves machined into the second lamella of both panels; the plate spans the joint width ( $480 \times 600$  mm, maximum thickness 30 mm, minimum 15 mm), which was noted as W-c (Figure 9). Variants differ by surface form: original ribbed (C), FD (flat + CW dowels), FR (rectangular), and FT (triangular), which is illustrated in Section 3.1.5. The baseline GC discretization uses  $\approx 45324$  elements.

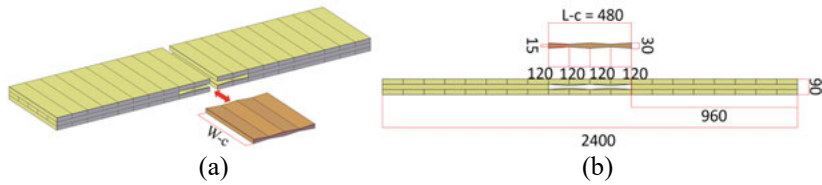


Figure 9 Designs of GC connection, (a) assembly illustration and (b) dimensions from front view. (unit in mm)

Furthermore, Double-surface (DS) connection (Figure 10) dealt with two rectangular timber tongues extending from opposed panel edges, locked by vertically inserted CW dowels (beech, diameter ( $D$ ) = 10 mm, length = 90 mm). The DS connector length (LC) was 240 mm, and its thickness matched one lamella (30 mm). The distance from dowel center to the panel end edge was  $d$  = 60 mm.

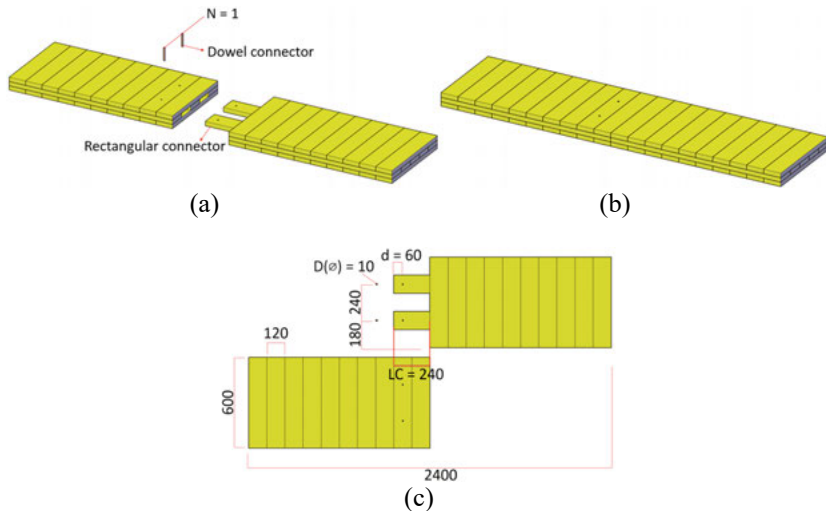


Figure 10 DS connection, (a) involved components, (b) assembled illustration, and (c) dimensions at front view. (unit in mm)

In the Half-lapped (HL) connection, each panel was half-lapped by removing 50% of thickness over a  $480 \times 600$  mm area (Figure 11); the two rebates were then mated and clamped with two through-height CW dowels (diameter ( $D$ ) = 10 mm, length = 90 mm) positioned at mid-span with an internal spacing of 350 mm. At mid-span the lower part thickness was  $TB$  = 45 mm, and the distance from dowel center to the upper panel edge was  $d$  = 240 mm.

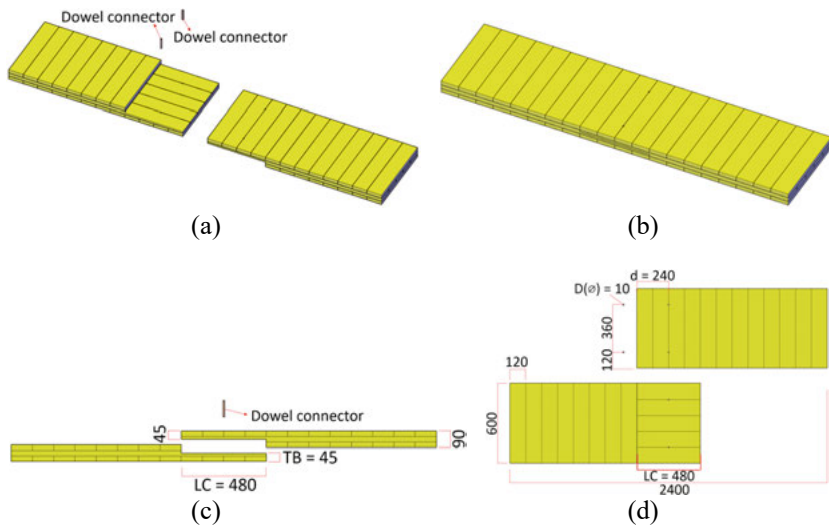


Figure 11 Geometries of HL connection, (a) before jointed, (b) jointed panel, (c) front view, and (d) top view. (unit in mm)

## 2.2. Experiments on glulam with edge connections (Paper IV)

Apart from the numerical simulation, the proposed connection concepts were adapted to GLT and tested experimentally. Six full-scale glulam floor-type specimens were fabricated and tested to evaluate the flexural performance of innovative adhesive-free timber edge connections. Each specimen comprised of two three-ply glulam panels joined along their end-grain at mid-span by densified-wood connectors. Structural characterization was performed in out-of-plane four-point bending to failure, with stiffness, strength, ductility, moment capacity, rotation, and failure modes recorded and analyzed according to timber testing standards.

### 2.2.1. Materials

During the experimental test, each specimen consisted of two identical 3-ply glulam panels with nominal panel dimensions  $1200 \times 300 \times 90$  mm (length  $\times$  width  $\times$  thickness); each lamella was 30 mm thick and manufactured from knot-bearing pine lumber sized  $1200 \times 120 \times 30$  mm. Panel geometry followed EN 408 and EN 16351 rules (lamination width/thickness  $\geq 4$ ) (CEN. EN 16351, 2021; SS. EN 408:2010+A1:2012, 2012). Moreover, lamellae were bonded using a polyurethane (PUR) adhesive under 0.6 MPa vertical press, per EN 14080 (EN 14080:2013, 2014). The mean density of the glulam was  $560 \text{ kg/m}^3$ , with moisture content 10–15% at fabrication.

Furthermore, connectors were made of beech veneers coated with synthetic resin and hot-pressed at  $130 \text{ }^\circ\text{C}$  to form high-density laminates ( $1350\text{--}1400 \text{ kg/m}^3$ ) (Figure 12). Two densified-wood panels ( $2000 \times 1000 \times 30$  mm) provided all connectors across the test matrix. Prior to assembly, all wood elements were sealed in air-tight plastic to limit moisture exchange and shrinkage;

$\pm 0.2$  mm dimensional allowance was applied to all connector geometries to achieve a designed interference fit.

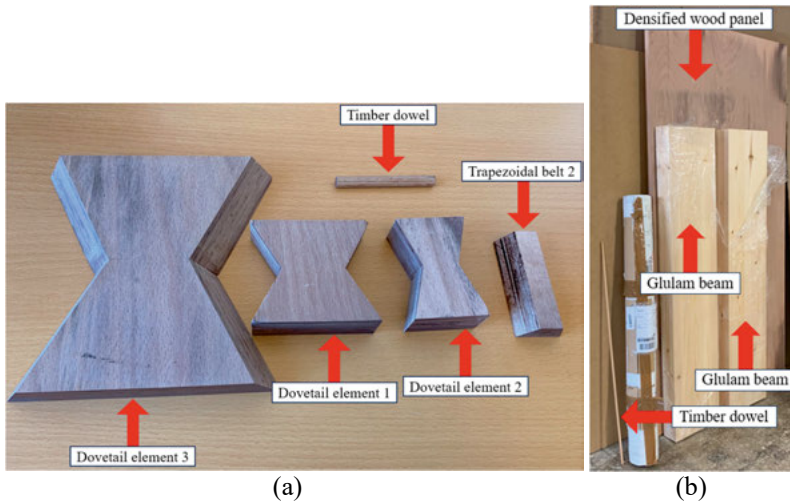


Figure 12 (a) densified wood connectors and (b) unsawn glulam beams, a densified wood panel, and a timber dowel.

As for the completed specimens, two glulam panels were joined at mid-span using one of six adhesive-free connection layouts (Specimens 1–6, depicted in Figure 13). Connectors were positioned within a 500 mm zone centered on the mid-span along the major (fiber) direction. Additionally, the CNC cutter reaches limit of 100 mm in the major direction which constrained some second-layer reinforcements to 200 mm in total (100 mm per panel edge). The six layouts were:

- **Specimen 1:** horizontal reinforcement at top and bottom layers with “timber elements 1” and trapezoidal belts 1.
- **Specimen 2:** flat plate (outer layer) plus side dovetail elements 1.
- **Specimen 3:** six vertical timber dowels only.
- **Specimen 4:** tongue-and-groove concept with one vertical dowel and two trapezoidal belts 2.
- **Specimen 5:** flat plate (middle layer) plus side dovetail elements 2.
- **Specimen 6:** horizontal reinforcement at outer and middle layers with dovetail elements 3 and a flat plate 3, respectively.

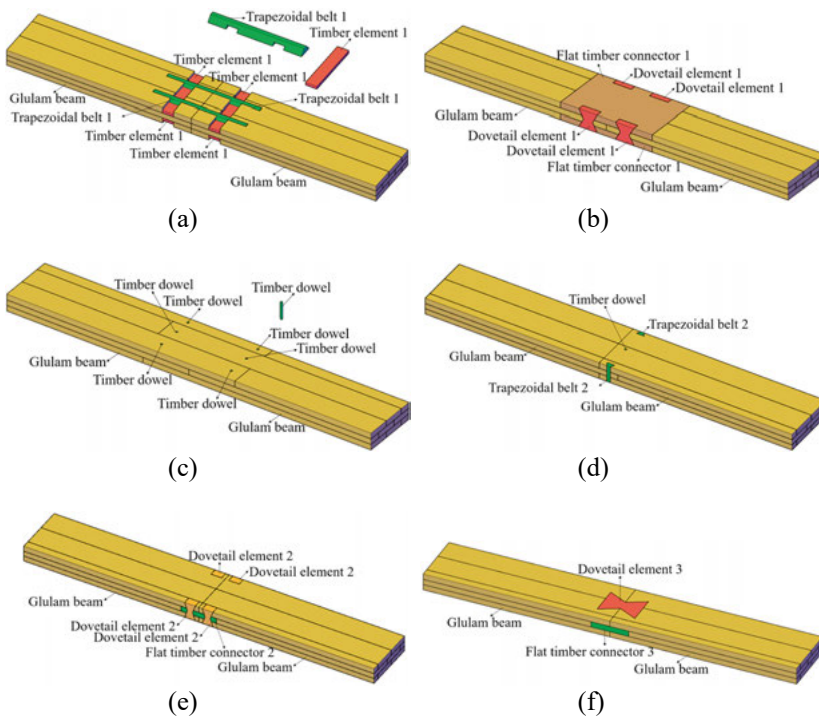


Figure 13 Examined specimens, (a) specimen 1, (2) specimen 2, (3) specimen 3, (4) specimen 4, (5) specimen 5, and (6) specimen 6.

### 2.2.2. Fabrication and machining

Based on the design in Section 2.2.1, panel edges (minor direction) were shaped on a 5-axis CNC milling system mounted on a vacuum holding bed to ensure positional accuracy. The operation created rounded internal corners because of the rotating cutter; these were then squared by light manual trimming to achieve 90° seats and continuous load paths. Where dowels were specified, through-holes were pillar-drilled after CNC to maintain alignment and surface finish. All connectors were CNC-milled from densified-beech panels and finished to the  $\pm 0.2$  mm interference tolerance.

Moreover, mating panel edges were aligned on a level bed, clamped, and the densified-wood connectors driven into their rebates/interlocks (without adhesives or metal fasteners) to achieve a dry, friction-dominated fit. For layouts employing vertical locking elements (dowels/belts), these were installed last to constrain slip normal to the joint. Additionally, manual “demolishing” (light chiseling) was employed locally to square CNC-rounded corners before fit-up.

### 2.2.3. Experimental testing

All specimens (overall test piece  $1980 \times 300 \times 90$  mm) were tested in four-point bending using a Shimadzu Autograph AG-X, 100 kN frame under displacement control at 2 mm/min to failure. Steel roller supports were spaced 1890 mm, and the two applied line loads were symmetrically located with 540

mm spacing about mid-span (Figure 14 (a)). Vertical displacements at the load points were recorded by the machine's default sensor ( $8 \mu\text{m}$  accuracy). The layout and procedures followed EN 408 (SS. EN 408:2010+A1:2012, 2012) and design conventions from Eurocode 5 (CEN. EN, 2004).

Furthermore, load and actuator displacements were recorded continuously from preload to post-peak softening. The principal global response was the load–displacement curve, from which elastic slope, yield, ultimate load, and failure displacement were obtained for each configuration.

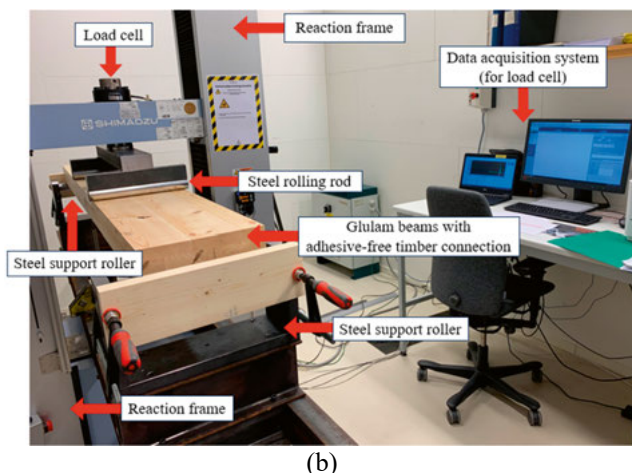
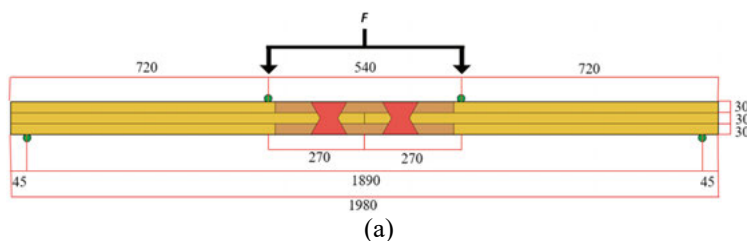


Figure 14 Four-point bending test setup, (a) sketches of four-point bending test setup for specimen 2 (unit in mm) and (b) setup in laboratory.

#### 2.2.4. Data acquisition and analysis procedure

At the data analysis phase of the experimental study, ductility ratio was calculated as the ratio of displacement at failure to yield displacement, using the criterion reported in Eq. (7).

$$\text{Ductility ratio} = \frac{\text{Displacement at failure (mm)}}{\text{Yield displacement (mm)}} \quad (7)$$

Bending strength  $f_m$  at failure was computed from the four-point bending relation (Eq. (8)):

$$f_m = \frac{3Fa}{bh^2} \quad (8)$$

where F is the maximum applied force at failure, a is the distance from support to load line, b represents specimen width, and h is depth.

Bending modulus  $E_m$  was obtained from the elastic-stage slope using Eq. (9):

$$E_m = \frac{FL^3}{awbh^3} \quad (9)$$

where L is clear span and w is the mid-span deflection used in the standard four-point formulation.

Effective joint stiffness  $EI_{eff}$  (rotational resistance in connection under out-of-plane bending) was derived from the elastic slope and geometry via Eq. (10) (Darzi et al., 2020):

$$EI_{eff} = \frac{a(3L^2 - 4a^2)}{48} \left( \frac{\Delta F}{\Delta w} \right) \quad (10)$$

After failure, each specimen was photographed and examined for: (i) delamination planes between lamellae, (ii) cross-grain shear near connectors, (iii) connector integrity (fracture vs. elastic deformation), and (iv) asymmetry/knots influencing crack paths.

### 2.3. LCA on slab systems and connections (Papers V & VI)

In addition to examining the structural performance of CLT-system, evaluating its environmental impact is another focus of this thesis. Goal and intended work: this work applies process-based LCA to quantify and compare the environmental impacts of CLT floor slab systems and an RC reference, with focus on how edge-connection choice influences whole-slab and connection-level burdens. Scope overview: two types of structural configurations are assessed with the following information.

(1) Structure type 1: CLT panels with edge connections

Four edge-connection typologies: BC connection (Section 2.1.3), DS connection (Section 2.1.3), TS connection (Section 2.1.3), and DSS connection (Section 2.1.1) (Zhang & Chui, 2020), benchmarked against an RC slab (Section 2.3.1) (Demertzi et al., 2020).

(2) Structure type 2: Adhesive-free CLT panels

A SCLT slab, three AFCLT (1–3), and an RC slab.

Two functional units (FU) were defined: (FU1) 1 m<sup>2</sup> of structural floor slab with edge connection designed for a uniformly distributed live load of 2.5 kN/m<sup>2</sup> over a 50-year reference period, and (FU2) 1 m of edge connection under the same service context. Based on the structure type 1, FU1 &

FU2 capture, respectively, the interaction between connections and panels and the stand-alone footprint of the connections. The structure type 2 has only considered FU1 since the concerning panel systems contained no edge connection. Besides, the geometries of all slab systems are described in Sections 2.3.1 and 2.3.2.

### 2.3.1. Functional units for structure type 1: CLT with edge connections

Since two FUs were applied in the studies of the structure type 1, this resulted in two scenarios (1 and 2). Each scenario implemented only one FU based on the same connection systems. However, scenario 1 studied CLT panels with edge connections, while scenario 2 included only edge connections.

#### Scenario 1: FU1 orientated

All CLT specimens were comprised of two jointed panels, each 1666 mm × 600 mm × 90 mm (length × width × thickness) with three 30 mm lamellae. The top surface area of all specimens was in accordance with FU1 as 1 m<sup>2</sup>. Connections BC, DS, and TS were timber-only; DSS combined timber splines with steel fasteners. The selected connections were adapted to the new CLT slab dimensions under this scenario, where the slab is shorter in the longitudinal direction and longer in the tangential direction, while the thickness remains the same. The reference RC slab reflected a conventional 160 mm concrete slab with two reinforcement layers.

**BC connection:** Two profiled panel edges were locked using eight CW elements—four rectangular inserts (600 × 30 × 15 mm) and four dovetail inserts (40–100 mm taper; with 30 × 15 mm openings 45 mm from each end), which are installed symmetrically on top and bottom faces (Figure 15 (b)); timber moisture content was taken as 10% (C. X. Chen et al., 2019). CNC milling was assumed for both panels and connectors (Harley et al., 2016; Jockwer et al., 2021; Tannert, 2016; Xin & Gattas, 2021).

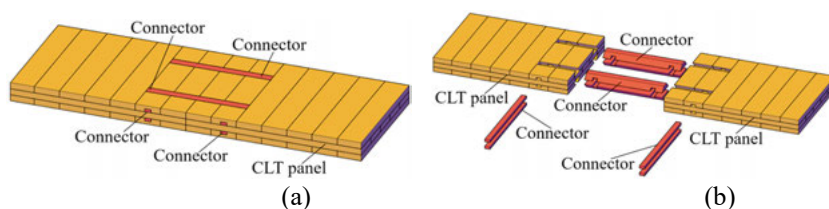


Figure 15 CLT panels with BC connection, (a) jointed view and (b) installation illustration.

**DS connection:** Two rectangular timber tongues from one panel engage the mating grooves in the other and are pinned by two 10 mm × 90 mm CW dowels, centered 60 mm from the panel edge (Figure 16 (b)). The total connection thickness and length are 30 mm and 240 mm, respectively.

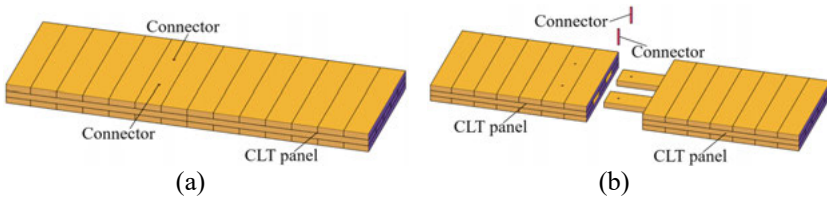


Figure 16 CLT panels with DS connection, (a) jointed view and (b) installation illustration.

**TS connection:** Two identical CW TS-connectors, with web tapering from 50 mm to 30 mm, are positioned along the panel length on the mid-span axis, spaced 200 mm apart and located 100 mm from each edge. Installation is carried out top-down without auxiliary fixings (Figure 17 (b)).

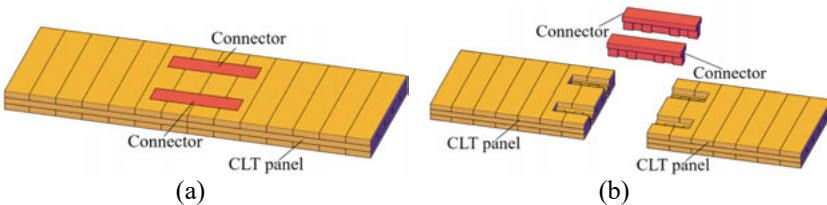


Figure 17 CLT panels with TS connection, (a) jointed view and (b) installation illustration.

**DSS connection** (Zhang & Chui, 2020): A plywood-spline joint reinforced with partial-thread self-tapping screws (PTS8160) spaced at 75 mm on both faces; washers are included. The modeled variant corresponds to DSS-8160/8/150-25W. The grain orientation of the outer and central layers is parallel to the joint plane (Figure 18 (b)).

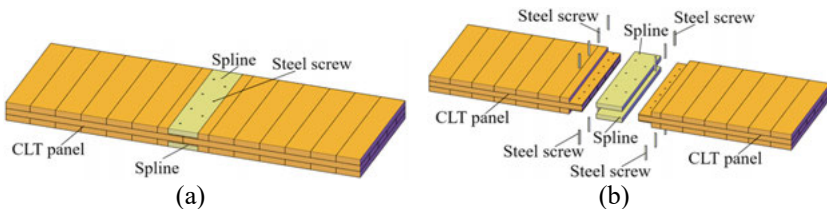


Figure 18 CLT panels with DSS connection, (a) jointed view and (b) installation illustration.

**Reference RC slab** (Demertzi et al., 2020) (Figure 19): Concrete C25/30 ( $\rho \approx 2500 \text{ kg/m}^3$ ) reinforced with A500NR rebars:  $\text{Ø}8 \text{ mm} @ 200 \text{ mm}$  in the top layer and  $\text{Ø}10 \text{ mm} @ 200 \text{ mm}$  in the bottom layer, providing  $\approx 10 \text{ kg/m}^2$  of steel.

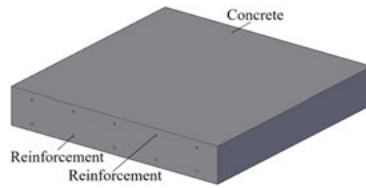


Figure 19 Axonometries of RC floor slab.

**Scenario 2: FU2 orientated**

For FU2 (1 m connection), panels were excluded, and connections were extended along the panel’s minor direction to 1 m. Components parallel to the joint axis were lengthened, while components perpendicular to it were duplicated at the appropriate spacing (e.g., DS dowels, TS) (Figure 20). This approach isolated the environmental signal of the connection per unit length.

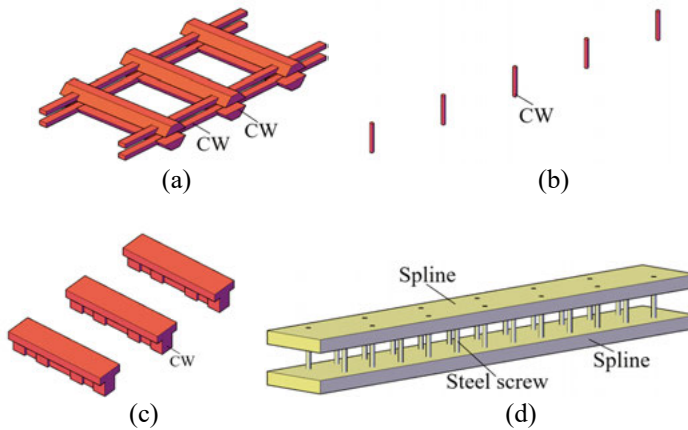


Figure 20 (a) b edge connection, (b) DS edge connection, (c) TS edge connection, and (d) DSS edge connection.

**2.3.2. Functional unit for structure type 2: Adhesive-free CLT**

In structure type 2, FU1 was followed in the LCA studies. The specimens involved are described below.

**SCLT (reference CLT)** (C. X. Chen et al., 2019): A 3-ply CLT panel with lamella of 30 mm thick each, bonded with a PUR adhesive (Figure 21). Scots pine was used; densities reported for inventory range from 466 to 517 kg/m<sup>3</sup> with the latter adopted in the consolidated bill of materials. Adhesives were also present in the finger joints. The maximum industrial panel size referenced was 3.45 m × 16 m.

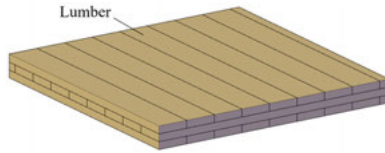


Figure 21 Configurations of SCLT.

**AFCLT1 (dovetail-jointed with service gaps)** (Baño & Moltini, 2021): An adhesive-free interlaminar connection formed by machined timber-to-timber dovetails (CNC-milled) between the outer and middle lamellae (Figure 22). The middle layer is gapped at 140 mm spacing to accommodate services. The 3-ply panel has a total thickness of 146 mm and dimensions of 1000 mm × 2500 mm for the inventory. Scots pine was used, with a density of 500 kg/m<sup>3</sup>. Adhesive was retained only in the finger joints of the boards.

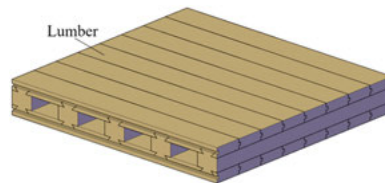


Figure 22 Configurations of AFCLT1.

**AFCLT2 (dowel-laminated)** (Sotayo, Bradley, Bather, Oudjene, et al., 2020): An adhesive-free connection was made using vertically inserted, hot-pressed beech dowels (10 mm diameter, 60 mm length; ~1300 kg/m<sup>3</sup>, 5% MC) through Scots pine lamellae (20 mm thick; ~556 kg/m<sup>3</sup>, 10% MC). The inventory test panel size was 600 mm × 1500 mm × 60 mm (Figure 23). Dowel density is two per 13 225 mm<sup>2</sup> of plan area. Finger-jointing adhesive is retained in the boards only.

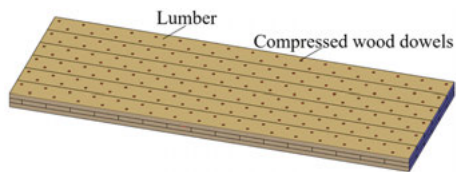


Figure 23 Configurations of AFCLT2.

**AFCLT3 (solid dovetail without internal gaps)** (Ilgin & Karjalainen, 2021): Adhesive-free interlaminar dovetailing, similar to AFCLT1 but without internal voids; 3-ply, each layer 40 mm thick (total 120 mm) (Figure 24). Inventory panel size: 2500 mm × 5000 mm; Scots pine density ~517 kg/m<sup>3</sup>; adhesive retained only in finger joints.

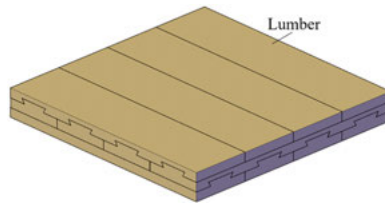


Figure 24 Configurations of AFCLT3.

**RC slab:** Same as the one studied in Section 2.3.1. To ensure functional comparability between different specimens, the RC reference slab was defined as a typical 160mm thick C25/30 slab, consistent with the reference design (Demertzi et al., 2020). The selected strength class is widely used in Swedish building practice for in-situ concrete elements under non-aggressive indoor environments (Boverket, 2004; Thomas Betong, 2018). Wood slabs (SCLT and AFCLT1-3) were modeled as precast panel products reported in the references, while the RC slab was modeled as a cast-in-place system. Therefore, all designs were compared per 1 m<sup>2</sup> of floor area for the same target (able to bear at least 2.5 kN per 1 m<sup>2</sup> for 50 years). However, considering that SCLT and AFCLT1-3 have different thicknesses (90 mm, 146 mm, 60 mm, and 120 mm) and lower densities compared to the RC slab, their load capacities may vary.

Although the compared floor slabs serve the same floor function, AFCLT1-3 cannot be proven to be structurally equivalent because they were directly adopted from the literature (Baño & Moltini, 2021; C. X. Chen et al., 2019; Ilgin et al., 2025; Sotayo, Bradley, Bather, Oudjene, et al., 2020) rather than fundamentally redesigned to match the flexural capacity and deflection limits of RC floor slabs. The RC reference design follows the traditional retrofit-oriented floor slab design proposed by Demertzi et al. (Demertzi et al., 2020). Therefore, the results should be primarily interpreted as a product-level comparison of different floor slab schemes per unit floor area, rather than an equal load-bearing capacity benchmark between all systems.

### 2.3.3. System boundaries and included life cycle modules

The assessment follows ISO 14040/14044 (ISO, 2006) and aligns with EN 15804 and EN 15978 (British Standards Institution, 2011; EN 15804:2012+A2:2019, 2019). A cradle-to-cradle boundary was applied (Figure 25), covering A1–A3 (raw material supply and production), A4–A5 (transport to site and installation), B1 (use—limited), C1–C4 (deconstruction and waste management), and D (potential benefits and burdens beyond the system boundary). In this study, C and D were reported within the EOL stage for comparability. Use-phase modules B2–B7 were excluded because the prefabricated slabs require no operational energy, water, or maintenance in the studied scenario, and reliable data were unavailable.

Biogenic carbon was also excluded due to: (1) focusing the comparison on process emissions and impacts under assumed conditions and (2) avoiding the influence of different carbon storage accounting methods on the results. According to EN 15804 (EN 15804:2012+A2:2019, 2019), biogenic carbon is

typically reported separately because it is sensitive to EOL scenarios (reuse, incineration, landfill) and service life span. Therefore, excluding biogenic carbon means that reported GWP values are relatively conservative for timber (i.e., the net climate benefit of carbon storage is neglected).

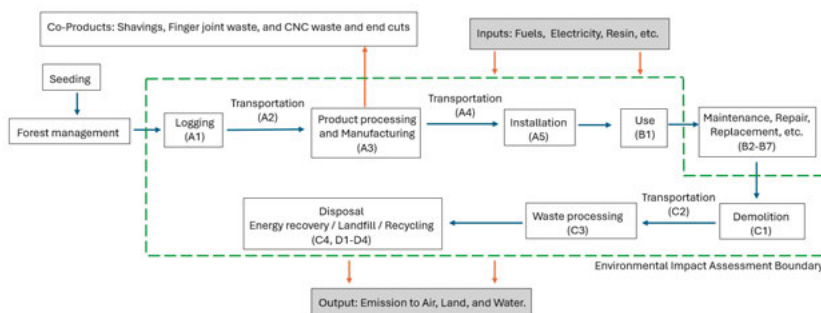


Figure 25 Life cycle framework and system boundary conditions.

In addition to the influence of geometry, the impacts of electricity mixes by location are also investigated based on structure type 2. To isolate the effect of electricity supply, manufacturing electricity is alternately modeled using country mixes for Norway, Sweden, Finland, and Saudi Arabia (all from Ecoinvent v3.5). Representative shares (used qualitatively in interpretation) are as follows: Norway is hydro-dominated (~87.39% hydro, ~3.82% wind); Sweden uses hydro (~39.86%), nuclear (~34.5%), and wind (~15.47%); Finland combines nuclear (~28.61%), hydro (~14.72%), wind (~7.61%), plus fossil shares; and Saudi Arabia is fossil-dominated (~50.69% oil, ~49.3% natural gas). Transport distances are not altered in these cases to focus the attribution on electricity mixes.

### 2.3.4. Inventory data and modeling assumptions

All life cycle models were implemented in SimaPro v9.4.0.3 using Ecoinvent v3.5 (Frischknecht & Rebitzer, 2005) as background data. Primary inventory parameters draw on our prior experimental work on AFCLT1–3, standard references for CLT manufacturing (Erol & Brad, 2013), and published LCA studies (Al-Najjar, 2021; Baño & Moltini, 2021; C. X. Chen et al., 2019; Demertzi et al., 2020; Puettmann et al., 2019b; Sotayo, Bradley, Bather, Oudjene, et al., 2020; Tighnavard Balasbaneh et al., 2022), with Swedish electricity contributions aligned to 2023 national statistics (Statens energimyndighet, 2023). Unless stated otherwise, electricity reflects Swedish conditions in 2023, and no service-life extension benefits are assumed.

Material provisioning and manufacturing follow a consistent mass/energy accounting approach across SCLT and AFCLTs. To produce 1 m<sup>3</sup> of finished panel, lumber input is 1.21 m<sup>3</sup> (Puettmann et al., 2019b); AFCLTs adjust this input to account for additional machining and geometry. Machining co-products are modeled explicitly and treated by cut-off (no substitution credit): milling shavings 3.45%, finger-joint waste 0.93%, and CNC residues/end-cuts 12.8%.

PUR adhesive consumption for conventional lamellae bonding is 6.44 kg/m<sup>3</sup> for a 3-ply SCLT (Puettmann et al., 2019b); AFCLTs eliminate lamella-surface bonding and retain PUR only for finger joints, scaled to actual lumber input. Timber machining is represented with a 4 × 8 CNC router operating at ≈417 mm/s (STYLECNC, 2025); CW elements are hot-pressed with a specific electricity demand of 1.5 kWh per 300 × 300 mm board (Xiamen Lith Machine Limited, n.d.).

For the DSS option, manufacturing electricity per screw is 0.000681 kWh, and installation electricity per screw is 8.6389 × 10<sup>-5</sup> kWh (Glasner et al., 2023; Landgrebe et al., 2018). Meanwhile, process electricity covers CLT production and CNC milling; AFCLT1 and 3 incur higher milling intensity than AFCLT2 due to more complex cutting. All material properties are summarized in Table 3.

Moreover, geography and logistics reflect Swedish suppliers and project locations. In this study, CLT-related slabs were assumed to be produced at Stora Enso (Ljusne), RC slabs at Thomas Betong AB (Heby), and the construction site is in Stockholm. Default one-way road transport distances are 242 km for CLT to site, 138 km for RC to site, and a uniform 150 km to waste-management facilities at EOL. Euro-class diesel lorry processes are taken from Ecoinvent. On-site erection is represented by a Kobelco TKE750G telescopic-boom crawler crane (rated power 254 kW) (Al-Najjar, 2021; Kobelco Construction Machinery Co., n.d.), with fuel/energy scaled linearly to each slab’s lifted mass per functional unit relative to the crane’s lifting capacity, consistent with the resolution of available inventory datasets. Site consumables are neglected.

Table 3 Material properties of elements in structure types 1 and 2.

Con- nection type	Sce- nario	Structural system	Material	Density (kg/m <sup>3</sup> )	Reference	Total weight (kg)
1	1	CLT + BC	Scots Pine (CLT)	556	(Ren et al., 2024c)	41.94
			Beech (CW joints)	1300		6.2478
			PUR	-		0.576
		CLT + DS	Scots Pine (CLT)	556	(Ren et al., 2024b)	41.94
			Beech (CW dow- els)	1300		0.01838
			PUR	-		0.576
		CLT + TS	Scots Pine (CLT)	556	(Ren et al., 2024c)	41.94
			Beech (CW joints)	1300		5.616
			PUR	-		0.576
		CLT + DSS	Scots Pine (CLT)	556	(Zhang & Chui, 2020)	41.94
			Scots Pine (splines)	517		2.1714
			Steel screws (PTS8160)	7850		0.45456
		PUR	-		0.576	

	RC	Concrete class C25/30	2500		400	
		Reinforcement A500NR ( $\varnothing 8$ & $\varnothing 10$ )	7850	(Demertzi et al., 2020)	5.053045	
	2	BC	Beech (CW joints)	1300	(Ren et al., 2024c)	9.6057
		DS	Beech (CW dowels)	1300	(Ren et al., 2024c)	0.045946
		TS	Beech (CW joints)	1300	(Ren et al., 2024c)	8.424
		DSS	Scots Pine (splines)	517	(Zhang & Chui, 2020)	3.619
	Steel screws (PTS8160)	7850	0.7576			
2	SCLT	Scots Pine	517	(C. X. Chen et al., 2019)	41.94	
		PUR	-		0.576	
	AFCLT1	Scots Pine	500	(Baño & Moltini, 2021)	51.525	
		PUR	-		0.184	
	AFCLT2	Scots Pine	556	(Sotayo, Bradley, Bather, Oudjene, et al., 2020)	30.024	
		CW dowels	1300		1.12	
	AFCLT3	PUR	-		0.0966	
		Scots Pine	517	(Ilgin & Karjalainen, 2021)	55.92	
	PUR	-		0.1932		

The use stage assumed no operational energy or water for the slabs and no maintenance, repair, or replacement (i.e., B1 has no operational loads, and B2–B7 are excluded in the reference case). EOL modeling differentiates timber-based, steel-based, and RC systems. For timber panels, 80% of wood mass is directly reused as structural timber, and 20% is sent to incineration with energy recovery (Tighnavard Balasbaneh et al., 2022). Module D credits are assigned as avoided materials/energy using SimaPro’s avoided-burden approach.

For RC slabs, demolition is modeled with a stone crusher; concrete fragments are landfilled in the base case, and 75% of reinforcing steel is recycled (Tighnavard Balasbaneh et al., 2022), with Module D reflecting avoided primary steel production where applicable. No concrete reuse credit is taken.

These assumptions are applied consistently to SCLT and AFCLT variants, with electricity-mix scenarios anchored in Swedish 2023 conditions and transport/installation scaled to actual product masses and geometries.

Furthermore, RC slab will absorb carbon dioxide ( $\text{CO}_2$ ) in the use stage. Therefore, GWP is the only impact category that receives influence from B1 stage based on RC slab. The total  $\text{CO}_2$  uptake ( $\text{TU}_{\text{carb}}$ ) is calculated based on Eq. (11) (Dervishaj et al., 2024; European Committee for Standardization (CEN), 2022):

$$TU_{\text{carb}} = (k_i \times \text{DoC}_i \times A_i) \left( \frac{\sqrt{t}}{1000} \right) \times U_{\text{max}} \times C \quad (11)$$

Where  $k$  represents the carbonation coefficient ( $\text{mm}/\text{year}^{0.5}$ ),  $\text{DOC}$  is the carbonation degree,  $A_i$  is the surface area that will have carbonation (top and bottom surfaces of RC slab are assumed to be exposed for carbonation),  $t$  is the expression of time in years,  $U_{\text{max}}$  refers to maximum theoretical  $\text{CO}_2$  absorption:  $0.49 \text{ kg CO}_2/\text{kg cement}$  (Andrade, 2020; Reis et al., 2021), and  $C$  is the cement content ( $300 \text{ kg cement}/\text{m}^3$ ) (CEMEX, n.d.). The RC is assumed to be indoor condition without cover. Hence,  $k$  is  $6.6 \text{ mm}/\text{year}^{0.5}$  and  $\text{DOC}$  is  $40\%$  (Dervishaj et al., 2024; European Committee for Standardization (CEN), 2022).

In addition, the modeled RC reference in this study is a typical and widely used type in the market. However, Sweden has been increasingly promoting low-carbon concrete options, which include blended cements and supplementary cementitious materials (SCMs) (e.g., slag or fly ash substitution) as well as reducing clinker usage. These methods can reduce the embodied GWP of concrete by lowering emissions from cement production (Helsing et al., 2023).

To avoid bias in interpretation, the RC slab results in this thesis should be considered as a baseline reference, instead of the optimal concrete solution. Low-carbon RC variants will reduce (but not completely eliminate) the dominance of RC in the production phase across most environmental impact categories.

### **2.3.5. Impact assessment method and impact categories**

Based on both structure types, environmental impacts were characterized using CML indicators: ADP, GWP, Ozone Depletion (ODP), HTP, Freshwater Aquatic Ecotoxicity (FAETP), Marine Aquatic Ecotoxicity (MAETP), Terrestrial Ecotoxicity (TETP), Photochemical Ozone Creation (POCP), Acidification (AP), and Eutrophication (EP).

## 3. Results and discussion

This Chapter provides the obtained results based on the three types of studies from Chapter 2, as well as the results analysis and discussion. Besides, the structural performance of the steel connection is provided and compared to the proposed connections. The limitations of this study are discussed.

### 3.1. Out-of-plane bending performance on CLT with edge connections (Papers II & III)

Based on the methodology and materials presented in Section 2.1, this Section provides the corresponding numerical results from the related verification models (1, 2, and 3) and the six proposed connections.

#### 3.1.1. Verification of numerical framework (models 1, 2, 3)

The modeling framework was first validated against two independent experimental studies: one at the joint (beam-to-beam) scale (models 1 and 2) and one at the plate (panel) scale (model 3). For the GLT end-connected beams with CW plates and dowels, the FE moment–rotation curve reproduced the experimental capacity within a few percent difference: BB-8-20 reached  $9.09 \text{ kN}\cdot\text{m}$  at  $1.88^\circ$ , compared with  $8.88 \text{ kN}\cdot\text{m}$  at  $1.77^\circ$  in the mean test, corresponding to +2% in capacity and +6% in rotation at failure (Figure 26 (a)). For BB-6-20, the FE moment was  $6.36 \text{ kN}\cdot\text{m}$  vs.  $6.40 \text{ kN}\cdot\text{m}$  from the experiment (−0.6%), confirming both stiffness and strength predictions over the elastic, yielding, and post-yield segments of the response (Figure 26 (b)). Material property tables used in these verifications (orthotropic elastic constants, interface laws, and strength components) are listed in Section 2.1.2 and underpin the remainder of the study.

At the panel scale (model 3), the AF-CLT benchmark with vertical CW dowels exhibited an experimental ultimate load of  $32.0 \text{ kN}$  and a mid-span displacement of  $85.4 \text{ mm}$  (Figure 26 (c)); the corresponding FE predictions were  $31.96 \text{ kN}$  and  $87.1 \text{ mm}$  (−0.1% and +1.9%). Agreement at both scales supports using the model for comparative design exploration of the new adhesive-free edge connections.

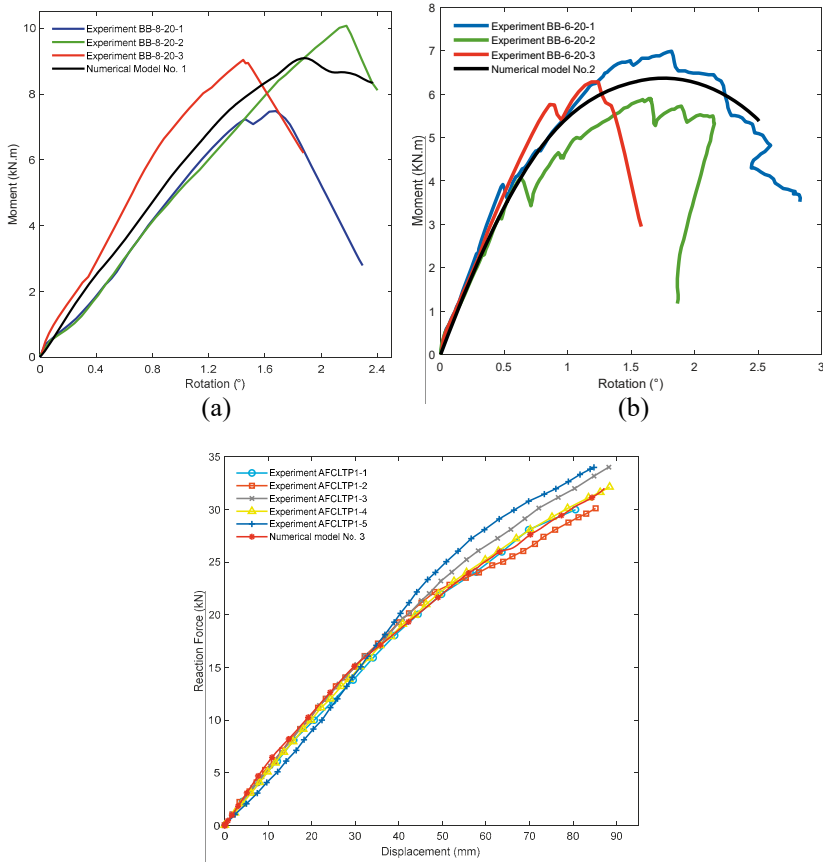


Figure 26 Comparison of verification model results, (a) verification model 1, (b) verification model 2, and (c) verification model 3.

### 3.1.2. Global behavior of six baseline connections

Based on the verified FE frames, the proposed six timber-based edge connections were numerically analyzed (geometries and materials are available at Sections 2.1.2 and 2.1.3). Figure 27 compares the baselines of each concept under identical four-point bending. All six connections showed a long linear elastic phase followed by a short, ductile nonlinear segment; none failed in a brittle manner.

The baseline BC connection achieved the greatest peak load (8.97 kN) and, in pairwise comparisons, exceeded TS by 206%, TS exceeded GT by 25.8%, and GT exceeded GC by 39.5%. Nevertheless, the BC concept exhibited the smallest displacement at peak ( $\approx 104.6$  mm), while TS, GC, and GT reached  $\approx 124.8$  mm, 130.6 mm, and 151.3 mm, respectively.

The ranking reflects how each concept engages the section: BC mobilizes both outer lamellae through dovetail belts and transverse locks, enhancing section-level action, whereas GT and GC primarily reinforce the second (transverse) lamella, which is intrinsically less effective for out-of-plane bending of

the full section. Locking mechanics also play a role: BC uses crossed CW elements to provide geometric lock, while TS/GT/GC rely more on sliding friction and local bearing in standard-wood paths.

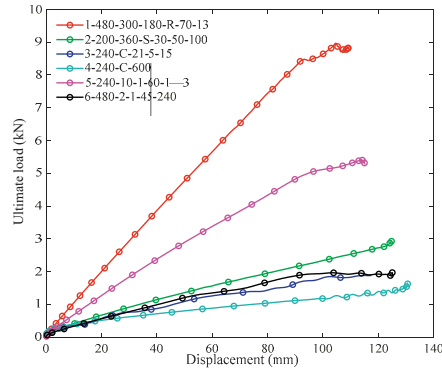


Figure 27 Load-displacement responses of BC (1-480-300-180-R-70-13), TS (2-200-360-S-30-50-100), GT (3-240-C-21-5-15), GC (4-240-C-600), DS (5-240-10-1-40-1-3), and HL connection (6-480-2-1-45-240).; titles in numbers are described in Section 3.1.5.

DS variants showed nearly coincident elastic slopes and typically brittle terminations shortly after peak load (Figure 28 (a)). This insensitivity of initial stiffness to parameter changes reflects that the rectangular tongues dominate bending transfer, and their cross-section and material remain invariant across DS cases; only the limited tongue region near mid-span actually rotates, while the regions near the dowels carry shear. By contrast, HL variants displayed more dispersed stiffness and larger plastic deformations prior to failure. The HL connection exhibited greater ductility but lower stability. Mechanistically, DS resists both sliding and global rotation through the combined action of the dowels and the mid-span rectangular tongues engaged with the CLT face, whereas HL primarily relies on the dowel line to block longitudinal slip.

These magnitudes were further compared through literature cross-referencing. CW timber joints in engineered-wood beams report a capacity of  $\approx 4.54$  kN (Mehra et al., 2021), approximately 20% lower than the DS average despite smaller members. Hybrid metallic LVL-splice/screw solutions can reach  $\approx 19.4$  kN but at  $\approx 77\%$  larger connector/panel volumes than used here, reducing their environmental parity and material-efficiency.

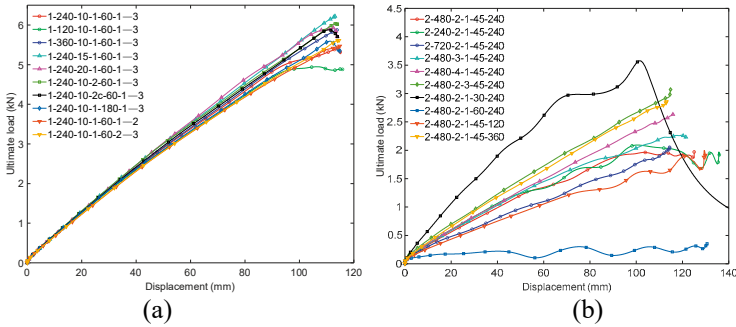


Figure 28 Load-displacement responses of all models regarding parametric studies, (a) DS connection, and (b) HL connection; titles in numbers are described in Section 3.1.5.

### 3.1.3. Strain evolution and lamination effects

Apart from the force-displacement performance, the mid-span strain histories from nine-gauge positions (Section 2.1.3) clarify how load is shared as nonlinearity develops. All configurations in Figure 29 show linear strain-load relationships in the elastic regime. In the TS, GT, and GC families, the bottom mid-span strains (gauges P7–P9) often remain small or become highly localized as failure approaches (Figure 29 (b)-(c)). This is consistent with the lack of robust tension bridging when reinforcement is concentrated in the transverse lamella: the bottom edges near the joint tend to separate, while compression localizes around connector edges. For TS, deformation of the bottom layer localizes near the corners of the TS-web/-flange about 240 mm from the joint.

At the side face (P4–P6), strains tend to drop toward zero at failure in BC, TS, and GC because delamination and rolling-shear develop around connector ends, consistent with prior four-point bending studies on three-layer CLT without connections. The BC concept stands apart: strain magnitudes around mid-span remains higher and more bending consistent until later in the loading, indicating better lamella coupling. Fracture initiation in BC occurs predominantly at the bottom mid-span region (Figure 29 (a)), whereas in TS/GT/GC the critical disturbances are associated with compression near connector edges in the top lamella and tension separation in the bottom lamella.

In DS, nine-point tracking revealed that the top longitudinal layer near mid-span carried the highest tensile/compressive demand, while the bottom longitudinal layer remained nearly inactive throughout much of the loading (Figure 29 (d)). Adding dowels tightened the joint, slightly elevating bottom-edge participation and balancing the mid-span strain distribution in the top layer. The short-tongue variant redirected demand earlier toward the tongue, consistent with its higher ductility.

In HL, the core transverse layer at mid-span dominated, showing that the lap geometry primarily anchored the connection through the core (Figure 29 (e)). Depth-wise measurements in DS further indicated a neutral-axis shift toward mid-depth, with compression concentrated in the top longitudinal layer and tension in the adjacent transverse layer, while bottom-layer strains remained near zero, explaining the limited influence of dowel penetration. By

contrast, HL showed fundamentally different through-depth patterns, since positions 4–6 belonged to separate half-lapped segments; changes in upper thickness or dowel placement reoriented the neutral axis and redistributed tension and compression between upper and lower halves.

These observations confirm the strong sensitivity of HL to section-level adjustments and highlight that local geometric modifications in both DS and HL govern the internal force transfer and strain evolution across the panel depth.

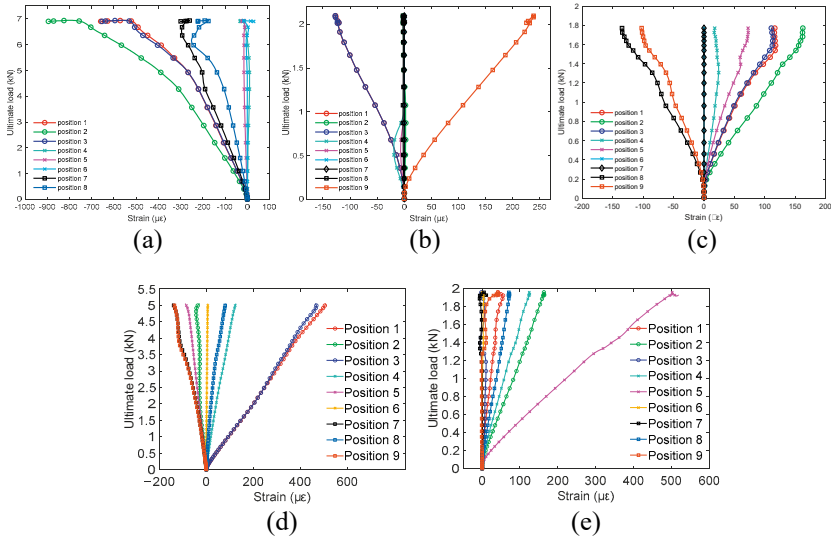


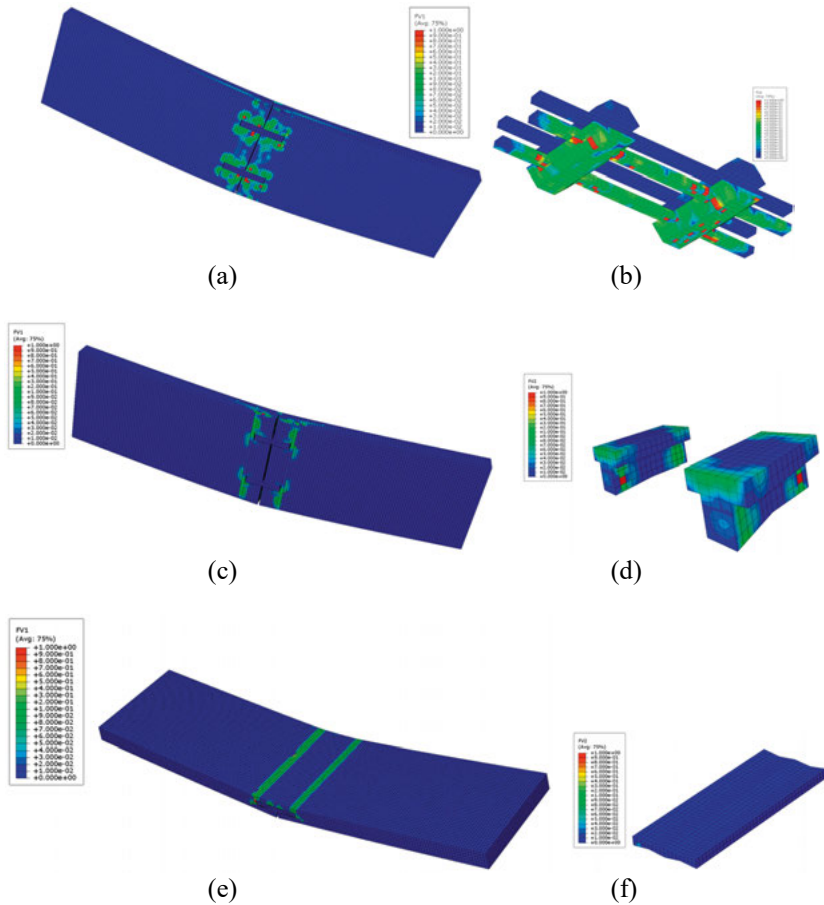
Figure 29 Load–strain diagrams under four-point bending test, (a) BC connection, (b) TS connection, (c) GC connection, (d) DS connection, and (e) HL connection.

### 3.1.4. Failure mode

In addition, the failure modes were collected and analyzed. In the BC connection (Figure 30 (a)-(b)), damage localized at the bottom mid-span, with additional compression-driven damage near connector corners at the top surface. Connectors placed in the third (tension) lamella attracted more damage than those in the first (compression) lamella, consistent with the tension-side demand. The TS connection exhibited similar tension-side dominance, with stress concentrations at the web corners; the flange operated mainly in compression as a seat and was less critical to locking (Figure 30 (c)-(d)). In the GT and GC layouts (Figure 30 (e)-(g)), the external/interlocking features were located in the second lamella; the response was disrupted primarily by compression near connector edges in the top lamella, while the bottom lamella remained comparatively unconstrained, leading to tension separation at mid-span. Deflection maps at failure were symmetric for BC and TS but became asymmetric for GT, reflecting the joint geometry. These patterns align with the mid-span strain histories and the global ductility/strength trade-offs described earlier.

Von Mises contours identified three DS hot-spot zones (Figure 30 (h)): (i) the top longitudinal layer between load points, (ii) the transverse layer near mid-span where the tongue rotates, and (iii) the region around dowels/tongues. Adding dowels reduced stress peaks around the dowels by altering the boundary condition of the rectangular connector. Failures were generally dowel shear perpendicular-to-grain (brittle trigger).

In HL (Figure 30 (i)), high stresses concentrated under the right-hand load at the upper panel top, under the left-hand load at the bottom, and between dowels and the right-hand load. With only two dowels, failure initiated at the dowel holes, indicating insufficient connector strength in the default HL geometry, an effect mitigated by using three/four dowels or improved placement. Ultimate-state deflection maps were longitudinally symmetric in DS about mid-span. HL peaked at the lower-panel outer edge (not at geometric mid-point) because the lower lap's free edge was weakly constrained. In both systems, deflection decayed nearly linearly from load points to support, consistent with the symmetric simple supports and out-of-plane bending.



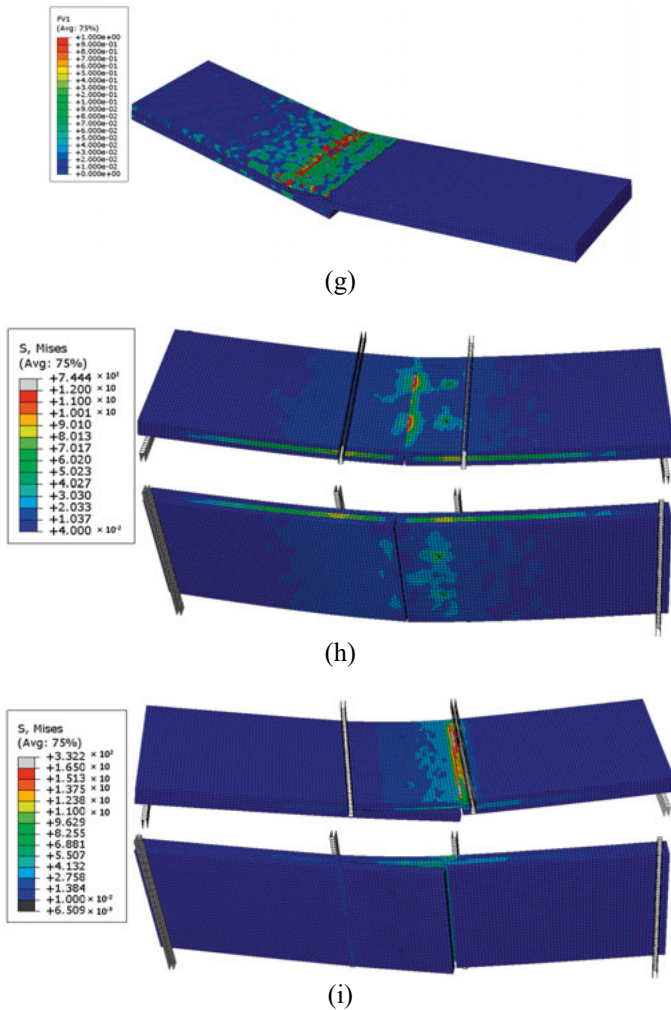


Figure 30 Contours of von Mises stress and failure modes, (a) CLT panel with BC connection, (b) BC connection, (c) CLT panel with TS connection, (d) TS connection, (e) CLT panel with GT connection, (f) GT connection, (g) CLT panel with GC connection, (h) CLT panel with DS connection, and (i) CLT panel with HL connection.

### 3.1.5. Parametric studies and performance within each type

Despite the six benchmark models, parametric studies were further conducted based on the baseline geometry within each connection type, which are placed at the first row in Tables 4, 6, 8, 10, 12, 14. This Section summarizes the design, parameters, and results of all parametric studies.

1) **BC connection (8 parameters; 12 models)**

- L-c: Dovetail longitudinal length; alignment along the central axis at the panel mid-span.
- L-d: Lateral spacing between dovetails.
- H-d: Longitudinal offset between the panel mid-span and dovetail-hole axis.
- LBCS: Cross-section of locking boards (R = rectangular, C = circular, T = triangular).
- W-a: Dovetail average width = (min + max)/2.
- PL: Lamella placement (e.g., 1 + 3 = top and bottom lamellae; 1 or 3 single-side).
- N: Number of dovetail connectors per participating lamella.
- MT: Connector material (CW baseline; S = standard wood in a control variant).

Table 4 Parametric study based on BC connection.

Connection	L-c (mm)	L-d (mm)	H-d (mm)	LBCS	W-a (mm)	P-L	N	MT
BC-480-300-180-R-70-1+3	480	300	180	R	70	1+3		
BC-480-300-180-R-70-1+3-1	480	300	180	R	70	1+3	1	
BC-240-300-180-R-70-1+3	240	300	180	R	70	1+3		
BC-480-200-180-R-70-1+3	480	200	180	R	70	1+3		
BC-480-400-180-R-70-1+3	480	400	180	R	70	1+3		
BC-480-300-60-R-70-1+3	480	300	60	R	70	1+3		
BC-480-300-180-C-70-1+3	480	300	180	C	70	1+3		
BC-480-300-180-T-70-1+3	480	300	180	T	70	1+3		
BC-480-300-180-R-90-1+3	480	300	180	R	90	1+3		
BC-480-300-180-R-70-3	480	300	180	R	70	3		
BC-480-300-180-R-70-1	480	300	180	R	70	1		
BC-480-300-180-R-70-1+3-S	480	300	180	R	70	1+3		S

It was noticed that the capacity increased as the dovetail length grew, with a 29% gain attributed to the stiffer connector while the lock geometry remained unchanged (Table 5). Increasing the lateral spacing between dovetails added about 5%, and moving the dovetail-hole axis farther from mid-span contributed an additional 9.5% by engaging more CW volume between the two end openings under compression (top) and tension (bottom). Changing the transverse lock from rectangular to circular or triangular had only  $\approx 1\%$  effect, as all three variants maintained similar volume and thickness, and therefore similar stiffness and contact area.

A wider dovetail (larger average width) increased capacity by about 7%. The location of reinforcement across lamellae was crucial: connectors in both

outer lamellae (1+3) yielded capacities 13% and 60% higher than using the first-only or third-only lamella, while third-only configuration outperformed first-only by 41%, underscoring tension-side dominance. Doubling the number of dovetails increased capacity by 47%, implying that roughly 94% of the peak load was borne by the dovetail system rather than the panel substrate.

Furthermore, using CW rather than standard wood in the connectors improved capacity by about 50%, demonstrating that connector strength governs ultimate capacity when the outer layers are properly engaged. Collectively, these observations identify outer lamellae engagement, connector volume/length, and connector count as the high-leverage design levers for the BC connection, whereas lock cross-section shape is comparatively unimportant when volume and thickness are held constant.

Table 5 Results of parametric study of BC connection.

Connection	Ultimate load (kN)	Flexural capacity (kN·m)	$EI_{eff}$ ( $10^3 \text{ Nm}^2$ )
BC-480-300-180-R-70-1+3	8.97	3.97	14.31
BC-480-300-180-R-70-1+3-1	6.09	2.69	10.20
BC-240-300-180-R-70-1+3	6.94	3.07	10.62
BC-480-200-180-R-70-1+3	8.73	3.86	13.35
BC-480-400-180-R-70-1+3	9.43	4.17	14.81
BC-480-300-60-R-70-1+3	8.19	3.62	12.36
BC-480-300-180-C-70-1+3	9.10	4.03	14.00
BC-480-300-180-T-70-1+3	9.08	4.02	13.96
BC-480-300-180-R-90-1+3	9.58	4.24	14.90
BC-480-300-180-R-70-3	7.96	3.52	12.34
BC-480-300-180-R-70-1	5.61	2.48	7.98
BC-480-300-180-R-70-13-S	5.99	2.65	8.62
Mean	7.97	3.53	12.29
Std. Dev.	1.38	0.64	2.40
COV	18.1%	18.2%	19.5%

## 2) TS connection (6 parameters; 12 models)

- L-c: Half-length of the TS-insert.
- L-d: Lateral spacing between the two inserts.
- Surface (web): C = ribbed, R = rectangular, and S = smooth.
- t-U: Flange thickness.
- W-L/W-U: Web/flange widths.

Table 6 Parametric study based on TS connection.

Connection	L-c (mm)	L-d (mm)	Web surface type	t-U (mm)	W-L (mm)	W-U (mm)
TS-200-300-S-30-50-100	200	300	S	30	50	100
TS-100-300-S-30-50-100	100	300	S	30	50	100
TS-300-300-S-30-50-100	300	300	S	30	50	100
TS-200-200-S-30-50-100	200	200	S	30	50	100
TS-200-400-S-30-50-100	200	400	S	30	50	100
TS-200-300-C-30-50-100	200	300	C	30	50	100
TS-200-300-R-30-50-100	200	300	R	30	50	100
TS-200-300-S-15-50-100	200	300	S	15	50	100
TS-200-300-S-0-50-100	200	300	S	0	50	100
TS-200-300-S-30-60-100	200	300	S	30	60	100
TS-200-300-S-30-50-80	200	300	S	30	50	80
TS-200-300-S-30-50-120	200	300	S	30	50	120

Based on the TS connection, shortening the TS-insert improved capacity by about 38%, a result attributed to steeper web angles and stronger anti-slip locking under compression. Additionally, bringing the two inserts closer together increased capacity by about 23% by promoting more even load sharing as non-linearity develops (Table 7).

Web surface engineering was the dominant factor: changing from a smooth to a rectangular or ribbed web increased capacity by up to 222% by enlarging effective contact area. Geometry changes that primarily increase volume had secondary effects: thicker flanges added 13% and wider webs added 23%, whereas flange width had only  $\approx 1\%$  impact because the flange primarily serves as a compressive seat while the web governs locking.

Notably, an aggressively contact-engineered TS variant (rectangular web) achieved an ultimate load of 9.45 kN ultimate load and a flexural capacity of 4.18 kN·m, rivaling the best BC variants reported in the study. These results suggest that the TS connection can match BC connection's performance when the web-panel interface is shaped to maximize contact and when length and spacing are optimized to mitigate differential load transfer between the two inserts.

Table 7 Results of parametric study of TS connection.

Connection	Ultimate load (kN)	Flexural capacity (kN·m)	$E_{I_{eff}}$ ( $10^3 \text{ Nm}^2$ )
TS-200-300-S-30-50-100	2.93	1.30	3.93
TS-100-300-S-30-50-100	4.04	1.79	2.73
TS-300-300-S-30-50-100	2.10	0.93	4.88
TS-200-200-S-30-50-100	3.61	1.60	2.77
TS-200-400-S-30-50-100	2.10	0.93	9.84
TS-200-300-C-30-50-100	5.70	2.52	15.25
TS-200-300-R-30-50-100	9.45	4.18	3.83
TS-200-300-S-15-50-100	2.87	1.27	3.46
TS-200-300-S-0-50-100	2.60	1.15	4.92
TS-200-300-S-30-60-100	3.62	1.60	3.87
TS-200-300-S-30-50-80	2.89	1.28	3.99
TS-200-300-S-30-50-120	2.98	1.32	2.57
Mean	3.74	1.66	5.17
Std. Dev.	2.04	0.90	3.71
COV	54.6%	54.6%	71.8%

3) ***GT connection (geometry of tongue/groove and dowel options)***

- Ag: Interlocking rib angle (modified in the second lamella only).
- t-g: Minimum tongue thickness (second lamella).
- d-ug: Minimum under-groove thickness (second lamella).
- CW: Optional dowels (with/without) used in selected variants.

All GT models positioned the joint at the panel mid-span.

Table 8 Parametric study based on GT connection.

Connection	L-c (mm)	MT	Ag ( $^{\circ}$ )	t-g (mm)	d-ug (mm)
GT-240-C-21-5-15	240	Standard wood	21	7.5	15
GT-120-C-21-5-15	120	Standard wood	21	7.5	15
GT-360-C-21-5-15	360	Standard wood	21	7.5	15
GT-240-S-21-5-15	240	CW	21	7.5	15
GT-240-Sd-21-5-15	240	Standard wood + CW dowel	21	7.5	15
GT-240-C-41-5-15	240	Standard wood	41	7.5	15
GT-240-C-21-10-15	240	Standard wood	21	12.5	15
GT-240-C-21-5-10	240	Standard wood	21	7.5	10
GT-240-C-21-5-20	240	Standard wood	21	7.5	20

In this group, a connection length of 240 mm was identified as optimal, delivering capacities 79% and 64% higher than 120 mm and 480 mm, respectively (Table 9). Shortening the joint length underdeveloped the interlocking ribs and shear transfer, whereas over-lengthening increased joint rotation, causing tensile limits to be reached sooner despite larger contact areas.

Replacing the second lamella with CW (instead of standard wood) increased capacity by 65%, confirming that a stronger transverse layer can effectively share load under shear. Adding dowels at the interface, however, reduced capacity by 6%, indicating that stress concentrations introduced by the dowels were not offset by additional shear transfer in this geometry.

Reducing the rib angle at the groove–tongue interface increased capacity by 47% by enlarging the effective shear contact. Minimum groove thickness had negligible effect ( $\approx 0\%$ ) because rib thickness and glue-enhanced edges govern separation, whereas a thicker tongue improved capacity by 13% through added connector volume and stiffness.

In contexts where reinforcement is limited to lamella 2 (due to fabrication or architectural constraints), these settings (CW in the transverse lamella, shallower ribs, and a thicker tongue) produce the most robust performance gains.

Table 9 Results of parametric study of GT connection.

Connection	Ultimate load (kN)	Flexural capacity (kN·m)	$EI_{eff}$ ( $10^3 \text{ Nm}^2$ )
GT-240-C-21-5-15	2.33	1.03	2.43
GT-120-C-21-5-15	1.30	0.58	1.19
GT-360-C-21-5-15	1.42	0.63	6.48
GT-240-S-21-5-15	3.85	1.70	2.69
GT-240-Sd-21-5-15	2.19	0.97	1.78
GT-240-C-41-5-15	1.58	0.70	2.48
GT-240-C-21-10-15	2.33	1.03	0.97
GT-240-C-21-5-10	0.84	0.37	2.67
GT-240-C-21-5-20	2.63	1.16	2.13
Mean	2.05	0.91	2.54
Std. Dev.	0.89	0.39	1.61
COV	43.6%	43.4%	63.3%

#### 4) ***GC connection (3 parameters; 8 models)***

- L-c: External plate length (connector axis aligned with panel mid-span).
- Surface: C (original ribbed), FD (flat + dowels), FR (rectangular), and FT (triangular).
- W-c: Plate width; an “×2” suffix denotes twin plates near the two side edges.

Table 10 Parametric study based on GC connection.

Connection	L-c (mm)	Connector's surface type	W-c (mm)
GC-240-C-600	240	C	600
GC-120-C-600	120	C	600
GC-360-C-600	360	C	600
GC-240-FD-600	240	FD	600
GC-240-FR-600	240	FR	600
GC-240-FT-600	240	FT	600
GC-240-C-240	240	C	240
GC-240-C-240×2	240	C	240 × 2

The results indicated that shorter external plates produced a modest 6% increase in capacity, consistent with narrower top/bottom surface angles that better resist slip-out (Table 11). In addition, the surface geometry had a strong influence on performance: compared with the original ribbed type, flat-with-dowels and rectangular surfaces increased capacity by about 10% and 66%, respectively, whereas a triangular profile decreased it by 34% due to smaller contact area. Narrowing a single plate improved capacity by 50%, while splitting into two narrow plates near the side edges increased it by 131% relative to the widest single plate. The twin-plate configuration also provided a notable stiffness advantage: the GC-240-C-240×2 variant achieved an effective stiffness  $EI_{eff}$  of  $\approx 14.31 \times 10^3 \text{ N}\cdot\text{m}^2$ , comparable to the stiffest BC baseline. This demonstrates that stiffness and peak strength may decouple depending on how the connector constrains rotation rather than solely on the load carried at peak.

Table 11 Results of parametric study of GC connection.

Connection	Ultimate load (kN)	Flexural capacity (kN·m)	$EI_{eff}$ ( $10^3 \text{ Nm}^2$ )
GC-240-C-600	1.67	0.74	2.28
GC-120-C-600	1.78	0.79	1.43
GC-360-C-600	1.18	0.52	3.33
GC-240-FD-600	1.83	0.81	3.13
GC-240-FR-600	2.78	1.23	1.41
GC-240-FT-600	1.10	0.49	3.37
GC-240-C-240	2.51	1.11	5.37
GC-240-C-240×2	3.85	1.70	14.31
Mean	2.09	0.92	4.33
Std. Dev.	0.918	0.41	4.23
COV	43.9%	43.8%	97.7%

5) ***DS connection (5 parameters; 10 models)***

- LC: Connector length along the span.
- D: Dowel diameter.
- N: Number of dowels per row; a “2c” suffix denotes two rows with closer row spacing (40 mm vs. 120 mm standard).
- d: Dowel-to-edge distance measured from the nearest lamellae edge.
- PL: Penetrated layers (top–middle–bottom), expressed as 1–2–3.

Table 12 Parametric study based on DS connection.

Connection	LC (mm)	D (mm)	N	d (mm)	PL
1-240-10-1-60-1—3	240	10	1	60	1—3
1-120-10-1-60-1—3	120	10	1	60	1—3
1-360-10-1-60-1—3	360	10	1	60	1—3
1-240-15-1-60-1—3	240	15	1	60	1—3
1-240-20-1-60-1—3	240	20	1	60	1—3
1-240-10-2-60-1—3	240	10	2	60	1—3
1-240-10-2c-60-1—3	240	10	2c	60	1—3
1-240-10-1-180-1—3	240	10	1	180	1—3
1-240-10-1-60-1—2	240	10	1	60	1—2
1-240-10-1-60-2—3	240	10	1	60	2—3

As for the DS connection, lengthening the rectangular tongue modestly increased capacity: extending from 240 to 360 mm raised the peak load by 9%, whereas shortening to 120 mm reduced it by 8% but enhanced ductility by triggering earlier rotation through a smaller lever arm (Table 13). Dowel diameter showed a clear optimum: Ø15 mm improved capacity by 15% compared with Ø10 mm, while Ø20 mm underperformed ( $\approx 10\%$  above baseline but below Ø15 mm) because the larger hole weakened the tongue cross-section enough to offset shear-area gains. Increasing the number of dowels raised strength by 12%; using two closely spaced rows improved performance by 9% but remained inferior to wider spacing, which distributed shear transfer more evenly and reduced stress peaks at the tongue–dowel interface. Longitudinal repositioning of dowels had negligible impact ( $\approx +4\%$ ), as the governing shear plane and tongue section remained constant. Likewise, varying penetration length within the studied range altered results by  $\leq 4\%$ , as all dowels already traversed the full transverse layer that carrying load. Overall, DS performance was controlled primarily by the tongue geometry and secondarily by dowel shear capacity: intermediate dowel diameters and wider row spacing offered the best trade-off, while very short tongues traded capacity for ductility.

Table 13 Results of parametric study of DS connection

Connection	Ultimate load (kN)	Displacement (mm)
1-240-10-1-60-1—3	5.40	114.07
1-120-10-1-60-1—3	4.95	106.52
1-360-10-1-60-1—3	5.88	113.92
1-240-15-1-60-1—3	6.23	113.14
1-240-20-1-60-1—3	5.93	112.46
1-240-10-2-60-1—3	6.04	113.23
1-240-10-2c-60-1—3	5.88	110.81
1-240-10-1-180-1—3	5.59	111.24
1-240-10-1-60-1—2	5.47	114.91
1-240-10-1-60-2—3	5.61	114.60
Mean	5.70	112.49
Std. Dev.	0.37	2.49
COV	6.51%	2.24%

6) ***HL connection (6 parameters; 10 models)***

- LC: Connector length along the span.
- DT1/DT2: Number of rows (upper/lower sub-assembly, where applicable).
- d: Dowel-to-edge distance measured from the nearest lamellae edge.
- TB: Thickness of the HL lower part at mid-span.

Table 14 Parametric study based on HL connection.

Connection	LC (mm)	DT1	DT2	TB (mm)	d (mm)
2-480-2-1-45-240	480	2	1	45	240
2-240-2-1-45-240	240	2	1	45	240
2-720-2-1-45-240	720	2	1	45	240
2-480-3-1-45-240	480	3	1	45	240
2-480-4-1-45-240	480	4	1	45	240
2-480-2-3-45-240	480	2	3	45	240
2-480-2-1-30-240	480	2	1	30	240
2-480-2-1-60-240	480	2	1	60	240
2-480-2-1-45-120	480	2	1	45	120
2-480-2-1-45-360	480	2	1	45	360

Varying the lap length from 240 to 720 mm shifted capacity only slightly (−4% to +6%), but shorter laps reduced ductility by up to 20%, indicating that longer laps allow greater rotational tolerance and a larger compression block before dowels govern (Table 15).

Increasing the number of dowels substantially boosted strength: +34% for added dowels and up to +55% when combined with favorable layouts, confirming that HL was connector-dominated and highly sensitive to redundancy. Furthermore, the sectional thickness proved decisive: increasing the upper half-thickness nearly doubled capacity (+81%), while excessive thinning reduced strength to 0.35 kN, underscoring the role of the upper layer as the compression flange. Moreover, dowel-to-edge distance also influenced performance, as moving dowels farther from the top edge increased capacity by 44% and stabilized behavior by mobilizing a larger lever arm and delaying local crushing. Overall, HL strength and stability depended primarily on dowel configuration and section geometry; maintaining adequate upper thickness and sufficient dowel redundancy was essential to prevent premature dowel-governed failure.

Table 15 Results of parametric study of HL connection.

Connection	Ultimate load (kN)	Displacement (mm)
2-480-2-1-45-240	1.98	125.06
2-240-2-1-45-240	2.09	100.52
2-720-2-1-45-240	2.05	114.44
2-480-3-1-45-240	2.27	119.66
2-480-4-1-45-240	2.65	116.20
2-480-2-3-45-240	3.07	114.84
2-480-2-1-30-240	3.58	101.56
2-480-2-1-60-240	0.35	130.67
2-480-2-1-45-120	2.00	129.43
2-480-2-1-45-360	2.86	113.12
Mean	2.29	116.55
Std. Dev.	0.87	10.26
COV	37.87%	8.81%

All parametric groups were tested under the same load/support/gauge definitions (Section 2.1.3), so that performance differences could be attributed directly to geometry/material changes in the connectors.

### **3.1.6. Design implications and scope**

Based on the performance observed, the results suggested a clear hierarchy of strategies. When strength governed, designs that directly engaged the outer lamellae and engineered the contact interface (such as BC with longer/wider and more numerous dovetails or TS with rectangular/ribbed webs and tuned length/spacing) consistently achieved the highest capacities. When serviceability governed, geometries that suppressed rotation without necessarily maximizing peak strength (such as twin, narrow GC plates near side edges) proved advantageous because they elevated  $EI_{eff}$  dramatically while keeping mass moderate. Where reinforcement had to remain in the transverse lamella, GT solutions benefited markedly from using CW in lamella 2, adopting shallower rib angles, and thickening the tongue; adding dowels in that interface proved counterproductive for capacity in this geometry set.

Across all families, the most powerful lever was not simply adding material but where and how the contact was created—surface shaping, placement, and the ability to couple tension and compression lamellae dominated the outcomes. For the DS connection, capacity improved most when the connection mobilized longer tongues and larger CW dowels ( $\text{\O}15$  mm), with two-row configurations and wider row spacing further stabilizing the response; short tongues could still be used, but they functioned best as a ductility-enhancing feature with a predictable strength penalty. For HL, performance hinged on preserving the upper-part thickness ( $\geq 45$  mm) as the effective compression flange, while increasing dowel-to-edge distance and introducing three or more dowels (especially in optimized layouts) enhanced both strength and reliability.

Collectively, the most influential levers emerged as tongue length, dowel diameter and dowel configuration in DS, and sectional thickness, dowel placement, and redundancy in HL. The magnitude of these effects was evident from the load capacity data: +8.80% (tongue length), +15.26% ( $\text{\O}15$  dowel), +11.71% (extra dowels) for DS, and +80.81% (upper-part thickness) and +55.05% (dowel number + layout) for HL.

## **3.2. Out-of-plane bending performance on glulam with edge connections (Paper IV)**

Except for the numerical studies, this Section provides the results of experimental tests based on the methodology and specimens described in Section 2.2.

### **3.2.1. Load–displacement response**

In the experimental studies based on glulam, all six specimens exhibited a clear elastic stage followed by post-yield softening governed by delamination and local shear in the lamellae near the edge connection (Figure 31). Specimens reinforced in the top/bottom layers (specimens 1–3) showed steeper elastic slopes than those reinforced through the transverse (middle) layer (specimens 4–6), indicating more efficient force transfer along the strong-axis lamella. Within the middle-layer group, higher elastic slopes tracked higher ultimate loads, suggesting that the geometric cuts at the panel edges (shear area

available for load transfer) had a greater influence on the post-yield deduction rate than connector details.

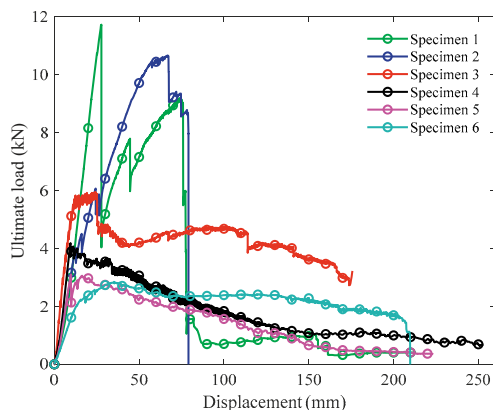


Figure 31 Load–displacement diagram of six specimens.

Moreover, ultimate loads spanned 2.85 kN to 11.74 kN across the matrix (Table 16). Specimen 1 achieved the highest capacity (11.74 kN), which was 312% greater than specimen 6 (2.85 kN). Specimens 1–2 (top/bottom reinforcement with belts/plates and dovetails) outperformed specimens 3–6 by about 64% on average, attributable to the reduced propensity for mid-depth delamination in the outer-layer reinforced layouts. It was found that the connection was routed through the transverse layer (specimens 4–6), premature delamination limited force transfer into the lamellae and capped capacity below the connector’s inherent strength. In specimen 3 (vertical dowels), capacity reflected a balance between dowel strength and lamellae delamination; friction at finger joints influenced the post-yield slope. This study showed that avoiding heavy milling in the transverse lamella layer and prioritizing outer-layer reinforcement increased load capacity.

Table 16 Ultimate load of six specimens under four-point bending.

No.	Tested specimens	Ultimate load (kN)
1	Specimen 1	11.74
2	Specimen 2	10.67
3	Specimen 3	5.96
4	Specimen 4	4.19
5	Specimen 5	3.10
6	Specimen 6	2.85
	Mean	6.42

### 3.2.2. Ductility

Ductility was computed as the ratio of displacement at failure to yield displacement, which ranged from 1.00 to 2.89 (mean 1.64) (Table 17). Specimen 6 reached the highest ductility (2.89), while specimen 4 had the lowest (1.00). Systems with tongue-and-groove plus vertical locking (4–5) showed a 65% reduction in ductility relative to other layouts, because delamination engaged the internal forces earlier and limited plastic redistribution between the connector and panel. By contrast, outer-layer reinforcement (specimens 1–2, 6) increased both yield and failure displacements by around 64% to 66% compared with middle-layer concepts, reflecting better engagement of tensile lamellae. The mean failure displacement (28.87 mm) exceeded a glulam baseline without a mid-span connection (25 mm) but remained below adhesive-free panels with only vertical dowels (35 mm), positioning these systems as moderately ductile for displacement-based design.

Additionally, specimen 1 (smaller densified-wood volume) and Specimen 2 (larger volume) achieved similar ductility (1.38 vs 1.32), indicating that connector volume alone did not govern ductility; stratification (depth) and milling geometry were more influential.

Table 17 Peak/yield displacements and ductility ratio.

No.	Tested specimen	Displacement at failure (mm)	Yield displacement (mm)	Ductility ratio
1	Specimen 1	27.65	20.06	1.38
2	Specimen 2	66.83	50.50	1.32
3	Specimen 3	24.17	10.95	2.21
4	Specimen 4	9.54	9.54	1.00
5	Specimen 5	9.83	9.25	1.06
6	Specimen 6	35.21	12.18	2.89
	Mean	28.87	18.75	1.64

### 3.2.3. Flexural properties (strength, modulus, effective stiffness)

Bending strength  $f_m$  ranged from 2.38 MPa to 9.78 MPa (mean 5.35 MPa). Specimen 1 performed the highest value (9.78 MPa), approximately 311% greater than specimen 6 (2.38 MPa). Two trends were observed: (i) longer connection length correlated with higher strength; and (ii) connections routed through the transverse layer (specimens 4–6) reduced strength by around 180% (group means 2.81 vs. 7.88 MPa), consistent with early delamination between the top and middle lamellae. The bending modulus  $E_m$  ranged from 0.62 GPa to 3.39 GPa, with the highest value in specimen 4 (3.39 GPa) and a comparably high value in specimen 1 (3.28 GPa). Effective joint stiffness  $EI_{eff}$  ranged from  $1.01 \times 10^4$  to  $5.49 \times 10^4 \text{ N} \cdot \text{m}^2$ , again peaking in specimen 4 ( $5.49 \times 10^4 \text{ N} \cdot \text{m}^2$ ) and closely followed by specimen 1 ( $5.31 \times 10^4 \text{ N} \cdot \text{m}^2$ ). These magnitudes were lower than those of reference glulam members without mid-span interruptions

reported in the literature (28.6–62.6 MPa; (Cai et al., 2021)), as the deliberate break at mid-span impaired load transfer from cross-grain to along-grain tension. Effective stiffness values also trended lower than those of larger test panels in related work due to geometry scaling effects.

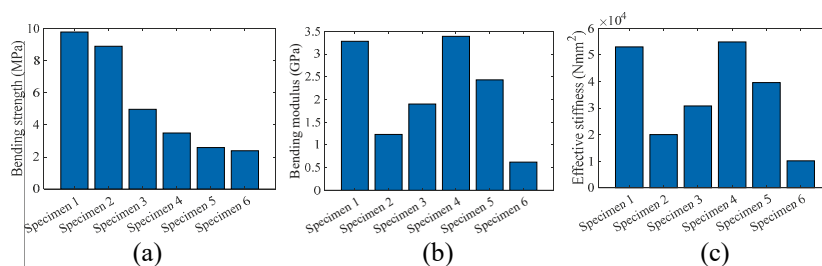


Figure 32 Flexural properties of six tested glulam beams, (a) bending strength, (b) bending modulus, and (c) effective stiffness of six tested specimens.

### 3.2.4. Rotation and moment resistance

Rotation at maximum moment ranged from  $0.81^\circ$  to  $5.65^\circ$ ; the largest rotation occurred in specimen 2 ( $5.65^\circ$ ), consistent with its high displacement capacity. Maximum moments followed the same capacity hierarchy: specimen 1 recorded the highest value (3.96 kN·m), followed by specimen 2 (3.60 kN·m), with the remaining layouts  $\leq 2.01$  kN·m. Longer connector length increased both rotation and moment (e.g., increasing length from 200 to 500 mm yielded up to +86% rotation and +76% moment in the best cases). Wider vertical connectors in the outer layer increased rotational capacity (up to +73%) by reducing solid outer lamellae width near mid-span. However, connector width did not increase moment capacity, which remained governed by reinforcement depth, longitudinal length, and geometry.

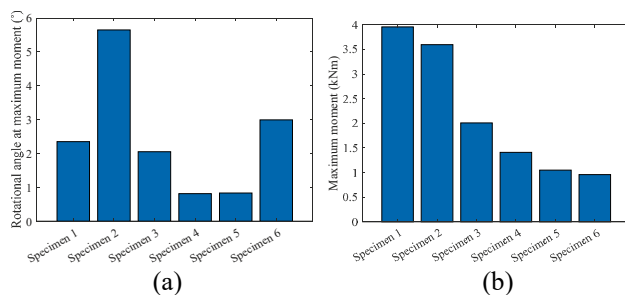


Figure 33 Bending performance of specimens 1–6: (a) rotational angle at maximum moment and (b) moment capacity.

### 3.2.5. Failure modes and connection mechanics

In all tested configurations (Figure 34), failure localized within the connection zone, most often governed by delamination between the top and middle lamellae. The progression of damage, however, differed across specimens, reflecting interaction between panel geometry and connector design.

In specimen 1, bottom-zone shear in the pine lamella initiated failure, followed by tensile rupture of the trapezoidal belt at the bottom edge. This sequence subsequently triggered half-depth delamination in the top belt along the grain, a response attributable to stiffness discontinuities between the 30 mm and 15 mm segments. Notably, the shear keys in timber “element 1” remained intact, highlighting their high parallel-to-grain shear stiffness.

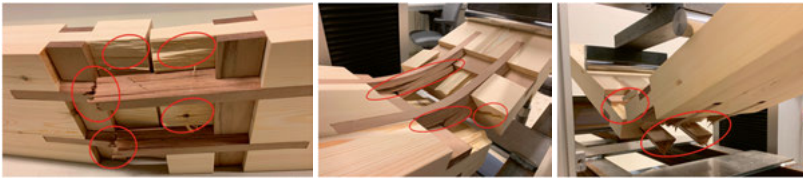
Specimen 2, by contrast, exhibited a single, concentrated shear–tension fracture across the middle lamella. The densified connectors showed no signs of damage, indicating substantial over-strength relative to the panel. This imbalance suggests that either reducing connector thickness/volume or increasing the thickness of the middle lamella could promote a more uniform failure progression.

As for specimen 3, the vertical dowels initiated cross-grain shear along the interface between the first and second lamellae. Here, the bottom lamella disengaged prematurely and contributed little to load transfer, implying insufficient activation of the dowel’s lower portion. An angled dowel insertion or alternative geometry may prevent this sliding and ensure more effective engagement of the bottom layer.

A different mechanism emerged in specimen 4, where the tongue-and-groove system, reinforced with one dowel and two belts, failed through dowel shear. The belts, however, remained intact, confirming their superior robustness as vertical connectors. Additional shear cuts were observed between adjacent belts on the same side, suggesting that thicker belts or greater spacing from the panel edge could mitigate such side-shear. Specimen 5 followed a similar trajectory, reproducing the delamination and side-shear patterns without actual connector fracture. This again points to an over-strength condition of the connectors relative to the panel edges and underscores the asymmetric nature of panel–connector interaction as the governing weakness.

Additionally, specimen 6 largely mirrored the dominant delamination between the top and middle lamellae observed elsewhere, while the bottom lamella remained inactive and undamaged. Cracks initiated at dovetail corners and were further influenced by surface knots, but the connectors themselves again showed no visible damage. This outcome suggests that the bottom connector either requires redesigning to become engaged or could be omitted in cases where capacity is primarily dictated by the upper lamella interface.

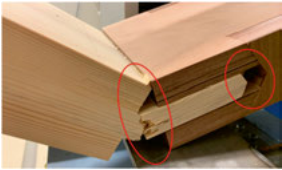
Moreover, these results revealed a consistent pattern: except for the slender dowels and the thin segment of the trapezoidal belt in specimen 1, densified-wood connectors were generally stronger than necessary, while the panel-edge geometry and transverse lamella ultimately controlled failure. Where delamination initiated early, the connectors transferred only a modest share of load. Consequently, refining the milled corner geometry and increasing the effective shear area in the lamellae appear to be more effective strategies for improving system capacity than further strengthening the connectors themselves.



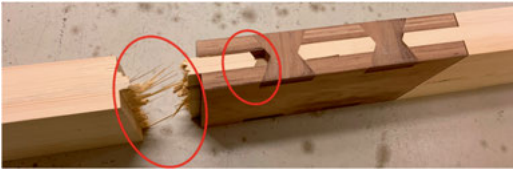
(a)

(b)

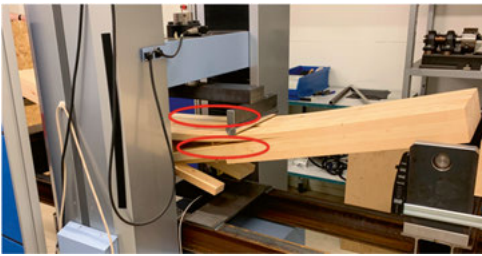
(c)



(d)



(e)



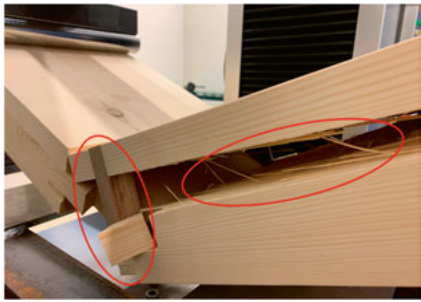
(f)



(g)



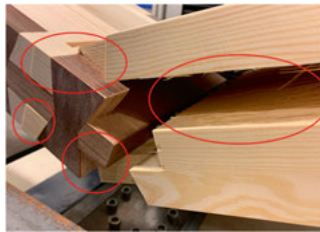
(h)



(i)



(j)



(k)



Figure 34 Failure modes.

### 3.2.6. Design recommendations

Based on the glulam experiments, the following points summarize the outstanding geometric and material choices for the proposed adhesive-free connections. They highlight the factors that affect capacity, stiffness, and ductility, and can be used as practical guidance when designing similar floor-type edge joints.

- **Reinforcement depth matters more than volume.** Outer-layer reinforcement consistently improved capacity and displacement metrics relative to middle-layer variants, even when densified-wood volume was smaller.
- **Connection length is a first-order driver.** Longer longitudinal engagement increased bending strength, rotation, and moment; for moment and rotation, the best cases rose by +76% and +86%, respectively.
- **Connector width increases rotation, not moment.** Wider vertical belts at the outer surface raised failure rotation (ductility) but did not increase moment capacity, which remained governed by depth, length, and geometry.
- **Dowel geometry requires re-engineering.** Vertical dowels were prone to shear at lamellae planes and to bottom-layer inactivity; angled insertion, increased cross-section, or hybrid belt–dowel concepts are promising.
- **Right-sizing connectors.** Undamaged plates/dovetails at failure indicate excess connector strength; reducing thickness/length where panels fail first can restore ductile balance and save material.

Additionally, effective stiffness values here were lower than those reported for larger, uninterrupted glulam members in the literature (Baño & Moltini, 2021; Cai et al., 2021; Mehra et al., 2021; Sotayo, Bradley, Bather, Oudjene, et al., 2020), which is expected given the intentional mid-span discontinuity and smaller geometry; likewise, bending strengths are well below continuous-span glulam. These differences validate that the edge-connection region governs structural response, and that improving lamellae interface integrity is the most direct path to raising global performance in floor-type members with mid-span joints.

### 3.3. Comparisons between proposed timber connections and typical steel connection

Connected to the verification model 4's settings in Section 2.1.1, this Section presents the performance of verification model 4 as well as the structural results of proposed timber connections when they are adapted to the dimensions and boundary conditions of verification model 4. Hence, the comparison between proposed timber connections and steel-based connections on CLT were obtained.

#### 3.3.1. Results of verification model 4

In verification model 4 (Section 2.1.1), the specimen in the experiment was tested with three repetitions. The results of three repetitions and the average value from the experimental test were compared with the numerical simulations. It was found that the numerical results matched the experimental results throughout the whole loading processing (Figure 35), where the elastic behaviors were similar and the failure values were close as well (especially experiment 2 and the average). Table 18 provides the maximum moment and the corresponding rotational angle at failure of each test, where the difference percentage between each of the experimental results and numerical simulation are presented as well. Based on the maximum bending moment, the average result from the experimental test (2.95 kNm) was 2.02% higher than that of the numerical model (2.89 kNm).

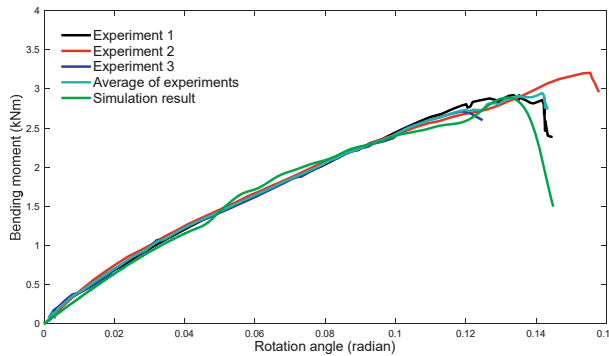


Figure 35 Verification comparison between experimental and numerical results.

Table 18 Results from verification model 4.

	Rotation angle at max moment (Radian)	Percentage	Max moment (kNm)	Percentage
Experiment 1	0.14	2.50%	2.92	1.16%
Experiment 2	0.16	17.82%	3.21	10.99%
Experiment 3	0.12	-10.01%	2.71	-6.08%
Average value	0.14	7.43%	2.95	2.02%
Numerical modeling	0.13	-	2.89	-

### 3.3.2. Geometries of timber connections on 5-ply CLT panel

In order to compare the structural performance of the self-developed six AF timber connections (Section 2.1.3) and the metallic connections in verification model 4, they should be applied on the panels with identical geometries and material properties. Therefore, these edge connections were adjusted and adapted to the 5-ply CLT panels (which were the same as verification model 4) based on their dimensions, element numbers, and placement locations (Figure 36).

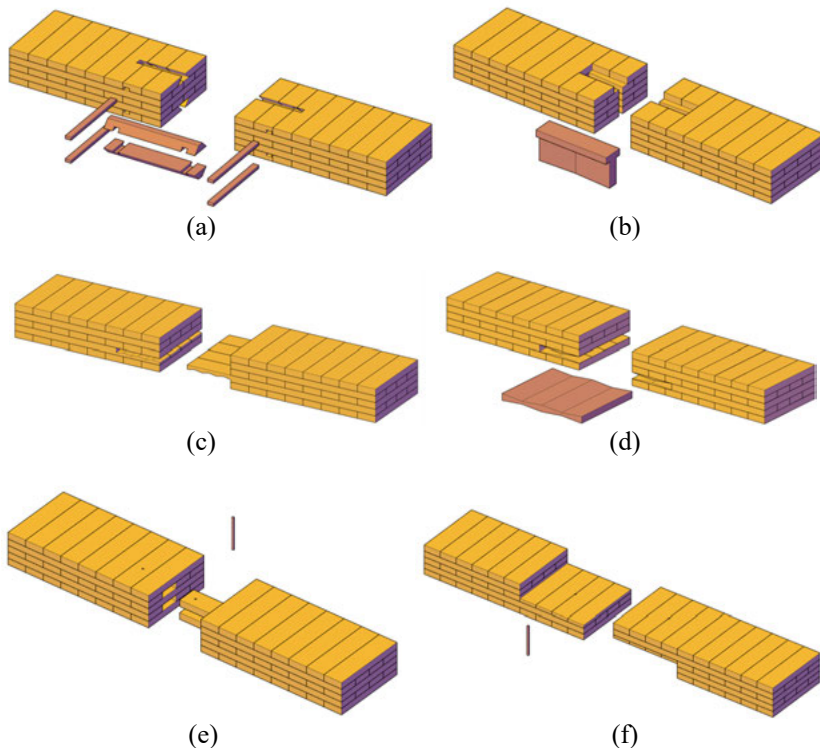


Figure 36 Six timber connections on 5-ply CLT panel, (a) AF Timber connection 1 – BC connection, (b) AF Timber connection 2 – TS connection, (c) AF Timber connection 3 – GT connection, (d) AF Timber connection 4 – GC connection, (e) AF Timber connection 5 – DS connection, and (f) AF Timber connection 6 – HL connection.

### 3.3.3. Results of proposed timber connections

By simulating the 5-ply CLT panels with six AF timber connections (Section 3.3.2) in ABAQUS and using the identical settings (out-of-plane four-point bending) as verification model 4, the bending results of all timber connections were obtained and compared with the steel connections in experiment (Figure 37). It was observed that AF timber connection 1 had the highest stiffness and the AF timber connection 2 had the lowest. This is because AF connection 1 was placed in the outermost lamellae layer and was parallel to the panel's

longitudinal direction, which bore load at its strong direction and locked the panel edge at the place with highest internal force.

As for AF timber connection 2, the loads were main held by the web's vertical surface, where load transfer highly depends on the web's angle and friction factor. Therefore, a minor amount of internal load from the CLT panel was transferred and carried by the connector itself, which causes a relatively lower stiffness. Meanwhile, AF timber connections 1, 3, 5, and 5 had higher stiffness than the steel connection.

Moreover, it was depicted that AF timber connections 1, 5 and 6 performed smaller ductility than the other specimens, which exhibited brittle failure at an earlier stage than others. The potential reason could be that effective connectors in these three samples were relatively small and the CW connectors endured the most force than the panels. Therefore, the CW connector broke before any other failures happen (such as failure from panels and adhesives), which caused this phenomenon.

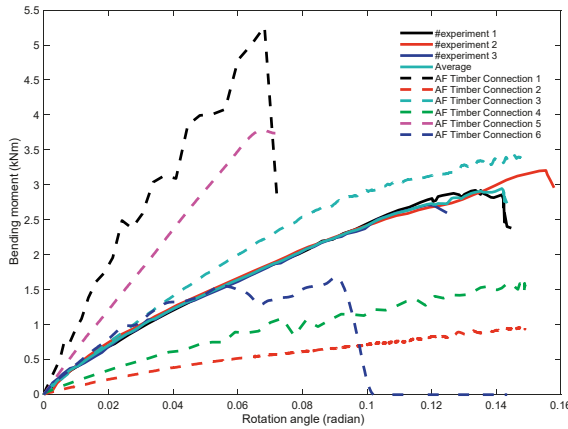


Figure 37 Bending moment and rotation angle graphs of steel and timber connections.

According to the results from Table 19, the bending moment of all six AF timber connections ranged from 0.96 kNm to 5.26 kNm. Compared with the moment of the steel connection, the six timber connections showed a difference range of -67.42% to 78.53%. It was noticed that AF timber connection 1 had the highest bending moment of 5.26 kNm, which is 78.53% higher than that of the steel connection. This can be explained by the differences in material properties between the CW connector (applied in AF timber connection) and plywood splines (applied in steel connection).

In the steel connection, the plywood splines were used together with the steel screws (vertically inserted). The steel screws were acting as a locker, absorbing the shear force and transferring it to the splines at the outermost layer. However, AF timber connection 1 was placed in the same location with thicker connector as well as higher material properties.

Furthermore, the AF timber connections 1, 3, and 5 exhibited higher moments than the steel AF connection by 78.53%, 16.06%, and -28.23%, AF timber

connections 2, 4, and 6 showed lower capacities (-67.42%, -45.16%, and -43.05%). These results indicated that (1) the enforcement in the lower part of the mid-span of the panel is more critical than the upper part, and (2) timber connectors are competitive with steel connection in terms of structural performance.

Table 19 Bending results of six AF timber connections and steel connection.

	Rotation angle at max moment (Radian)	Percentage	Max moment (kNm)	Percentage
AF Timber connection 1	0.07	-53.21%	5.26	78.53%
AF Timber connection 2	0.15	4.94%	0.96	-67.42%
AF Timber connection 3	0.15	2.82%	3.42	16.06%
AF Timber connection 4	0.15	4.16%	1.62	-45.16%
AF Timber connection 5	0.07	-52.29%	3.78	28.23%
AF Timber connection 6	0.09	-36.20%	1.68	-43.05%
Steel connection	0.14	-	2.95	-

### 3.4. Structure type 1: Environmental performance of edge connections and CLT with edge connections (Paper V)

Apart from the structural behavior of CLT slab interacting with timber connections, their environmental performances were analyzed and summarized in the current Section, which is based on the pure slab elements (structure type 1) from Section 2.3.1.

#### 3.4.1. Scenario 1 (FU1: 1 m<sup>2</sup> slab including edge connection)

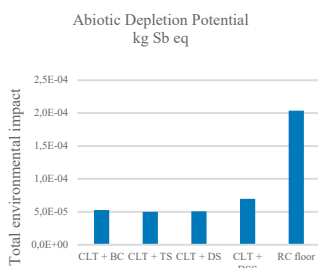
Under Scenario 1, the system-level comparison across the ten CML midpoint indicators showed that all CLT-based slabs outperform the RC reference, with the largest separations observed in ADP, GWP, ODP, HTP, FAETP, MAETP, AP, and EP. As quantified in Table 20, the percentage differences between timber slabs and RC are pronounced (ADP 75.5%, GWP 90.1%, ODP 79.5%, HTP 82.7%, FAETP 90.0%, MAETP 86.8%, AP 78.1%, and EP 76.9%) whereas the gaps are smaller in TETP and POCP, indicating lower material sensitivity in those categories. These patterns corroborate the established climate and resource advantages of timber under Swedish conditions and provide a quantitative basis for the conclusions drawn here.

Within the CLT cohort, CLT+DS and CLT+TS consistently emerge as the lowest-impact performers across most categories. DS is slightly lower than TS in six indicators (GWP, ODP, FAETP, MAETP, POCP, EP), while TS leads in four (ADP, HTP, TETP, AP). By contrast, CLT+DSS is the highest-impact timber option, with GWP, FAETP, and MAETP approximately doubling relative to the other CLT slabs. These rankings, visible in Figure 38 and Table 20,

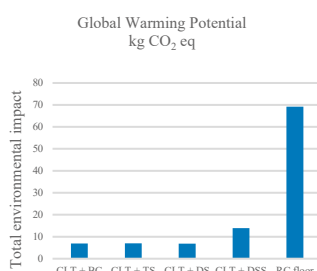
reflect the compounding effects of steel burdens in DSS and mass/processing effects associated with the heavier timber geometries.

Table 20 Total environmental impacts based on FU1.

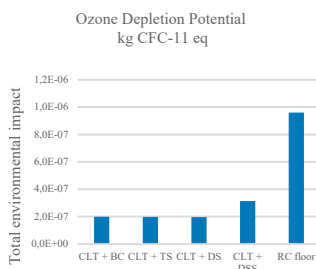
Categories	Unit	CLT + BC	%	CLT + TS	%	CLT + DS	%	CLT + DSS	%	RC floor slab	%
ADP	kg Sb eq	5.259E-05	74.2	4.989E-05	75.5	5.067E-05	75.1	6.959E-05	65.8	2.037E-04	0
GWP	kg CO <sub>2</sub> eq	6.938	90.0	7.014	89.9	6.846	90.1	13.884	79.9	69.207	0
ODP	kg CFC-11 eq	1.99E-07	79.2	1.98E-07	79.3	1.97E-07	79.5	3.13E-07	67.4	9.59E-07	0
HTP	kg 1.4-DB eq	7.347	81.7	6.938	82.7	7.034	82.5	11.075	72.4	40.173	0
FAETP	kg 1.4-DB eq	3.738	89.5	3.630	89.8	3.568	90.0	8.368	76.6	35.695	0
MAETP	kg 1.4-DB eq	7254.297	86.5	7460.617	86.1	7086.827	86.8	16922.130	68.4	53568.766	0
TETP	kg 1.4-DB eq	0.143	39.5	0.136	42.6	0.140	40.7	0.168	28.9	0.237	0
POCP	kg C <sub>2</sub> H <sub>4</sub> eq	6.275E-03	55.5	6.430E-03	54.4	6.268E-03	55.5	1.096E-02	22.2	1.409E-02	0
AP	kg SO <sub>2</sub> eq	0.051	77.6	0.050	78.1	0.051	77.8	0.073	68.2	0.230	0
EP	kg PO <sub>4</sub> <sup>3-</sup> eq	0.017	76.6	0.017	76.4	0.017	76.8	0.031	57.8	0.074	0



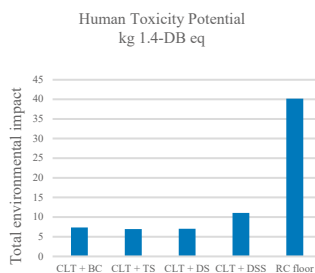
(a)



(b)



(c)



(d)

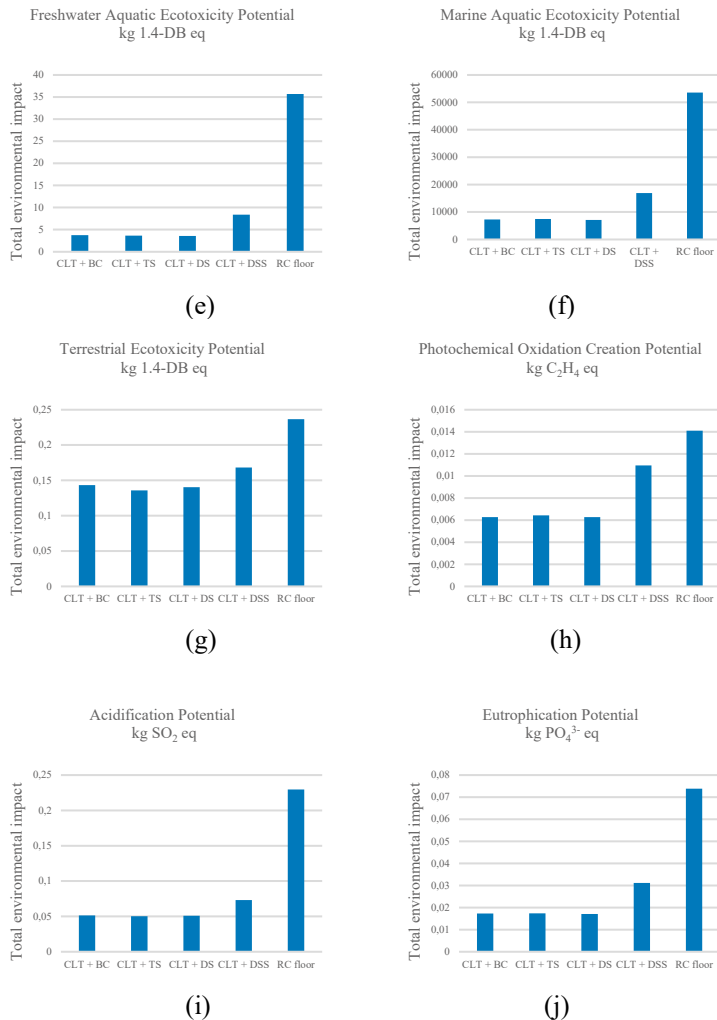


Figure 38 Total environmental impact of five floor slab systems per FU1 for categories of: (a) ADP, (b) GWP, (c) ODP, (d) HTP, (e) FAETP, (f) MAETP, (g) TETP, (h) POCP, (i) AP, and (j) EP.

Furthermore, decomposing the slab into panels and connections clarifies the mechanisms behind these rankings. It was observed that the DS connection is effectively negligible at the slab scale, contributing <0.1% in every indicator (functionally zero at FU1). At the opposite end, the DSS connection contributes around 10% of the slab impact in seven categories (AP, EP, POCP, TETP, ODP, GWP, ADP) and substantially more in toxicity-oriented indicators (FAETP 38.2%, MAETP 26.5%, HTP 18.5%), a profile primarily driven by steel production. The BC and TS connections sit between these extremes, with connection shares typically in the -6% to +6% range; negative values arise

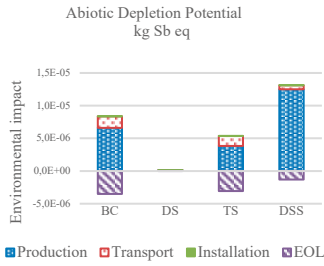
from timber reuse credits at EOL. The component-level attribution therefore aligns with the whole-system ranking: mass-light, timber-only geometries push connection shares toward zero, whereas steel shifts toxicity and resource indicators upward.

Moreover, the mass distribution across slab concepts explains why DS appears ‘invisible’ under FU1. DS accounts for only 0.04% of the timber slab mass, the lowest among all connections; by comparison, BC represents  $\approx 12.8\%$ , TS  $\approx 11.7\%$ , and DSS  $\approx 5.8\%$  of slab mass. Because transport burdens scale with mass, BC and TS are penalized more strongly than DS on a per-slab basis, and this penalty grows with joint density at the building scale. This mass advantage is a key reason DS maintains its lead in categories sensitive to mass-dependent logistics.

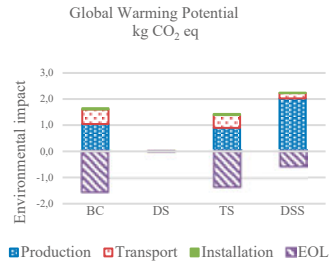
In addition, the observed impact differences between DS and TS can be interpreted through process-level contributions. Although DS is lowest overall in six indicators, TS leads in ADP, HTP, TETP, and AP (Figure 38). Tracing contributions reveal that TS uses more sawn wood and generates more municipal solid waste and waste wood than DS, which elevates MAETP and EP while leaving other levers comparatively favorable; conversely, DS’s extremely low mass and simple machining keep impacts uniformly suppressed. In effect, DS minimizes the board through geometry and mass efficiency, whereas TS achieves selective wins in categories less sensitive to those drivers.

#### **3.4.2. Scenario 2 (FU2: 1 m of connection; panels excluded)**

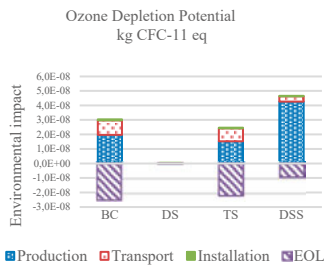
Under Scenario 2, the stage analysis indicates that production is the dominant contributor for all connection types and impact categories, with transport remaining a second-order term (typically 45%–99% lower than production) and installation contributing only marginally because lifting energy is low and the operations are simple, primarily drilling and self-tapping (Figure 39). Category sensitivities align with the compiled inventory: ADP and HTP are chiefly driven by electricity; GWP and ODP by heat supply; FAETP and MAETP by municipal solid-waste handling; TETP by wood-ash mixtures; POCP by adhesives; and AP/EP by diesel. These levers are strongest for DSS, whose steel-based materials amplifies electricity and processing dependencies, and more muted for timber-only variants in which sawn-wood production is the principal driver. Transport burdens scale closely with connection mass: heavier timber-only concepts such as BC and TS exhibit higher transport shares than DSS and DS yet remain well below production in absolute terms. In HTP, FAETP, MAETP, TETP, and POCP, production exceeds transport by approximately 27× to 96×, underscoring that improvements to mill energy mixes, waste management, and material formulations generally matter more than logistics within the Swedish distance assumptions.



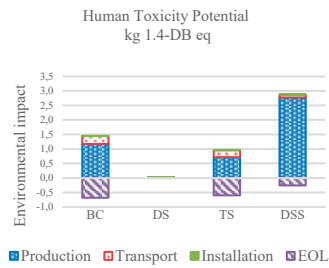
(a)



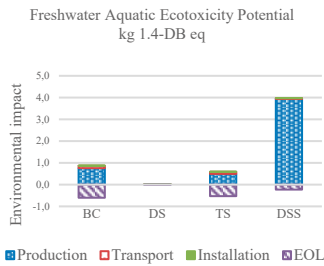
(b)



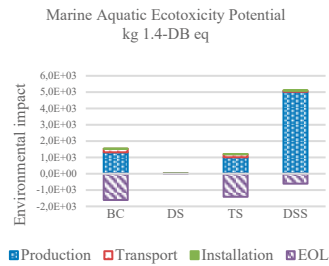
(c)



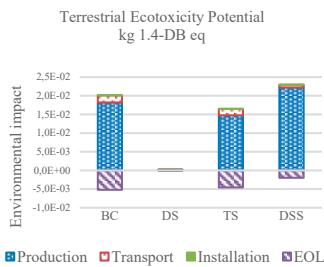
(d)



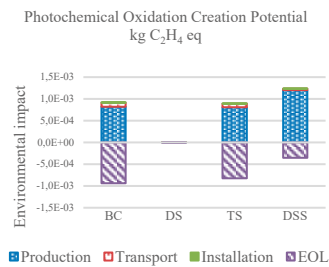
(e)



(f)



(g)



(h)

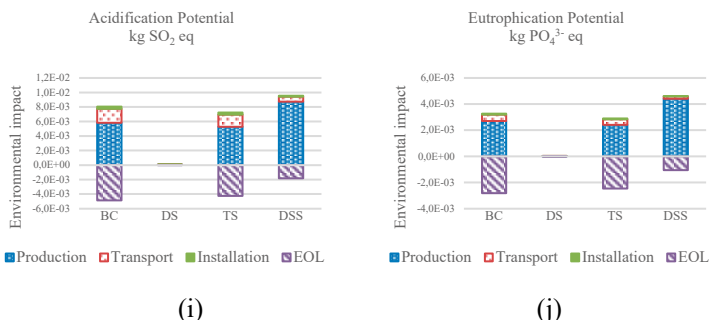


Figure 39 Environmental impact stage contribution of four connections per FU2 for categories of: (a) ADP, (b) GWP, (c) ODP, (d) HTP, (e) FAETP, (f) MAETP, (g) TETP, (h) POCP, (i) AP, and (j) EP.

When the connection is assessed independently, the EOL treatment and associated D-phase credits become decisive, particularly for timber-only geometries (Table 21). As Table 22 depicts, excluding EOL (thereby removing reuse or energy-recovery credits) substantially increases impacts sharply for BC and TS: GWP increases by  $\sim 11.9\times$  for BC (1188.3%) and  $\sim 14.6\times$  for TS (1458.1%), accompanied by multi-fold increases in FAETP and POCP (up to  $\sim 56\times$  for POCP in BC). DS is comparatively less sensitive because its lower mass yields less recoverable timber, while DSS remains relatively insensitive across most categories due to the predominance of steel in its production profile (although notable differences persist for FAETP and MAETP). The inference is clear: inclusion of D-phase benefits is critical to represent the performance of timber-only connections accurately under FU2, and the effect intensifies with larger, mass-rich configurations.

Table 21 Total environmental impacts of floor slab systems studied (per FU2) through LCA including EOL stage.

Impact categories	Unit	BC edge connection with EOL	DS edge connection with EOL	TS edge connection with EOL	DSS edge connection with EOL
ADP	kg Sb eq	4.839E-06	8.557E-08	2.277E-06	7.698E-06
GWP	kg CO <sub>2</sub> eq	0.112	0.004	0.080	1.438
ODP	kg CFC-11 eq	5.523E-09	1.209E-10	2.939E-09	2.647E-08
HTP	kg 1.4-DB eq	0.767	0.014	0.361	1.348
FAETP	kg 1.4-DB eq	0.265	0.007	0.060	0.828
MAETP	kg 1.4-DB eq	-79.977	6.185	-209.106	1450.017
TETP	kg 1.4-DB eq	1.499E-02	1.456E-04	1.198E-02	1.947E-02
POCP	kg C <sub>2</sub> H <sub>4</sub> eq	-1.613E-05	1.973E-08	7.302E-05	8.864E-04
AP	kg SO <sub>2</sub> eq	3.188E-03	2.630E-05	2.965E-03	7.316E-03
EP	kg PO <sub>4</sub> <sup>3-</sup> eq	4.531E-04	8.377E-06	4.294E-04	3.083E-03

Table 22 Total environmental impacts of floor slab systems studied (per FU2) through LCA excluding EOL stage.

Impact categories	Unit	BC edge connection without EOL	DS edge connection without EOL	TS edge connection without EOL	DSS edge connection without EOL
ADP	kg Sb eq	7.698E-06	9.924E-08	4.784E-06	1.288E-05
GWP	kg CO <sub>2</sub> eq	1.438	0.010	1.243	2.169
ODP	kg CFC-11 eq	2.647E-08	2.210E-10	2.131E-08	4.510E-08
HTP	kg 1.4-DB eq	1.348	0.017	0.871	2.837
FAETP	kg 1.4-DB eq	0.828	0.010	0.554	3.956
MAETP	kg 1.4-DB eq	1450.017	13.504	1132.667	5064.111
TETP	kg 1.4-DB eq	1.947E-02	1.670E-04	1.590E-02	2.271E-02
POCP	kg C <sub>2</sub> H <sub>4</sub> eq	8.864E-04	4.337E-06	8.645E-04	1.226E-03
AP	kg SO <sub>2</sub> eq	7.316E-03	4.605E-05	6.585E-03	9.287E-03
EP	kg PO <sub>4</sub> <sup>3-</sup> eq	3.083E-03	2.096E-05	2.736E-03	4.551E-03

### 3.4.3. Cross-scenario synthesis

Synthesizing results across FU1 (1 m<sup>2</sup> slab including the edge connection) and FU2 (1 m of connection, panels excluded) yields a consistent ranking in most midpoint categories: DS ≈ TS < BC << DSS. DS attains the lowest impacts primarily by minimizing mass and machining requirements, while TS performs closely by balancing advantages in ADP, HTP, TETP, and AP despite its higher wood input. BC carries a modest penalty driven by added mass and processing, and DSS is consistently disadvantaged by the burdens and toxicity footprint associated with steel manufacturing. Where EOL reuse and energy-recovery are credited, mass-rich timber solutions (BC and TS) recover more benefit than DS simply because they contain more recoverable wood; however, they do not surpass DS at the slab scale when impacts are aggregated across categories.

Additionally, these conclusions are sensitive to the chosen system boundary. A1–A5-only scopes (such as those used in Swedish climate declarations) reduce the absolute advantage of timber connections by omitting D-phase benefits, although the relative ordering of DS, TS, BC, and DSS generally remains intact. In an A-only view, the optimization focusses shifts on production-stage material and energy choices, whereas design-for-reuse strategies reveal their value only in cradle-to-cradle scopes that include D-phase credits. The stage analysis, therefore, offers practical guidance: when assessments exclude EOL, prioritize mill energy, material recipes, and machining efficiency; when assessments are cradle-to-cradle, place additional emphasis on reusability and recovery pathways.

Furthermore, scaling from slabs to whole buildings, edge connections constitute a small but non-negligible share of total impacts. Extrapolations from slab-level shares and stage sensitivities indicate that DS contributes on the order of ~0.01% – 0.05% of whole-building GWP, BC and TS typically remain

$\leq 0.2\% - 0.5\%$ , and DSS can approach  $\sim 1\%$  in toxicity-oriented indicators in joint-dense layouts while staying  $\leq 0.3\%$  for GWP in typical designs. These bounds are indicative rather than prescriptive, as project-specific values will vary with span strategy, panelization, grid geometry, joint density, transport distances, and sourcing. Nonetheless, even tenths or hundredths of a percent accumulate under sectoral net-zero pathways, particularly when multiplied across portfolios of projects, reinforcing the value of mass-efficient, timber-only geometries and careful boundary-aware optimization.

#### **3.4.4. Implications for design and manufacturing**

For standard floor slab joints, the environmentally preferable default is a light, timber-only detail, with DS and TS consistently emerging as first choices. DS should be prioritized where minimizing mass and machining overhead is critical, while TS is attractive in contexts where ADP, HTP, TETP, and AP are the primary decision indicators. By contrast, DSS should be limited to localized necessities (such as specific stiffness requirements or assembly constraints) rather than deployed in long, repetitive runs, given its toxicity and resource burdens; a simple way to shrink FAETP, MAETP, and HTP without undermining a timber panel strategy is to reduce the count of steel-rich joints.

Moreover, improvement measures should be aligned with category-specific drivers identified in the stage analysis. Decarbonizing electricity reduces ADP and HTP; decarbonizing and optimizing process heat lowers GWP and ODP; minimizing municipal-solid-waste generation curbs FAETP and MAETP; controlling wood-ash pathways mitigates TETP; optimizing adhesive recipes and dosages diminishes POCP; and reducing diesel use in logistics decreases AP and EP. These levers are most consequential in production, whereas transport fuel switching (e.g., to renewable diesel) offers benefits but remains second-order within the distances modeled here. Because EOL credits strongly influence timber-only connections, design-for-reuse becomes central to realizing D-phase benefits in practice; selectable, non-destructive connectors, reversible detailing, and thorough documentation should therefore be integrated from the outset. To prevent boundary-driven misinterpretation of performance, stakeholders should also state system boundaries explicitly in targets and declarations, ensuring that optimization choices are consistent with whether assessments are A-only or cradle-to-cradle.

#### **3.4.5. Generalizability and limitations**

In this thesis, these findings are grounded in a Swedish context with short transport distances and a low-carbon electricity mix. Regions with more carbon-intensive grids or longer logistics would see larger A-phase burdens and potentially narrower absolute gaps, but two inferences are robust: production dominates, and steel content disproportionately drives toxicity-related indicators. Forestry dynamics (biogenic carbon timing, land-use change, biodiversity) are not explicitly resolved here and would refine the GWP narrative if modeled dynamically. Similarly, varying recycled content in steel, adhesive formulations, and mill energy mixes would shift ADP/HTP/FAETP/MAETP/POCP. These sensitivities point to fruitful

directions for future scenario testing around supplier mixes and circular design choices.

### **3.4.6. Conclusions and discussion**

Based on the LCA results for structure type 1, the following points summarize the main conclusions about how CLT, adhesive-free CLT, and RC systems perform across FU1 and FU2 and impact categories, including implications for slab- and building-scale design choices:

- At FU1, CLT slabs substantially reduce impacts compared with RC in eight categories, with smaller but still meaningful improvements in TETP and POCP; CLT+DS and CLT+TS are the most favorable timber options.
- The DS connection's slab-level contribution is <0.1% across all categories, while DSS contributes around 10% in most categories and far more in FAETP/MAETP/HTP because of steel.
- At FU2, production dominates; transport is second-order, and installation is minor; category sensitivities can be traced to specific upstream processes (electricity, heat, MSW, diesel, adhesives).
- EOL modeling is decisive for timber-only connections (excluding D-phase can inflate GWP by ~12 – 15× for BC/TS), with similarly large effects in POCP and FAETP (but has smaller effects for DSS in most categories).
- At the building scale, edge-connection shares are small but non-negligible (DS ~0.01% – 0.05% of building GWP; BC/TS ≤0.5%; DSS up to ~1% in toxicity indicators), so minimizing steel and designing for reuse remain justified, especially under net-zero pathways.

### **3.5. Structure type 2: LCA on CLT, adhesive-free CLT, and RC slabs (Paper VI)**

In this Section, the focus moves from full slab systems with connections to the slabs themselves, treated as individual structural elements. Structure type 2 (Section 2.3.2) represents slab configurations of CLT, AFCLT, and RC slab, all modeled under the same LCA framework, assumptions, and scenarios as structure type 1 (Sections 2.3.3, 2.3.4, and 2.3.5). The purposes are: (1) isolate and compare the environmental impacts solely generated by the panel products, excluding the effects of edge connections and secondary components and (2) identify key factors of the environmental performance of CLT and related wood slabs, such as wood species, adhesive use, panel thickness, and reinforcement strategies. This will provide a clearer foundation for understanding how product-level design choices affect the overall climate and carbon footprint of slab systems.

### 3.5.1. Whole-life performance across ten CML indicators

Within structure type 2, the five slabs display a clear hierarchy across all mid-point categories: AFCLT2 (dowel-laminated, adhesive-free) is the lowest-impact option, while RC is the highest overall, often by an order of magnitude. Using GWP as an anchor, AFCLT2 totals 3.779 kg CO<sub>2</sub>-eq per FU1; SCLT, AFCLT1, AFCLT3, and RC register 7.013, 7.974, 10.576, and 61.932 kg CO<sub>2</sub>-eq, respectively. Expressed relative to the best performer, RC ranges from 519% to 1784.3% across categories, underscoring the burden of cement, reinforcement, and mass-driven operations.

Within the timber family the ranking is stable in every category: AFCLT2 is consistently lowest, SCLT and AFCLT1 cluster in the mid-range, and AFCLT3 is highest. The mechanisms behind this pattern are structural rather than incidental: AFCLT2 eliminates surface adhesives and avoids complex CNC milling, so it carries less electricity demand, fewer board/connector inputs, and lower total mass per FU1. AFCLT3, by contrast, is heavier and milling-intensive; those two features propagate through several indicators. The full set of AFCLT2 totals illustrates the breadth of its advantage (Table 23).

Furthermore, two exceptions to the ‘RC is worst’ rule appear at TETP and POCP, where RC’s totals are lower than those of the heaviest timber option (AFCLT3). At the production phase, TETP is 0.1623 kg 1,4-DB-eq for RC vs. 0.242 kg 1,4-DB-eq for AFCLT3; POCP is 0.00996 kg C<sub>2</sub>H<sub>4</sub>-eq for RC vs. 0.01592 kg C<sub>2</sub>H<sub>4</sub>-eq for AFCLT3. The difference is linked to wood-processing and waste-treatment profiles, including contributions from wood ash management and sawing; nevertheless, RC remains dominant in most other categories due to concrete and steel production plus mass-driven stages.

Table 23 Total environmental impacts within structure type 2.

Categories	Unit	SCLT	AFCLT1	AFCLT2	AFCLT3	RC slab
ADP	kg Sb eq	4.986E-05	4.077E-05	2.401E-05	5.082E-05	1.81 E-04
GWP	kg CO <sub>2</sub> eq	7.013	7.974	3.779	10.576	61.932
ODP	kg CFC-11 eq	1.982E-07	1.646E-07	8.249E-08	2.107E-07	7.783E-07
HTP	kg 1,4-DB eq	6.932	7.068	4.078	9.000	30.034
FAETP	kg 1,4-DB eq	3.627	4.227	2.360	5.436	20.409
MAETP	kg 1,4-DB eq	7457.867	8726.051	4472.192	10907.686	34655.31
TETP	kg 1,4-DB eq	0.136	0.179	0.095	0.221	0.200
POCP	kg C <sub>2</sub> H <sub>4</sub> eq	0.006	0.009	0.004	0.011	0.0106
AP	kg SO <sub>2</sub> eq	0.050	0.062	0.031	0.076	0.205
EP	kg PO <sub>4</sub> <sup>3-</sup> eq	0.017	0.024	0.012	0.031	0.061

### 3.5.2. Phase-resolved contributions and controlling mechanisms

Production (A1–A3) is the controlling phase for all slabs, frequently exceeding 100% of the whole-life total because EOL credits (Module D) are negative and

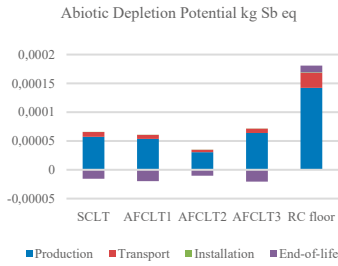
pull totals downward. Across categories (Figure 40), production contributes 110.05% – 181.34% for SCLT, 113.07% – 192.45% for AFCLT1, 108.22% – 196.68% for AFCLT2, 109.80% – 177.17% for AFCLT3, and 67.97% – 153.24% for RC. Dominance is most pronounced in GWP, FAETP, MAETP, POCP, and EP, where raw material production and process electricity overwhelm smaller stage contributions.

Furthermore, subdividing timber variants further can clarify their driving factors. Sawn-wood production largely governs GWP and contributes materially to MAETP because both the volume and density of lumber scale the impacts; thus, any design decision that lowers board input yields immediate climate and marine ecotoxicity benefits. Process electricity for CLT production and CNC milling is the primary lever behind FAETP; for that reason, AFCLT1/AFCLT3, with more complex milling, score worse than AFCLT2 despite their adhesive-free laminations. For ADP, ODP, and HTP, the balance shifts between PUR and lumber mass: SCLT carries more PUR, increasing ADP/ODP, whereas AFCLT1/AFCLT3 carry more wood and electricity, which can drive HTP above that of SCLT; HTP is 7.068 and 9.000 kg 1,4-DB-eq for AFCLT1 and AFCLT3, both higher than SCLT's 6.932, indicating the outsized role of wood mass in this category. AP and EP correlate with final product mass and incineration/raw-material extraction: the heaviest wood design, AFCLT3 ( $\approx 56.1$  kg per FU1), records the highest AP and EP among timber slabs.

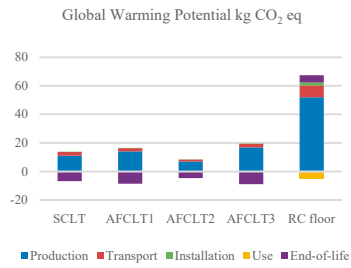
Moreover, transport (A4) and installation (A5) are consistently minor for all slabs because logistics are domestic, installation procedures are simple, and energy demand scales with mass; switching to renewable electricity for trucks and cranes would trim already small shares but would not alter rankings.

Considering the EOL behavior and Module D, the timber systems assume 80% reuse as structural timber and 20% incineration with energy recovery; credits are modeled as avoided burdens in SimaPro, so they appear as negative contributions to several categories. As a fraction of the total, EOL exhibits its greatest influence for wood in GWP (85.02-122.99%), ODP (55.39-90.84%), FAETP (65.2-80.28%), MAETP (86.39-108.77%), POCP (50.27-67.97%), and EP (52.68-71.65%), again with negative signs that offset production. Heavier timber products have larger absolute credits because reuse mass is higher; thus, AFCLT3 shows the largest EOL credit among timber slabs, and AFCLT2 the smallest. That said, “designing heavier to chase credits” is counterproductive because production still dominates and mass increases impacts elsewhere.

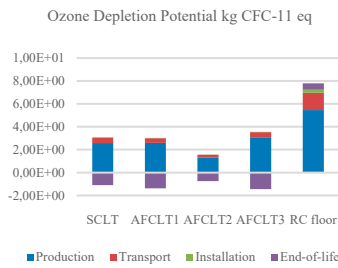
In addition, the RC slab lacks obvious energy recovery in most categories (except for GWP which absorbed CO<sub>2</sub> for 5.49 kg) because concrete is land-filled while only 75% of reinforcement is recycled; its EOL share therefore stays low (2.91% – 62.55%) relative to the total and is typically positive. This points to waste-concrete treatment as the main EOL issue; credible mitigation comes from mass reduction, low-carbon binders, and higher-value concrete reuse/recycling routes.



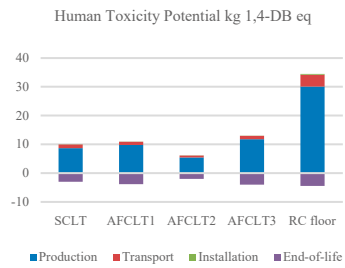
(a)



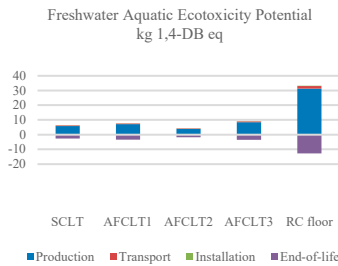
(b)



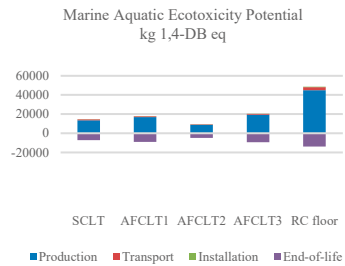
(c)



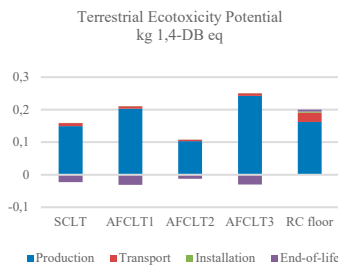
(d)



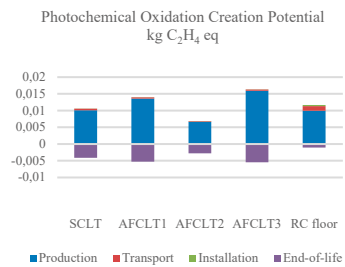
(e)



(f)



(g)



(h)

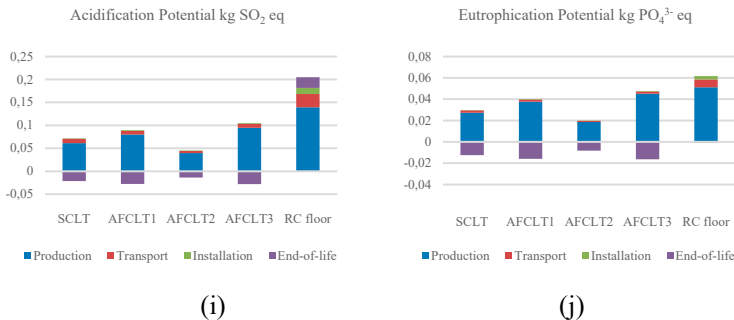


Figure 40 Environmental impact from structure type 2: (a) ADP, (b) GWP, (c) ODP, (d) HTP, (e) FAETP, (f) MAETP, (g) TETP, (h) POCP, (i) AP, and (j) EP

### 3.5.3. Geographic electricity scenarios

Varying only the manufacturing electricity mix among Norway, Sweden, Finland, and Saudi Arabia leaves the timber ranking unchanged (AFCLT2 remains the lowest-impact option and AFCLT3 the highest) but widens the separations on clean grids and compresses them on fossil-heavy grids (Figure 41). Illustratively, SCLT's GWP exceeds AFCLT2 by 189.44% with Norwegian electricity, 185.59% with Swedish, 139.2% with Finnish, and 96.98% with Saudi electricity. Norway's hydropower-dominant grid yields the lowest impacts overall, whereas Saudi Arabia's oil/gas grid generates the highest; Sweden generally outperforms Finland across categories, consistent with larger shares of hydro/nuclear/wind and a smaller coal fraction. Aggregating across indicators shows that GWP, ODP, MAETP, TETP, POCP, and AP are most sensitive to electricity in this modeling, while certain toxicity categories do not respond uniformly: under the Saudi case, FAETP and MAETP occasionally underperform Finland, underscoring that grid effects are not monotonic across all endpoints. The country-specific tables for SCLT/AFCLT1 and AFCLT2/AFCLT3 corroborate these patterns in absolute terms; for example, AFCLT2 GWP shifts from 3.65–3.78 kg CO<sub>2</sub>-eq on Norway/Sweden to 6.48 kg CO<sub>2</sub>-eq in Finland and 30.35 kg CO<sub>2</sub>-eq in Saudi Arabia, while AFCLT3 ranges from 10.41–10.58 kg CO<sub>2</sub>-eq in the Nordics and 30.35 kg CO<sub>2</sub>-eq in Saudi Arabia.

The reasons AFCLT2 leads are structural and process-integrated: minimal machining, adhesive-free lamination, and lean mass combine to lower electricity demand, eliminate PUR, and reduce transport/installation energy, yielding cross-category gains. By contrast, AFCLT1 and AFCLT3 remove surface PUR but introduce electricity-intensive milling and higher lumber inputs; the reduction in adhesive is partly offset by greater board mass and power consumption, which explains why HTP can exceed SCLT despite lower PUR. Contribution analyses within production identify the same levers (sawn wood, PUR, electricity, board bonding, and waste-wood handling) with consistently smaller magnitudes for AFCLT2. For RC, impacts reflect three compounding features: emissions-intensive cement and steel production, a weight penalty that amplifies mass-linked stages, and limited EOL recovery. Credible pathways to narrow the timber–concrete gap therefore pair section mass control (e.g.,

voided/waffle geometries) with clinker substitution via low-carbon binders, complemented by improved concrete reuse.

Moreover, sensitivity patterns across the four grids indicate that design effects dominate when manufacturing occurs on clean electricity, whereas grid composition can overshadow design on fossil-heavy mixes. This interaction has practical implications for siting and procurement: producing timber slabs on hydropower- or nuclear-heavy grids accentuates AFCLT2's advantage; on oil/gas grids, absolute impacts rise and inter-timber differences compress. Although the models hold other parameters constant to isolate electricity, real projects can expect additional variability from transport distances, EOL infrastructure, and regional recycling markets. Even so, the phase-resolved shares and the directionality of the improvement levers remain robust, guiding priority actions irrespective of location.

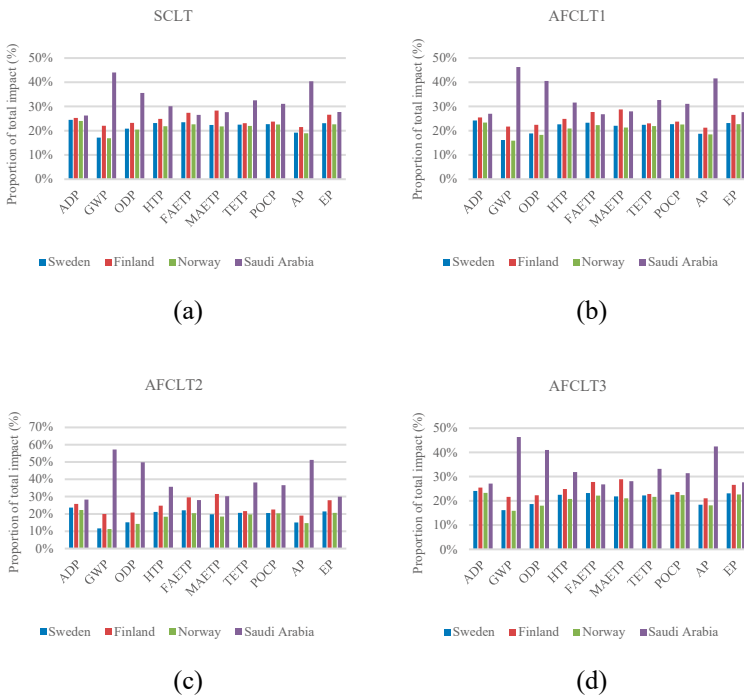


Figure 41 Environmental impact based on structure type 2 in different regions (based on relation between impact of location and that of total for all locations), per functional unit 1: (a) SCLT, (b) AFCLT1, (c) AFCLT2, and (d) AFCLT3.

### 3.5.4. Practical implications for designers and policy makers

For timber slabs, prioritizing mass minimization, geometry simplification, and efficient nesting reduces lumber demand and electricity per FU1, yielding immediate reductions in GWP, FAETP, AP, and EP. Where milling cannot be avoided, routing and toolpath optimization can curb FAETP-sensitive electricity. Managing co-products adds a second layer of gains: re-processing shavings

and end-cuts to displace structural stock, recycling CNC waste, or valorizing residues for process heat improves both production and Module D outcomes without inflating mass. PUR minimization aids ADP/ODP/HTP, but adhesive choices alone do not compensate for heavy or electricity-intensive designs; the whole system must be tuned.

For RC, policy instruments that incentivize low-carbon cement, section-mass optimization, and high-value concrete recycling directly target the categories that keep RC far above timber. In parallel, electrifying transport and craning on renewable grids offers modest but reliable reductions across systems without upsetting the fundamental ranking.

Furthermore, three conclusions follow from the evidence. First, AFCLT2 is the most sustainable slab for the studied functional unit and boundary because it aligns low mass, low electricity, and adhesive-free assembly; its advantage strengthens on clean grids and persists on fossil-heavy grids. Second, EOL credits for timber are meaningful (especially in GWP, MAETP, and EP) but remain secondary to production; designing heavier to amplify credits is counterproductive given production dominance and mass-linked penalties. Third, RC remains the outlier in overall burden; although it outperforms AFCLT3 in TETP and POCP, its production and EOL profiles keep it far above timber alternatives in the aggregate. These points jointly frame a practical design doctrine: start with lean timber geometry that minimizes lumber and milling, limit adhesives where structurally viable, and co-locate manufacturing with low-impact electricity to lock in whole-life gains.

### **3.6. Uncertainty considerations in LCA results**

The LCA results presented in Sections 3.4 and 3.5 include uncertainties that mainly influence absolute impact magnitudes and relative differences between slab alternatives. The key uncertainties can be categorized by: (i) background datasets, (ii) inventory assumptions, and (iii) EOL modeling and substitution choices.

The background datasets (Ecoinvent v3.5) are general and may not fully reflect the specific conditions of suppliers in lumber, adhesives, steel products, fuels, and waste management. Moreover, the electricity in the reference case was modeled based on Swedish 2023 conditions (Statens energimyndighet, 2023), and the geographic electricity scenarios show that different electricity mixes can affect results significantly because slab production and CNC machining are electricity-based. Therefore, impact indicators linked to energy production and upstream process (e.g., GWP, ODP, and toxicity-related categories) may vary if actual supply chains differ from the applied datasets.

Furthermore, assumptions are made when original data are unavailable or simplified, which bring uncertainties as well: such as CNC machining intensity (particularly relevant for AFCLT variants with complex geometries), handling/distribution of machining residues, adhesive consumption estimated based on literature, and installation energy consumption based on mass. To maintain comparability, these modeling choices are consistent across all

comparison systems, but they bring uncertainties to electricity- and process-dominated indicators, particularly FAETP and HTP.

As for EOL modeling and module D, 80% of timber is assumed to be directly reused as structural timber and 20% is incinerated with energy recovery. The benefits of module D are modeled using the avoided-burden approach. Since module D of timber appears as a negative contribution, it can significantly reduce the production impact and total impact. Therefore, results including module D should be interpreted as conditional benefits in practice.

High reuse rates for CLT require certain conditions that can not be guaranteed in traditional demounting practice: design for disassembly, controlled deconstruction to avoid damage, traceability/documentation to support re-certification, and market/logistics preparation (e.g., standardized dimensions and handling). If these conditions are not met, reuse rates may be lower and Module D benefits would decrease accordingly. In addition, the credit from incineration depends on which energy source is substituted. In the future, decarbonization of electricity and heat may lead to cleaner substitutes, reducing the avoided-burden credit from energy recovery. Thus, the contribution from incineration is less than that from direct material reuse in the long run.

Compared with the current EOL design, a more conservative EOL scenario (0% or 25–50% reuse) would reduce benefits from module D and increase total impact from timber product, particularly for GWP, while rankings driven by mass and electricity intensity are expected to remain roughly similar.

For RC slab, EOL outcomes are less sensitive to reuse rate assumption in this study because concrete is landfilled and only reinforcing steel is recycled (75%), resulting in smaller module D effects than timber reuse scenarios.

### 3.7. Limitations

The analysis and conclusions of this thesis are framed within certain boundaries and modeling choices to ensure comparability and practical application value. Besides, the structural study focuses on out-of-plane four-point bending of the jointed panels, representative of floor slab applications. While this is an application case for many slab systems, direct extrapolation to other effects (e.g., diaphragm shear, in-plane bending, seismic requirements) should be adjusted based on particular circumstances. The FE models are calibrated based on laboratory data and established theories of timber mechanics; they are used to explore parametric sensitivities within proposed families of joints and intentionally prioritize clarity of predictions over exhaustive material nonlinearities.

Furthermore, the LCA adopts EN/ISO-consistent system boundaries and scenarios to enable like-for-like comparisons among connection options and slab types. Inventory datasets reflect Swedish conditions for materials, transport, and electricity where relevant; these choices are typical for Nordic projects and provide a clear baseline that readers can adjust to their own contexts. Additionally, use-phase processes are limited to those directly affecting the prefabricated slab systems, and EOL scenarios are specified to examine reuse and recovery pathways for timber systems alongside standard demolition and recycling assumptions for RC. Moreover, the FU1 comparison is defined

per 1 m<sup>2</sup> of floor area under the same targeted load condition and service life. However, the slab alternatives are not fully functionally identical in a structural sense because their thicknesses and densities are different. Therefore, the LCA outcomes should be interpreted as environmental performance per floor area, rather than as impacts per equal bending resistance or equal serviceability performance.

Nevertheless, this thesis aims to achieve a balance between specificity and universality: the samples, models, and procedures are detailed to support validation and comparison, and the assumptions are described so that designers and researchers can translate the findings into relevant systems, alternative combinations, or other geographical contexts as needed.

## 4. Conclusions and future work

This Chapter offers the conclusions of the studies provided in this thesis, which included key results, implications, and reflections. Besides, the future work beyond this thesis is also discussed.

### 4.1. Conclusions

This thesis examined the interface where structural performance and environmental performance are balanced in EWP systems: the panel edge connection. In accordance with the thesis aim and the five objectives (Section 1.5), the work progressed from (i) concept development based on literature review, to (ii) FE modeling, laboratory testing, and sensitivity analysis, and (iii) cradle-to-cradle LCA at both slab and connection scales. Accordingly, the following conclusions directly address RQ1-RQ4: RQ1-RQ2 demonstrated the structural response, failure mechanisms, and design factor impacts of six adhesive-free wood connections through validation; RQ3-RQ4 verified how the choice of connectors/materials and adhesive-free slab variants influences the impact on modules A, B1, C, and D through unified LCA. The main outcomes include: (1) validated structural performance of timber-based edge connections, achieving competitive stiffness, strength, and ductility in out-of-plane bending; (2) parametric design results revealing relations between the geometric and material factors and the load-bearing capacity, and rotation; and (3) LCA results demonstrating that adhesive-free, all-timber alternatives significantly reduce environmental impact at the floor scale with the advantageous remaining under different electricity-mix and EOL pathways. These findings support specification of reversible, low-impact CLT floor slabs without reducing structural performance.

#### 4.1.1. Structural performance

This section reports the conclusions primarily for RQ1-RQ2 and corresponds to objectives 2–3. In the numerical validation process, the FE framework (orthotropic continuum lamellae, frictional timber-timber contact, and a quadratic, stress-based failure check implemented in VUSDFLD) was verified based on three independent experiments (glulam beam-to-beam with densified-wood plates/dowels; adhesive-free CLT with vertical densified-wood dowels; and a plywood-spline CLT specimen with steel screws). Among these verifications, benchmark comparisons showed small differences ( $\approx+2\%$  in capacity,  $\approx+7.3\%$  in rotation), providing a series of reliable settings and values for subsequent design exploration and sensitivity analyses. Additionally, the modeling choices, boundary conditions, and measurement protocols were kept unchanged across connection families so that observed performance

differences derive from connection architecture and parameter changes rather than differences from modeling methods.

Furthermore, under the four-point bending with harmonized geometry and support conditions, the six proposed timber-only connections (BC, TS, GT, GC, DS, and HL) achieved the following ranges at system level:

- Ultimate load 2.85–11.74 kN (mean 6.42 kN), with the best configuration exceeding the weakest by 312% due to improved engagement of outer lamellae and superior rotation restraint.
- Ductility ratios 1.00–2.89 (mean 1.64), reflecting stable post-yield mechanisms rather than brittle, connector-governed failures.
- Bending strength 2.38–9.78 MPa (mean 5.35 MPa), with significant reductions when the joint path traversed the transverse lamella (group means ~2.81 vs. 7.88 MPa), highlighting the importance of avoiding load paths that concentrate rolling-shear demand in cross layers.
- Effective flexural rigidity with joint ( $EI_{eff}$ ) up to  $5.49 \times 10^4$  N·m<sup>2</sup>, indicating that rotation control at the joint line is a primary factor of system stiffness.

Across examined families, three common behaviors were concluded:

1. The concepts that coupled the outer lamellae layers (either by positioning interlock designs near to the outer lamellae or by spanning them with shaped elements), which were the highest tension and compression zones, consistently depicted higher stiffness and capacity.
2. The rotation restraint outweighs the importance of local strength increases. Raising connector's properties without improving joint-line rotation control would not linearly enhance the structural performance. Conversely, small geometric changes that stiffen the rotational spring at the interface produced measurable system-level improvements.
3. The load through the transverse lamella layer depressed bending strength and led to rolling-shear-type responses. The connections that minimize demand in cross layers and maintain longitudinal lamellae continuity performed best.

In addition, six full-scale glulam floor-type specimens joined by densified-wood connectors in the experimental studies confirmed the mechanisms observed numerically: (1) nonlinear and stable load–displacement curves were obtained before failure, (2) the panel's capacity was governed by bending in the timber elements rather than brittle connector rupture, and (3) elastic behavior in the FE models was similar but with different stiffness. Moreover, the failure examinations showed that the lamination-interface activity and cross-grain shear near connectors appeared only when geometry funneled demand into the cross layers. Otherwise, the cracks initiated in timber zones consistent with section-level stress distributions. These experimental tests support the thesis' key claim that proposed timber-only connectors can deliver predictable, ductile system behavior under out-of-plane bending.

Additionally, a DSS connection with plywood spline and STS representing common market product was numerically verified and then used as a reference. Although the DSS solution provides high initial stiffness and capacity (2.9479 kNm), screw groups concentrate shear in the cross lamellae and rotation localizes at the splines. Besides, it was noticed that several timber-only variants (notably from AF timber connection 1 – BC connection, AF timber connection 3 – GT connection, and AF timber connection 5 – DS connection) approached or exceeded the DSS configuration in bending stiffness and capacity within the same test conditions and geometry. It was achieved without metal fasteners or glue and improved the ductility and reparability at the same time.

#### **4.1.2. Environmental performance**

The conclusions that address RQ3-RQ4 are reported in this section, which concerns objectives 4 and 5. For the environmental performance of the proposed timber connection based on slab scale (FU1) and per-connection scale (FU2) in structure type 1, the LCA results showed significant advantages for timber systems compared with steel-based and RC elements across midpoint indicators, with the most notable indicator being GWP according to policies:

- For FU1 (1 m<sup>2</sup> slab including edge connection): typical RC  $\approx 69$  kg CO<sub>2</sub>-eq, vs.  $\approx 4$ –7 kg CO<sub>2</sub>-eq for the evaluated CLT variants, which is a notably lower than values for timber. The EOL scenarios that enable reuse and energy recovery provided substantial reduction on the environmental impacts from timber.
- For FU2 (1 m connection): the environmental impact from connection became independent from other components in this case. Timber-only joints consistently outperformed steel-reinforced ones by avoiding burdens in material production and by improving compatibility with circular EOL pathways (disassembly, component reuse). Moreover, it revealed that the connector choice itself is an obvious contributor to embodied impact differences in CLT floor slabs.

Furthermore, the same methods and CML indicator set were applied in the structure type 2, which comprised of AF CLTs, SCLT, and RC slabs (without edge connections). The material intensity and chemistry components influenced the environmental performance: steel- and glue-rich solutions tended to achieve higher impact values than timber-only ones in most cases (except for TETP and POCP). Additionally, adhesive-free CLT variants AFCLT2 repeatedly returned the lowest impact among timber options, while AFCLT3 performed worst (within AFCLTs only) due to greater mass used. Nevertheless, clean electricity mixes widened these gaps by lowering the environmental burdens of CNC machining and panel production, while the fossil-heavy mixes compressed them. The absolute magnitudes shifted with scenario assumptions (electricity mix and transport), while the relative ranking remained stable. This indicated the advantages of timber-only approaches for less environmental impact in the construction sector.

Based on the structural performance and LCA analysis, the suggestions and actionable guidance for designs could be summarized:

- Engage outer lamellae. Prioritize connector geometries and placements that couple areas with highest tension and compression, thereby maximizing section efficiency and limiting rotation at the joint line. (BC, optimized DS, twin-plate GC, and HL with preserved flange thickness exemplify this principle.)
- Control rotation first, then add strength. Before increasing local load-bearing capacity, the overlap length, tongue and tenon dimensions, and plate layout should be adjusted to enhance the rotational stiffness of the joint. Once rotation is controlled, a predictable incremental gain can be obtained by moderately increasing the connector's diameter/number or material properties.
- Keep demand out of cross layers. Avoid load paths that mainly pass through the transverse lamellae or create stress hot-spots in cross-grain shear. If it is unavoidable, use geometries that distribute shear (e.g., dual elements rather than single wide inserts).
- Prefer timber-only, glue-free connectors for circularity and carbon. Under FU1, the quality of the floor slab is dominant, but the choice of connectors still influences its impact; under FU2, this difference is more pronounced. Timber-only joints also enable dry assembly, inspection, and disassembly for reuse, aligning structural choices with EOL benefits observed in the LCA.

#### **4.1.3. Reflections and summary**

Despite the presented results and works, this thesis still has certain limitations and limited scope of validity. The structural performance studied focuses on out-of-plane bending, which is a governing action for many floor slabs but not a proxy for all demands (e.g., in-plane diaphragm shear, cyclic/seismic inputs). Moreover, the strength checks used instantaneous failure criteria rather than progressive damage evolution. This was sufficient for comparative design guidance, but future work may refine post-peak modeling. In addition, the LCA boundaries and inventory datasets reflected Swedish/Nordic conditions and standard EN/ISO practices, while rankings were stable across electricity scenarios. The absolute values will vary with local supply chains and project specifics. These limitations have been outlined so that practitioners can adjust their research findings and methodology, based on their own circumstances.

For structural designers, this study provides a validated prototype of all-timber edge connections, with parametric maps illustrating how small geometric changes can lead to significant improvements in stiffness and load-bearing capacity. For environmental study teams, the LCA revealed the environmental benefits of using glue-free all-timber connectors at the component and floor levels, including reliable EOL compensation available under reuse and energy recovery conditions. For standards development, the findings advocate for: (i) explicitly considering inter-panel rotational constraints in the stiffness formulas for CLT floor slabs; (ii) developing guidelines for woodworking high-

density timber connectors; and (iii) incorporating connector selection into the carbon accounting of the entire building, given its measurable contribution to carbon emissions and its impact on the circularity.

Furthermore, edge connections determine whether precast CLT panels behave as rigid, continuous slabs or as loosely coupled components constrained by node rotation and interlayer shear. This thesis demonstrated that well designed and arranged adhesive-free, all-wood connectors can tightly bond with outer layers and control rotation, achieving system-level stiffness, load-bearing capacity, and ductility comparable to steel-involved and RC structures, while significantly reducing environmental impacts and enabling recyclable EOL disposal solutions. An integrated modeling-testing-life LCA approach provides a practical template for synergistically optimizing structural and environmental performance: (1) designing rotation control and edge connections, (2) validating through calibrated FE analysis and conducting targeted testing; and (3) assessing impacts within certain functional units and scenarios that fully consider geometry and manufacturing realities. Through these steps, designers can specify robust, repairable, and climate-compliant adhesive-free edge connections for CLT slabs, thereby helping buildings achieve decarbonization.

In addition, the outcomes obtained in this thesis indicate a broader future for large-volume timber manufacturing: (1) CNC machining makes it easier to achieve high precision in woodworking, (2) the increasing knowledge of high-density timber products, (3) structural connectors are expected to once again be dominated by wood. Therefore, using wood element is not only for aesthetic or heritage considerations, but also because data has demonstrated that timber connectors are efficient, predictable, and low carbon. In this sense, the connection concepts and design rules proposed in this thesis contribute to the development of a new generation of wood panel flooring, enabling it to be outstanding in both structural and environmental performance.

## **4.2. Future work**

This work showed that edge connections shape both the strength of CLT floor slabs and their carbon profile. The next step is to apply and study these joints from the laboratory into real-buildings scale over time. Long-term tests under moisture cycles, creep, and temperature variation can reveal how stiffness, slip, and rotation evolve in service. Additionally, fire and repair studies can add an understanding of safety and reversibility for glue-free details, since circular use is one of the advantages of timber-only connections.

Furthermore, the scope of structural testing can be expanded. For example, cyclic and seismic loading can test ductility and energy dissipation capacity. Not only out-of-plane bending can be analyzed, but also the effects of in-plane diaphragms and the connection performance at openings. Using full-size floor slab strips with actual support, surface layers, and sound-absorbing layers, their service performance, vibration characteristics, and construction tolerances can be clearly defined.

On the other hand, the FE framework can include progressive damage, rolling-shear softening, and moisture-dependent properties. Manufacturing studies

can investigate CNC limits, fit-up allowances, and assembly speed so that geometry choices support both performance and production convenience.

Moreover, the LCA part can consider dynamic power mix, regional forestry data, and measured output from machining, which can refine the inventory list. Uncertainty analysis and scenario scope can enhance the robustness of decision-making. Subsequently, techno-economic and social indicators can be added to construct a more comprehensive sustainability picture, allowing for a better comparison of different construction components.

## References

- Adhikari, S., & Ozarska, B. (2018). Minimizing environmental impacts of timber products through the production process “From Sawmill to Final Products.” *Environmental Systems Research*, 7(1). <https://doi.org/10.1186/s40068-018-0109-x>
- Akter, S. T., Olsson, A., & Bader, T. K. (2025). Stiffness and Strength of Scots Pine Wood Under Compression Perpendicular to the Grain and Rolling Shear Loading. *Applied Sciences*, 15(19), 10775. <https://doi.org/10.3390/app151910775>
- Al-Najjar, A. (2021). *Full life cycle assessment of a cross laminated timber modular building in Sweden*.
- American National Standards Institutes (ANSI). (2018). ANSI/APA PRG 320-2018: Standard for Performance-Rated Cross-Laminated Timber. In *The Engineered Wood Association (APA)*.
- American Wood Council. (2018). NDS Supplement National Design Specification Design Values for Wood Construction. In *Journal of Chemical Information and Modeling*.
- Andersen, J. H., Rasmussen, N. L., & Ryberg, M. W. (2022). Comparative life cycle assessment of cross laminated timber building and concrete building with special focus on biogenic carbon. *Energy and Buildings*, 254. <https://doi.org/10.1016/j.enbuild.2021.111604>
- Andrade, C. (2020). Evaluation of the degree of carbonation of concretes in three environments. *Construction and Building Materials*, 230. <https://doi.org/10.1016/j.conbuildmat.2019.116804>
- Anshari, B., Guan, Z. W., Kitamori, A., Jung, K., Hassel, I., & Komatsu, K. (2011). Mechanical and moisture-dependent swelling properties of compressed Japanese cedar. *Construction and Building Materials*, 25(4), 1718–1725. <https://doi.org/10.1016/J.CONBUILDMAT.2010.11.095>
- ASTM D2718. (2000). Standard Test Methods for Structural Panels in Planar Shear (Rolling Shear). *American Society for Testing and Materials*, 00(2011).
- Atnoorkar, S., Ghatpande, O. A., Haile, S. L., Goetsch, H. E., & Harris, C. B. (2023). Carbon intensity of mass timber materials: impacts of sourcing and transportation. *Frontiers in Built Environment*, 9. <https://doi.org/10.3389/fbuil.2023.1321340>
- Australian Bureau of Agricultural and Resource Economics and Sciences. (2017). *Australia's forests at a glance 2017: with data to 2015–16*.
- Bahrami, A., Edås, M., Magnenat, K., & Norén, J. (2022). The behavior of cross-laminated timber and reinforced concrete floors in a multi-story building. *International Journal of Advanced and Applied Sciences*, 9(6), 43–50. <https://doi.org/10.21833/ijaas.2022.06.006>

- Bahrami, A., Vall, A., & Khalaf, A. (2021). Comparison of Cross-Laminated Timber and Reinforced Concrete Floors with Regard to Load-Bearing Properties. *Civil Engineering and Architecture*, 9(5), 1395–1408. <https://doi.org/10.13189/cea.2021.090513>
- Baño, V., & Moltini, G. (2021). Experimental and numerical analysis of novel adhesive-free structural floor panels (TTP) manufactured from timber-to-timber joints. *Journal of Building Engineering*, 35, 102065. <https://doi.org/10.1016/J.JOBE.2020.102065>
- Boverket. (2004). *Boverkets handbok om betongkonstruktioner, BBK 04*. Boverket. [https://www.boverket.se/globalassets/publikationer/dokument/2004/boverkets\\_handbok\\_om\\_betongkonstruktioner\\_bbk\\_04.pdf?utm\\_source=chatgpt.com](https://www.boverket.se/globalassets/publikationer/dokument/2004/boverkets_handbok_om_betongkonstruktioner_bbk_04.pdf?utm_source=chatgpt.com)
- British Standards Institution. (2004). EN 789, Timber structures -Tests methods-Determination of mechanical properties of wood based panels. In *British Standard*.
- British Standards Institution. (2011). BS EN 15978:2011 - Sustainability of construction works : assessment of environmental performance of buildings : calculation method. In *British Standard* (Number November).
- Brown, J. R., & Li, M. (2021). Structural performance of dowelled cross-laminated timber hold-down connections with increased row spacing and end distance. *Construction and Building Materials*, 271, 121595. <https://doi.org/10.1016/J.CONBUILDMAT.2020.121595>
- Cai, Z., Senalik, C. A., & Ross, R. J. (2021). Chapter 12: Mechanical properties of wood-based composite materials. In: Wood handbook - wood as an engineering material. *USDA - General Technical Report*.
- CEMEX. (n.d.). *RC Concrete Mixes*. Retrieved February 9, 2026, from [https://www.cemex.co.uk/products/readymix-concrete/bs-designated-mixes/rc-concrete-mixes?utm\\_source=chatgpt.com](https://www.cemex.co.uk/products/readymix-concrete/bs-designated-mixes/rc-concrete-mixes?utm_source=chatgpt.com)
- CEN. EN. (2004). BS EN 1995-1-1:2004 - Eurocode 5: Design of timber structures - Part 1-1: General - Common rules and rules for buildings. *Eurocode 5, 1*(2004).
- CEN. EN 16351. (2021). *Timber structures - Cross laminated timber - Requirements*. Comité Européen de Normalisation.
- Chen, C. X., Pierobon, F., & Ganguly, I. (2019). Life Cycle Assessment (LCA) of Cross-Laminated Timber (CLT) produced in Western Washington: The role of logistics and wood species mix. *Sustainability (Switzerland)*, 11(5). <https://doi.org/10.3390/su11051278>
- Chen, J., Xiong, H., Furuta, T., Lu, Y., & Abbas, N. (2022). Experimental and analytical studies on mechanical performance of innovative energy-dissipating hold-down for CLT structures. *Construction and Building Materials*, 317. <https://doi.org/10.1016/j.conbuildmat.2021.125966>
- Chen, Z., Gu, H., Bergman, R. D., & Liang, S. (2020). Comparative life-cycle assessment of a high-rise mass timber building with an equivalent reinforced concrete alternative using the athena impact estimator for buildings. *Sustainability (Switzerland)*, 12(11). <https://doi.org/10.3390/su12114708>

- Conway, M., Mehra, S., Harte, A. M., & O’Ceallaigh, C. (2021). Densified wood dowel reinforcement of timber perpendicular to the grain: a pilot study. *Journal of Structural Integrity and Maintenance*, 6(3). <https://doi.org/10.1080/24705314.2021.1906090>
- Dadej, K., & Surowska, B. (2016). *Analysis of Cohesive Zone Model Parameters on Response of Glass-Epoxy Composite in Mode II Interlaminar Fracture Toughness Test Development of a physically consistent Virtual Crack Closure Technique (VCCT) View project Enhanced beam-theory modelling of delamination in laminated beams View project*. <https://www.researchgate.net/publication/319753750>
- Dan, B., Zhongwei, G., Annette, H., Peer, H., Salim, B., François, D., & Marc, O. (n.d.). *Technical Note 3 Properties of Compressed Wood*. Interreg NWE. Retrieved June 20, 2023, from <https://vb.nweurope.eu/media/10253/tech-brief-03-properties-of-compressed-wood.pdf>
- Darzi, S., Karampour, H., Bailleres, H., Gilbert, B. P., & McGavin, R. L. (2020). Experimental study on bending and shear behaviours of composite timber sandwich panels. *Construction and Building Materials*, 259, 119723. <https://doi.org/10.1016/J.CONBUILDMAT.2020.119723>
- Demertzi, M., Silvestre, J., Garrido, M., Correia, J. R., Durão, V., & Proença, M. (2020). Life cycle assessment of alternative building floor rehabilitation systems. *Structures*, 26. <https://doi.org/10.1016/j.istruc.2020.03.060>
- Dervishaj, A., Malmqvist, T., Silfwerbrand, J., & Gudmundsson, K. (2024). A digital workflow for assessing lifespan, carbonation, and embodied carbon of reusing concrete in buildings. *Journal of Building Engineering*, 96. <https://doi.org/10.1016/j.jobe.2024.110536>
- EN 14080:2013. (2014). Timber structures — Glued laminated timber and glued solid timber — Requirements. *BSI Standards Publication*, (June).
- EN 15804:2012+A2:2019. (2019). *Sustainability of construction works - Environmental product declarations - Core rules for the product category of construction products*. CEN European Committee for Standardisation.
- Erol, K., & Brad, D. (2013). CLT Handbook: Cross-laminated Timber. In *Book*. FPIInnovations.
- Eslami, H., Jayasinghe, L. B., & Waldmann, D. (2024). Experimental and numerical study on shear behavior of a demountable CLT-concrete composite shear connection. *Construction and Building Materials*, 425, 135982. <https://doi.org/10.1016/J.CONBUILDMAT.2024.135982>
- European Committee for Standardization (CEN). (2022). *Sustainability of construction works - environmental product declarations - product Category Rules for concrete and concrete elements (EN 16757:2022)*. <https://www.sis.se/en/produkter/construction-materials-and-building/construction-materials/concrete-and-concrete-products/ss-en-167572022/>
- European Scots Pine Wood*. (n.d.). Retrieved June 10, 2023, from <https://www.matweb.com/search/datasheet.aspx?mat-guid=1d218996ea634b37b4290c2ac38a69ab&n=1&ckck=1>
- Flores, E. I. S., Saavedra, K., Hinojosa, J., Chandra, Y., & Das, R. (2016). Multi-scale modelling of rolling shear failure in cross-laminated timber

- structures by homogenisation and cohesive zone models. *International Journal of Solids and Structures*, 81, 219–232. <https://doi.org/10.1016/J.IJSOLSTR.2015.11.027>
- Forest Service, U., & Products Laboratory, F. (2010). *Wood Handbook, Wood as an Engineering Material*. [www.fpl.fs.fed.us](http://www.fpl.fs.fed.us).
- Frischknecht, R., & Rebitzer, G. (2005). Theecoinvent database system: A comprehensive web-based LCA database. *Journal of Cleaner Production*, 13(13–14). <https://doi.org/10.1016/j.jclepro.2005.05.002>
- Gama, B. A., & Gillespie, J. W. (2011). Finite element modeling of impact, damage evolution and penetration of thick-section composites. *International Journal of Impact Engineering*, 38(4), 181–197. <https://doi.org/10.1016/J.IJIMPENG.2010.11.001>
- Gao, Z., Zhang, X., Wang, Y., Yang, R., Wang, G., & Wang, Z. (2016). Measurement of the Poisson's ratio of materials based on the bending mode of the cantilever plate. *BioResources*, 11(3). <https://doi.org/10.15376/biores.11.3.5703-5721>
- Glasner, D., Ringhofer, A., Hubmann, G., & Braun, W. (2023). ENERGY DEMAND FOR THE DRIVING IN OF SELF-TAPPING TIMBER SCREWS AND ITS APPLICABILITY. *13th World Conference on Timber Engineering, WCTE 2023*, 6. <https://doi.org/10.52202/069179-0475>
- Global Alliance for Buildings and Construction. (2024). *2023 Global Status Report for Buildings and Construction*. <https://doi.org/10.59117/20.500.11822/45095>
- Group, K. (2002). Handbook of finnish plywood. In *Screen*.
- Harley, T., White, G., Dowdall, A., Bawcombe, J., McRobie, A., & Steinke, R. (2016). Dalston Lane - The world's tallest CLT building. *WCTE 2016 - World Conference on Timber Engineering*.
- Hashin, Z. (1980). Failure Criteria for Unidirectional Fiber Composites. *Journal of Applied Mechanics*, 47(2), 329–334. <https://doi.org/10.1115/1.3153664>
- Helsing, E., Malaga, K., & RISE. (2023). *Orsakar användning av klimatförbättrad betong med slagg, flygaska och silikastoft utlakning av farliga ämnen i dricks-vattenanläggningar?* B&t. [https://byggteknikforlaget.se/orsakar-anvandning-av-klimatforbatttrad-betong-med-slagg-flygaska-och-silikastoft-utlakning-av-farliga-amnen-i-dricks-vattenanlaggningar/?utm\\_source=chatgpt.com](https://byggteknikforlaget.se/orsakar-anvandning-av-klimatforbatttrad-betong-med-slagg-flygaska-och-silikastoft-utlakning-av-farliga-amnen-i-dricks-vattenanlaggningar/?utm_source=chatgpt.com)
- Hemmilä, V., Adamopoulos, S., Karlsson, O., & Kumar, A. (2017). Development of sustainable bio-adhesives for engineered wood panels-A Review. In *RSC Advances* (Vol. 7, Number 61). <https://doi.org/10.1039/c7ra06598a>
- Ilgin, H. E., & Karjalainen, M. (2021). Preliminary Design Proposals for Dove-tail Wood Board Elements in Multi-Story Building Construction. *Architecture*, 1(1). <https://doi.org/10.3390/architecture1010006>
- Ilgin, H. E., Pajunen, S., Leivo, V., & Karjalainen, M. (2025). Structural performance of a novel dovetailed timber panel subjected to out-of-plane bending. *Case Studies in Construction Materials*, 23. <https://doi.org/10.1016/j.cscm.2025.e05095>

- International Energy Agency., & Global Alliance for Buildings and Construction. (2019). *2019 global status report for buildings and construction*. International Energy Agency.
- ISO. (2006). ISO 14044:2006. *Environmental Management - Life Cycle Assessment - Requirements and Guidelines, ISO 14044, International Organization for Standardization, 2006(7)*.
- Jockwer, R., Brühl, F., Cabrero, J. M., Hübner, U., Leijten, A., Munch-Andersen, J., & Ranasinghe, K. (2021). Modern connections in the future eu-rocode 5 - Overview of current developments. *World Conference on Timber Engineering 2021, WCTE 2021*.
- Kellenberger, D., & Althaus, H. J. (2009). Relevance of simplifications in LCA of building components. *Building and Environment, 44(4)*. <https://doi.org/10.1016/j.buildenv.2008.06.002>
- Kobelco Construction Machinery Co., LTD. (n.d.). *TKE750G Telescopic Boom Crawler Crane*. Retrieved March 6, 2025, from [www.kobelco-europe.com](http://www.kobelco-europe.com)
- Kraenzlein, P., Hindman, D. P., & Phillips, A. R. (2026). Half-lap cross laminated timber panel-to-panel connections using hardwood dowels. *Construction and Building Materials, 510*. <https://doi.org/10.1016/j.conbuildmat.2026.145273>
- Kretschmann, D. E. (2010). Chapter 5 - Mechanical Properties of Wood. *Wood Handbook - Wood as an Engineering Material*.
- Kulak, P., Lachowicz, H., Moskalik, T., Piętka, J., Aniszewska, M., & Gendek, A. (2023). The Structural, Physical, and Mechanical Properties of Wood from Scots Pine (*Pinus sylvestris* L.) Affected by Scots Pine Blister Rust. *Forests, 14(11)*. <https://doi.org/10.3390/f14112161>
- Kurzinski, S., Crovella, P., & Kremer, P. (2022). Overview of Cross-Laminated Timber (CLT) and Timber Structure Standards across the world. *Mass Timber Construction Journal, 5(1)*.
- Landgrebe, D., Götze, U., Bergmann, M., Schmidt, A., & Selbmann, R. (2018). Evaluation of manufacturing processes for the production of graded ultrafine grained materials. *Procedia Manufacturing, 21*. <https://doi.org/10.1016/j.promfg.2018.02.093>
- Larsen, H. J., & Munch-Andersen, J. (2011). *CIB-W18 Timber Structures-A review of meeting 1-43 CIB-W18 Timber Structures-A review of meetings 1-43 4 CONNECTIONS CONTENT*.
- Larsson, M., Yoshida, H., Umetani, N., & Igarashi, T. (2020). Tsugite: Interactive design and fabrication of wood joints. *UIST 2020 - Proceedings of the 33rd Annual ACM Symposium on User Interface Software and Technology*. <https://doi.org/10.1145/3379337.3415899>
- Li, M., Dong, W., & Lim, H. (2019). Influence of Lamination Aspect Ratios and Test Methods on Rolling Shear Strength Evaluation of Cross-Laminated Timber. *Journal of Materials in Civil Engineering, 31(12)*. [https://doi.org/10.1061/\(asce\)mt.1943-5533.0002977](https://doi.org/10.1061/(asce)mt.1943-5533.0002977)
- Li, Z., Wang, X., He, M., Shu, Z., Huang, Y., Wu, A., & Ma, Z. (2021). Mechanical performance of pre-fabricated metal dovetail connections for

- Cross-Laminated Timber (CLT) structures. *Construction and Building Materials*, 303. <https://doi.org/10.1016/j.conbuildmat.2021.124468>
- Liu, Y., Guo, H., Sun, C., & Chang, W. S. (2016). Assessing cross laminated timber (CLT) as an alternative material for mid-rise residential buildings in cold regions in China-A life-cycle assessment approach. *Sustainability (Switzerland)*, 8(10). <https://doi.org/10.3390/su8101047>
- Ljunggren, F., Fredriksson, M., Johansson, N., & Sasic Kalagasidis, A. (2025). Cross-laminated timber: a state-of-the-art review of moisture, fire, acoustics, and energy-related aspects. In *Wood Material Science and Engineering*. <https://doi.org/10.1080/17480272.2025.2507145>
- Lukić, I., Premrov, M., Passer, A., & Žegarac Leskovar, V. (2021). Embodied energy and GHG emissions of residential multi-storey timber buildings by height – A case with structural connectors and mechanical fasteners. *Energy and Buildings*, 252, 111387. <https://doi.org/10.1016/J.ENBUILD.2021.111387>
- Mehra, S., O’Ceallaigh, C., Hamid-Lakzaeian, F., Guan, Z., & Harte, A. M. (2018). Evaluation of the structural behaviour of beam-beam connection systems using compressed wood dowels and plates. *WCTE 2018 - World Conference on Timber Engineering*.
- Mehra, S., O’Ceallaigh, C., Sotayo, A., Guan, Z., & Harte, A. M. (2021). Experimental characterisation of the moment-rotation behaviour of beam-beam connections using compressed wood connectors. *Engineering Structures*, 247, 113132. <https://doi.org/10.1016/J.ENG-STRUCT.2021.113132>
- Mehra, S., O’Ceallaigh, C., Sotayo, A., Guan, Z., & Harte, A. M. (2022). Experimental investigation of the moment-rotation behaviour of beam-column connections produced using compressed wood connectors. *Construction and Building Materials*, 331. <https://doi.org/10.1016/j.conbuildmat.2022.127327>
- Mirianon, F., Fortino, S., & Toratti, T. (2008). *A method to model wood by using ABAQUS finite element software Part I. Constitutive model and computational details*.
- MIT Climate Portal Writing Team. (2023). *How does the climate impact of cross-laminated timber compare to steel or concrete?* [https://climate.mit.edu/ask-mit/how-does-climate-impact-cross-laminated-timber-compare-steel-or-concrete?utm\\_source=chatgpt.com](https://climate.mit.edu/ask-mit/how-does-climate-impact-cross-laminated-timber-compare-steel-or-concrete?utm_source=chatgpt.com)
- Nakano, K., Karube, M., & Hattori, N. (2020). Environmental impacts of building construction using cross-laminated timber panel construction method: A case of the research building in Kyushu, Japan. *Sustainability (Switzerland)*, 12(6). <https://doi.org/10.3390/su12062220>
- Nero, R., Christopher, P., & Ngo, T. (2022). Investigation of rolling shear properties of cross-laminated timber (CLT) and comparison of experimental approaches. *Construction and Building Materials*, 316. <https://doi.org/10.1016/j.conbuildmat.2021.125897>
- Oh, J. W., Park, K. S., Kim, H. S., Kim, I., Pang, S. J., Ahn, K. S., & Oh, J. K. (2023). Comparative CO2 emissions of concrete and timber slabs with

- equivalent structural performance. *Energy and Buildings*, 281. <https://doi.org/10.1016/j.enbuild.2022.112768>
- Pozza, L., Ferracuti, B., Massari, M., & Savoia, M. (2018). Axial – Shear interaction on CLT hold-down connections – Experimental investigation. *Engineering Structures*, 160. <https://doi.org/10.1016/j.eng-struct.2018.01.021>
- Puettmann, M., Sinha, A., & Ganguly, I. (2019a). Life Cycle Assessment of Cross Laminated Timbers Produced in Oregon. *Journal of Green Building*, 14(4).
- Puettmann, M., Sinha, A., & Ganguly, I. (2019b). Life cycle energy and environmental impacts of cross laminated timber made with coastal douglas-fir. *Journal of Green Building*, 14(4), 17–33. <https://doi.org/10.3992/1943-4618.14.4.17>
- Ramage, M. H., Burrridge, H., Busse-Wicher, M., Fereday, G., Reynolds, T., Shah, D. U., Wu, G., Yu, L., Fleming, P., Densley-Tingley, D., Allwood, J., Dupree, P., Linden, P. F., & Scherman, O. (2017). The wood from the trees: The use of timber in construction. *Renewable and Sustainable Energy Reviews*, 68, 333–359. <https://doi.org/10.1016/J.RSER.2016.09.107>
- Reis, D. C., Quattrone, M., Souza, J. F. T., Punhagui, K. R. G., Pacca, S. A., & John, V. M. (2021). Potential CO2 reduction and uptake due to industrialization and efficient cement use in Brazil by 2050. *Journal of Industrial Ecology*, 25(2). <https://doi.org/10.1111/jiec.13130>
- Ren, H., Bahrami, A., Cehlin, M., & Wallhagen, M. (2024a). A state-of-the-art review on connection systems, rolling shear performance, and sustainability assessment of cross-laminated timber. *Engineering Structures*, 317, 118552. <https://doi.org/10.1016/J.ENG-STRUCT.2024.118552>
- Ren, H., Bahrami, A., Cehlin, M., & Wallhagen, M. (2024b). Flexural Behavior of Cross-Laminated Timber Panels with Environmentally Friendly Timber Edge Connections. *Buildings*, 14(5). <https://doi.org/10.3390/buildings14051455>
- Ren, H., Bahrami, A., Cehlin, M., & Wallhagen, M. (2024c). Proposing new adhesive-free timber edge connections for cross-laminated timber panels: A step toward sustainable construction. *Case Studies in Construction Materials*, 20, e02975. <https://doi.org/10.1016/J.CSCM.2024.E02975>
- Rogeanu, N., Latteur, P., & Weinand, Y. (2021). An integrated design tool for timber plate structures to generate joints geometry, fabrication toolpath, and robot trajectories. *Automation in Construction*, 130. <https://doi.org/10.1016/j.autcon.2021.103875>
- Sitnikova, E., Guan, Z. W., Schleyer, G. K., & Cantwell, W. J. (2014). Modelling of perforation failure in fibre metal laminates subjected to high impulsive blast loading. *International Journal of Solids and Structures*, 51(18), 3135–3146. <https://doi.org/10.1016/J.IJSOLSTR.2014.05.010>
- Sotayo, A., Bradley, D., Bather, M., Sareh, P., Oudjene, M., El-Houjeyri, I., Harte, A. M., Mehra, S., O’Ceallaigh, C., Haller, P., Namari, S., Makradi, A., Belouettar, S., Bouhala, L., Deneufbourg, F., & Guan, Z.

- (2020). Review of state of the art of dowel laminated timber members and densified wood materials as sustainable engineered wood products for construction and building applications. *Developments in the Built Environment*, 1, 100004. <https://doi.org/10.1016/J.DIBE.2019.100004>
- Sotayo, A., Bradley, D. F., Bather, M., Oudjene, M., El-Houjeyri, I., & Guan, Z. (2020). Development and structural behaviour of adhesive free laminated timber beams and cross laminated panels. *Construction and Building Materials*, 259, 119821. <https://doi.org/10.1016/J.CONBUILDMAT.2020.119821>
- SS. EN 408:2010+A1:2012. (2012). *Timber structures – Structural timber and glued laminated timber – Determination of some physical and mechanical properties*. Comit'ee Europ'een de Normalisation.
- Statens energimyndighet. (2023). *Scenarier över Sveriges energisystem 2023*.
- STYLECNC. (2025). *STYLECNC - 4x8 Wood CNC Router Machine*. <https://www.stylecnc.com/cnc-wood-router/4x8ft-wood-cnc-router-for-sale.html?gQT=1>
- Swedish Wood. (n.d.). *Properties of softwood*. Retrieved September 15, 2025, from <https://www.swedishwood.com/wood-facts/about-wood/from-log-to-plank/properties-of-softwood/>
- Swedish Wood. (2022). Design of timber structures, Volume 2: Rules and formulas according to Eurocode 5. *Swedish Wood*, 3.
- Tannert, T. (2016). Improved performance of reinforced rounded dovetail joints. *Construction and Building Materials*, 118. <https://doi.org/10.1016/j.conbuildmat.2016.05.038>
- Tétreault, M. G., Rollo, G., Oudjene, M., & Fafard, M. (2023). Experimental Investigation on the Mechanical Characteristics of a Novel Hybrid Densified Wood-Filled Aluminum Tube Dowel for Timber Connections †. *Engineering Proceedings*, 43(1). <https://doi.org/10.3390/eng-proc2023043044>
- Thomas Betong. (2018). *Välj rätt betong*. [https://thomasbetong.se/wp-content/uploads/sites/6/2024/04/Valj-ratt-betong\\_2024.pdf?utm\\_source=chatgpt.com](https://thomasbetong.se/wp-content/uploads/sites/6/2024/04/Valj-ratt-betong_2024.pdf?utm_source=chatgpt.com)
- Tighnavard Balasbanch, A., Sher, W., Yeoh, D., & Koushfar, K. (2022). LCA & LCC analysis of hybrid glued laminated Timber–Concrete composite floor slab system. *Journal of Building Engineering*, 49, 104005. <https://doi.org/10.1016/J.JOBE.2022.104005>
- Wang, T., Wang, Y., Crocetti, R., & Wålinder, M. (2022). In-plane mechanical properties of birch plywood. *Construction and Building Materials*, 340. <https://doi.org/10.1016/j.conbuildmat.2022.127852>
- Xiamen Lith Machine Limited. (n.d.). *Laboratory Electronic Industry Widen Flat Automatic Hot Press Machine*. Retrieved May 22, 2025, from [https://www.lithmachine.com/laboratory-electronic-industry-widen-flat-automatic-hot-press-machine\\_p267.html](https://www.lithmachine.com/laboratory-electronic-industry-widen-flat-automatic-hot-press-machine_p267.html)
- Xin, Z., & Gattas, J. (2021). Structural Behaviors of Integrally-Jointed Plywood Columns with Knot Defects. *International Journal of Structural Stability and Dynamics*, 21(2). <https://doi.org/10.1142/S021945542150022X>

- Xu, B.-H., Yu, K.-B., Jiao, S.-Y., Zhao, Y.-H., & Zhang, B. (2023). Pull-Out Performance of Timber Joints with Glued-In Densified Wood Dowels. *Journal of Materials in Civil Engineering*, 35(8). <https://doi.org/10.1061/jmcee7.mteng-15610>
- Younis, A., & Doodoo, A. (2022). Cross-laminated timber for building construction: A life-cycle-assessment overview. *Journal of Building Engineering*, 52, 104482. <https://doi.org/10.1016/J.JOBE.2022.104482>
- Yvonne, M. (2007). *Manual for LS-DYNA Wood Material Model 143*.
- Zhang, S., & Chui, Y. H. (2020). Characterizing flexural behaviour of panel-to-panel connections in cross-laminated timber floor systems. *Structures*, 28. <https://doi.org/10.1016/j.istruc.2020.10.040>

**Papers**

Associated papers have been removed in the electronic version of this thesis.

For more details about the papers see:

<http://urn:nbn:se:hig:diva-49495>